INFORMATION TO USERS

This manuscript has been reproduced from the microfilm master. UMI films the text directly from the original or copy submitted. Thus, some thesis and dissertation copies are in typewriter face, while others may be from any type of computer printer.

The quality of this reproduction is dependent upon the quality of the copy submitted. Broken or indistinct print, colored or poor quality illustrations and photographs, print bleedthrough, substandard margins, and improper alignment can adversely affect reproduction.

In the unlikely event that the author did not send UMI a complete manuscript and there are missing pages, these will be noted. Also, if unauthorized copyright material had to be removed, a note will indicate the deletion.

Oversize materials (e.g., maps, drawings, charts) are reproduced by sectioning the original, beginning at the upper left-hand corner and continuing from left to right in equal sections with small overlaps.

ProQuest Information and Learning
300 North Zeeb Road, Ann Arbor, MI 48106-1346 USA
800-521-0600

UMI®

INVESTIGATING THE STRUCTURAL AND CHEMICAL PROPERTIES OF SELF-ASSEMBLED MONOLAYERS AS A FUNCTION OF HYDROCARBON CHAIN LENGTH AND TERMINAL FUNCTIONAL GROUP

by

CHANDRA SEKHAR PALLA

A Dissertation submitted to the Graduate Faculty in Engineering in partial fulfillment of the requirements for the degree of Doctor of Philosophy, The City University of New York

2003

ProQuest Information and Learning Company
300 North Zeeb Road
P.O. Box 1346
Ann Arbor, MI 48106-1346

This manuscript has been read and accepted for the Graduate Faculty in Engineering in satisfaction of the dissertation requirement for the degree of Doctor of Philosophy.

9/12/2003 — Date

Alexander Gouzi — Chair of Examining Committee

9/15/2003 — Date

Mumtaz K. Kazimi — Executive Officer

Professor Charles Maldarelli

Professor Lane Gilchrist

Professor Leslie Isaacs

Professor Rasti Levicky

Supervisory Committee

THE CITY UNIVERSITY OF NEW YORK

Abstract

INVESTIGATING STRUCTURAL AND CHEMICAL PROPERTIES OF SELF-ASSEMBLED MONOLAYERS AS A FUNCTION OF HYDROCARBON CHAIN LENGTH AND TERMINAL FUNCTIONAL GROUP

by

Chandra Sekhar Palla

Advisor: Professor Alexander Couzis

In nature, self-assembly results in supermolecular hierarchical organizations of interlocking components that provides very complex systems. SAMs offer unique opportunities to increase fundamental understanding of self-organization, structure-property relationships, and interfacial phenomena. The ability to tailor both head and tail groups of the constituent molecules makes SAMs excellent systems for a more fundamental understanding of phenomena affected by competing intermolecular, molecular-substrates and molecule-solvent interactions like ordering and growth, wetting, adhesion, lubrication, and corrosion.

In this research we have investigated how the intermolecular interactions, mostly van der Waals interchain interactions, depend on the hydrocarbon chain length and terminal functional group, and how these interactions in turn determine the structure, mechanism of formation, and also packing density of the monolayers. We have considered octadecyltrichlorosilane (OTS, 18 carbon chain with methyl termination), undecyltrichlorosilane (UTS, 11 carbon chain with methyl termination), 11-cyano undecyltrimethoxysilane (CUTMS, 11 carbon chain with cyano (C≡N) termination) and aminopropyltrimethoxysilane (APS, 3 carbon chain with amine (NH_2) termination)

varying in chain length and terminal functional groups. FTIR results showed that molecules with long hydrocarbon chain formed densely packed, ordered crystalline structures and the order in the structure decreased with decrease in the hydrocarbon chain length. The order also decreased with addition of hydrophilic terminal group, for the same hydrocarbon chain length, due to affinity of hydrophilic terminal group to the substrate. The packing density of these monolayers, likewise, also depended on the chain length and terminal group. The packing density decreased with decrease in hydrocarbon chain length, and also with incorporation of hydrophilic surface group for the same chain length. FTIR and ellipsometer results showed that low chain molecules with hydrophilic surface group, like APS, have tendency of forming multilayers.

We investigated the mechanism of formation of monolayers as a function of temperature. Self-assembled monolayers formation is initiated by three distinct growth regimes: (i) island-like growth regime below phase transition temperature (ii) homogeneous growth regime at high temperatures (above phase transition) and (iii) mixed regime at intermediate regimes. Phase transition temperature decreased with decrease in chain length. OTS showed island-like growth regime at temperatures below 16°C, and CUTMS showed homogeneous growth regime at room temperatures. At 0°C, CUTMS showed presence of liquid-like and solid-like structure, indicating mixed growth regime for CUTMS monolayer at these temperatures.

We successfully demonstrated the modification of cyano terminal group of CUTMS monolayer into carboxylic group using a simple in situ hydrolysis reaction approach for the surface transformation. We have investigated the reaction kinetics and conversion both by contact angle measurements and FTIR. COOH surface is very

sensitive to the surrounding pH. We studied the local structure, primarily the surface 2-D distribution of the COOH and COO^-, by varying pH. We also evaluated the molar absorptivities of COOH, COO^- and CN moieties from simple stoichiometric analysis.

We also successfully demonstrated the use of SAMs as model membranes to study the sorption properties of various volatile organic vapors, and in turn understand the prominent interactions that govern the absorption process. We studied the absorption of polar acetone vapors and non-polar hexane vapors. Acetone vapors, being polar, showed affinity towards polar surfaces. Acetone vapors showed strong hydrogen bonding with hydrophilic silicon surfaces, weak hydrogen bonding with APS and CUTMS surfaces and primarily physisorption with UTS and OTS surfaces. Effect of partial pressure on the absorption is also studied. Acetone vapors agreed reasonably well with Langmuir sorption model, except at high partial pressures when the condensation of the vapors became significant.

Interactions of hexane vapors also depended on the properties of the underlying monolayers. Moreover, alignment of the absorbed hexane vapors exhibited a strong correlation with the structure of the underlying monolayer. Absorbed hexane structure varied from all-trans on OTS monolayer to liquid like structure on clean silicon wafer. We also modeled the alignment of hexane molecules on the OTS (methyl terminated) monolayer using interfacial energy arguments.

Acknowledgements

I would like to express my deepest gratitude to my advisor, Prof. Alexander Couzis for the continuous encouragement, guidance and support during my doctoral study. He has been a mentor, a friend and a philosopher, and has been a pleasure working with him for my thesis. I am very much in debt to him for the support and advice he has provided me not only professionally but also personally.

I would also like to thank Prof. Charles Maldarelli for his guidance, support and the discussions we had during group meetings and other occasions. He has been a role model for me to keep my patience, no matter how difficult the situation is.

I would like to thank Changzai Chi for the numerous discussions we had together. We entered college same year, joined the interfacial group together and did almost everything together. It has been a pleasure to know him personally so well. One of the sweetest moments of my Ph.D is to be the Best Man for his marriage. I would also like to thank Nitin Kumar, especially, for getting me started with the Ph.D work, teaching me patiently all the experimental techniques.

I would like to extend my special thanks to my special friends Kavitha, Mariella and Vaidharbhi for being with me during my stay here. They have constantly encouraged me and it was great to interact with them. Kavitha, especially, has been a constant source of inspiration for me and it is pleasure to know her personally so well. I would also like to extend my thanks to my past and present roommates Pradeep, Anil, Manoj, Ravi and Jeevan for bearing with me. My due thanks to Dr. Fan, Hongjie, Qing Song, Ashish and Jose.

I would also like to thank Andy and Xu for their assistance.

Finally I would like to thank my parents and family for all the support, encouragement and believing in me all these years.

Table of Contents

ABSTRACT iii

ACKNOWLEDGEMENTS vi

TABLE OF CONTENTS vii

LIST OF FIGURES xii

LIST OF TABLES xvi

CHAPTER 1: INTRODUCTION 1

1.1 ORGANIC THIN FILMS 1

1.2 APPLICATIONS AND CHALLENGES 4

1.3 SELF-ASSEMBLED MONOLAYERS 7

1.4 SURFACE ENGINEERING USING SAMS 10

1.5 OUTLINE OF RESEARCH 12

1.5.1 Objective 12

1.5.2 Structure and Packing Density of SAMs 12

1.5.3 Modification of SAMs 13

1.5.4 SAMs as Model Membranes 14

1.6 REFERENCES 16

CHAPTER 2: BACKGROUND: A BRIEF OVERVIEW OF SELF-ASSEMBLED MONOLAYERS 18

2.1 INTRODUCTION 18

2.2 INTERACTIONS INVOLVED IN THE FORMATION OF SELF-ASSEMBLED MONOLAYERS 19

2.3 MECHANISM OF FORMATION OF SILOXANE SELF-ASSEMBLED MONOLAYERS 20

2.4 EFFECT OF SOLVENT 21

2.5 EFFECT OF WATER CONTENT IN SOLVENT 23

2.6 EFFECT OF SURFACE HYDRATION 23

2.7 EFFECT OF TEMPERATURE ON MECHANISM OF FORMATION 25

2.8 REFERENCES 27

CHAPTER 3: EFFECT OF CHAIN LENGTH AND TERMINAL FUNCTIONAL GROUP ON STRUCTURE, MORPHOLOGY, MECHANISM OF FORMATION AND PACKING DENSITY OF SELF-ASSEMBLED MONOLAYERS 35

3.1. INTRODUCTION 35

3.2 EXPERIMENTAL SECTION 37

3.2.1 Materials 37

3.2.2 Cleaning Protocol 38

3.2.3 Monolayer Preparation 39

3.2.3.1 OTS Monolayer 39

3.2.3.2 UTS Monolayer 39

3.2.3.3 CUTMS Monolayer 39

3.2.3.4 APS monolayer 40

3.2.3.5 LB film of Stearic Acid 40

3.2.4 Contact Angle Measurements 40

3.2.5 Ellipsometry 41

3.2.6 IR Measurements 41

3.2.7 AFM Imaging 42

3.3 RESULTS AND DISCUSSIONS 42

3.3.1 Structure and Properties of Monolayers 42

3.3.2 Packing Density 45

3.3.3 Effect of Temperature on Mechanism of Formation 49

3.4 CONCLUSIONS 49

3.5 REFERENCES 50

CHAPTER 4: MODIFICATION OF SELF-ASSEMBLED MONOLAYERS: CONVERSION OF TERMINAL CN FUNCTIONAL GROUP TO COOH GROUP 57

4.1 INTRODUCTION 57

4.2 EXPERIMENTAL SECTION 60

4.2.1 Materials 60

4.2.2 Modification of CUTMS Monolayer 61

4.3 RESULTS AND DISCUSSIONS 61

4.3.1 Formation of CUTMS Monolayer 61
4.3.2 Conversion of CN to COOH groups 66
4.3.3 pH Dependence of COOH groups 67
4.3.4 Calculation of Molar Absorptivities for evaluation of Number Densities 67
4.4 CONCLUSIONS 71
4.5 REFERENCES 72
CHAPTER 5: SAMS AS MODEL MEMBRANES: ABSORPTION OF ACETONE AND HEXANE VAPORS ON DIFFERENT MONOLAYERS 89
5.1 INTRODUCTION 89
5.2 EXPERIMENTAL SECTION 96
5.2.1 Materials 96
5.2.2 Flow Conditions 97
5.2.3 Quantitative Prediction of Molecular Coverage 98
5.3 RESULTS AND DISCUSSIONS 98
5.3.1 Properties of Various Monolayers 98
5.3.2 Absorption of Acetone Vapors on Monolayers 99
5.3.2.1 Effect of Partial Pressure 104
5.3.2.2 Langmuir Model 107
5.3.2.3 Assumptions in Langmuir Model 108
5.3.2.4 BET Model 109
5.3.2.5 Effect of Surface Tension on Absorption 110
5.3.3 Absorption of Acetone Vapors on Monolayers 111
5..3.3.1 Effect of Partial Pressure 114
5.3.3.1 Langmuir Model 116
5.3.3.2 BET Model 116
5.3.3.3 Model Prediction of Structure of Hexane Vapors on Methyl Terminated Monolayers 116
5.4 CONCLUSIONS 119
5.5 REFERENCES 121
CHAPTER 6: FUTURE WORK 144

6.1 STRUCTURE OF MONOLAYERS 144
6.2 SURFACE ENGINEERING OF SAMS 145
6.3 SAMS AS MODEL MEMBRANES 146
REFERENCES 148

List of Figures

Figure 1.1: Cartoon depicting the potential applications of SAMs 17

Figure 2.1: Cartoon of a surfactant molecule showing all the forces involved in the formation of a self-assembled monolayer 31

Figure 2.2: Cartoon depicting the mechanism of formation of self-assembled monolayer 32

Figure 2.3: Effect of surface hydration of monolayer formation (a) on hydrated substrate OTS forms island-like fractal structures (b) on partailly hydrated substrate island size decreases and (c) on dehydrated substrate only dot-like structure are seen (courtesy Nitin et al) 33

Figure 2.4: π-A isotherm of OTS molecules exhibiting different phases 34

Figure 2.5: Effect of temperature on mechanism of formation of monolayers: OTS showing three different growth patterns depending on temperature of deposition (a) forms island-like structures below critical temperature (b) at T= 25 °C, forms less islands (c) above critical temperature, shows homogeneous growth pattern (courtesy Carraro et al) 34

Figure 3.1: Cartoon depicting the surfactant molecules considered to study the effects of hydrophobic chain length and terminal functional group 51

Figure 3.2: Cartoon depicting the procedure for preparation of self-assembled monolayers 52

Figure 3.3: IR Spectra of different monolayers formed on silicon crystal 53

Figure 3.4: Sample spectrum of a monolayer, showin methylene and methyl asymmetric and symmetric vibrations, used for peak fit duirng packing density measurements 54

Figure 3.5: Calibration curve, showing the linear variation in area of asymmetric methylene stretching frequency with the concentration of OTS surfactant concentration, for obtaining ε_{bulk} 54

Figure 3.6: Schematic of various monolayers 55

Figue 3.7: AFM image of CUTMS monolayer formed at room temperatures taken in contact mode. Absence of islands indicates homogenous growth regime at room temperatures 56

Figure 3.8: Spectrum of CUTMS monolayer formed at 0°C. Peak splits for methylene asymmetric and symmetric stretches indicate the existence of LC-LE phases in equilibrium 56
Figure 4.1: Typical spectrum of CUTMS monolayer formed on silicon crystal 78
Figure 4.2: Variation in contact angle of CUTMS monolayer with deposition time 80
Figure 4.3: Variation in contact angle as reaction proceeds 81
Figure 4.4: Fraction of COOH and CN groups present as reaction proceeds (Cassie's Equation) 82
Figure 4.5: Spectrum shows increase in COOH peak at 1702 cm^{-1} and decrease in CN peak at 2253 cm^{-1} as reaction proceeds 83
Figure 4.6: Decrease in CN peak intensity as reaction proceeds 84
Figure 4.7: (a) Spectrum of CUTMS monolayer after reaction at low pH (2.0) (only COOH present) (b) spectrum of monolayer at pH 7.5 (both COOH and COO^- present) 85
Figure 4.8: (a) LB film of stearic acid at pH 2.0 (b) LB film immersed in calcium chloride solution of pH 11.5 (c) LB film again immersed in a solution pH of 2.5 (d) again immersed in a sodium hydroxide solution of pH 10.5 86
Figure 4.9 (a) Cartoon CN terminated monolayer converted to COOH terminal groups (b) Schematic showing the dependence of COOH terminal groups on the pH of the environment (c) showing the distribution of COOH and COO^- groups at an intermediate pH value 88
Figure 5.1: Spectra of acetone present in three different phases; clearly showing surface induced perturbation in C=O peak 123
Figure 5.2: Experimental flow cell used to measure the sorption properties of volatile organic vapors 124
Figure 5.3: Kinetics of absorption of acetone vapor on clean Si surface 125
Figure 5.4: Amount of acetone absorbed on different surfaces 125
Figure 5.5: IR spectra of acetone absorbed on different monolayers 126
Figure 5.5: Zoomed IR spectra of acetone vapor absorbed on (a) CUTMS monolayer (b) OTS monolayer and (c) UTS monolayer 126

Figure 5.6: Effect of partial pressure on acetone absorption on Si surface with time 128
Figure 5.7: Effect of partial pressure on acetone absorption on different surfaces 128
Figure 5.8: IR spectra of acetone vapors absorbed on Si crystal as a function of partial pressure 129
Figure 5.9: IR spectra of acetone vapors absorbed on APS monolayer as a function of partial pressure 129
Figure 5.10: IR spectra of acetone vapors absorbed on CUTMS monolayer as a function of partial pressure 130
Figure 5.11: IR spectra of acetone vapors absorbed on partial-OTS monolayer as a function of partial pressure 130
Figure 5.12: IR spectra of acetone vapors absorbed on OTS monolayer as a function of partial pressure 131
Figure 5.13: IR spectra of acetone vapors absorbed on UTS monolayer as a function of partial pressure 131
Figure 5.14 (a): Linear regime of Langmuir sorption model (b) Langmuir fit 132
Figure 5.15 (a): Linear regime of BET sorption model (b) BET fit 133
Figure 5.16(a): Effect of surface tension of the monolayers on the amount of acetone absorbed (b) Effect of polar and dispersive components of surface tension of the monolayers on the amount of acetone absorbed 134
Figure 5.17: Amount of hexane absorbed on different monolayers 136
Figure 5.18: Spectra of absorbed hexane on different monolayer surfaces **136**
Figure 5.19: Amount of hexane absorbed as a function of partial pressure with time 138
Figure 5.20: Amount of hexane absorbed as a function of partial pressure 138
Figure 5.21: Spectra of absorbed hexane on Si crystal as a function of partial pressure 139
Figure 5.22: Spectra of absorbed hexane on APS monolayer as a function of partial pressure 139
Figure 5.23: Spectra of absorbed hexane on CUTMS monolayer as a function of partial pressure 140

Figure 5.24: Spectra of absorbed hexane on UTS monolayer as a function of partial pressure 140
Figure 5.25: Spectra of absorbed hexane on OTS monolayer as a function of partial pressure 141
Figure 5.26: Showing the strong correlation between the structure of the absorbed hexane molecules on the monolayer and the structure of the corresponding underlying monolayer 141
Figure 5.27 (a): Linear regime of Langmuir sorption model (b) Langmuir fit 142
Figure 5.28 (a): Linear regime of BET sorption model (b) BET fit 143
Figure 6.1: Formation of CdS nanoparticles (a) on OTS surface (b) on modified CUTMS monolayer 147

List of Tables

Table 3.1: Showing the methylene and methyl stretches of the spectra shown in figure 3.3. Also shows the contact angle and ellipsometer measurements for all the monolayers 53

Table 4.1: In situ transformation of monolayers into different functional groups 76

Table 4.2: Peak positions of important vibrations of between CUTMS liquid and monolayer spectra. The difference in spectral values is not considerably different, indicating that the monolayer formed resembles a liquid-like structure 79

Table 4.3: Peak Positions of methylene symmetric and asymmetric vibrations of CUTMS monolayer prepared in different solvents. Data shows that there is no considerable effect of solvent on the monolayer structure of CUTMS 79

Table 4.4: Peak positions of methylene symmetric and asymmetric vibrations for OTS self-assembled monolayer and Stearic acid LB film. Both of them form a densely packed, crystalline structure 79

Table 4.5: Peaks of COOH and COO^- (bounded and unbounded) of stearic acid LB film at various pH values. Integrated absorbance values are also given in the table. No differentiation was drawn between bounded and unbounded COOH and COO^- in the calculation of the integrated absorbance values 87

Table 5.1: Showing the vibrational frequencies of C=O peak of acetone present in hydrogen bonded, physically adsorbed (or condensed) or vapor phase states in the presence of OTS, UTS, CUTMS and clean Silicon substrate 127

Table 5.2: Langmuir parameters 132

Table 5.3: BET model parameters 133

Table 5.4: Polar and Dispersive components of surface tension of the monolayers 135

Table 5.5: Showing the methylene asymmetric and symmetric stretches of absorbed hexane vapors. (values not in parethesis). Values in the parenthesis represent that of the corresponding monolayers 137

Table 5.6: Langmuir parameters 142

Table 5.7: BET parameters 143

Chapter 1

Introduction

1.1 Organic Thin Films

The properties of organic thin films, and particularly thin polymeric films and molecular monolayers and multilayers, offer many challenging scientific and technological opportunities for devices. Already we have seen that many thin organic films are being used in microelectronic, either in new applications or by replacing existing materials. The prospects are good for much more. In fact, molecular thin films are expected to be the wave of the future, especially with the ability to modify molecular structure, i.e. the ability to do molecular engineering. Dimensions of current devices are continually being reduced and are almost to the molecular level. It is tantalizing, therefore, to consider the possibility of information processing and storage at the molecular level. Here it is obvious that the properties and attributes of the individual molecules and their interactions must be taken into account. Chemists can synthesize many types of molecules and optimize some desired property; hence a whole host of possibilities exists. Films can be fabricated by spinning from solution, by the langmuir-blodgett technique or by self-assembly from solution. Surface science experimental techniques can identify and verify desired structures. All these aspects have made it possible to produce new films, characterize them, and ascertain their structure and desired properties.

Now not only are the technological applications of these molecular films being exploited, but also the many new opportunities they offer to study film structure and

phase transitions in two dimensions. Cooperative effects similar to those in liquid crystals have been observed, but much more understanding is needed to optimize these interactions for molecular films. Understanding of the relationship between structure and desired properties is in its infancy. What is desired is the ability to make a molecular film with some specific property by a combination of synthetic chemistry and the physics of assembly and fabrication. Optical and electrical properties are of interest for their impact on microdevices. Although much has been done in this field of research and development, there is still far to go before we can take full advantage of the capabilities of organic films. One must reflect on the many membranes in the human body with their myriad functions. How we can understand and mimic some of those processes is the question and challenge for molecular scientists today.

Molecular films, ordered thin organic films in a thickness range from a few nanometers to several hundred nanometers, show considerable technological promise, and further scientific investigation could prove to be very fruitful. Electronic and optical devices presently incorporate structures that are in this thickness range or approaching it, and organic thin films have been proposed to replace both passive and active components traditionally fabricated with other materials. Scientific studies of molecular interactions in thin-film structures leading to an understanding of the collective properties of ordered arrays have recently been possible with organic films, characterized in more detail by a number of the newer surface science techniques. Biological lipid membranes exhibit a variety of different functions, and attempts to produce synthetic thin-film analogues have excited the imagination of many. For these reasons it is necessary to investigate the

physical, chemical, biological, and theoretical aspects of thin molecular films, and their potential assessed.

Chemists have been able to synthesize molecules with many different conformations and chemical structures exhibiting a wide variety of functions. Although collective phenomena have been studied, more emphasis needs to be placed on the design and control of important collective properties so as to make these molecules into useful materials. The future for thin molecular solids lies in designing organized films to perform new and special functions. Of interest are arrays with cooperative properties different from those of the individual molecular components and perhaps possessing some functional enhancement. Liquid crystal displays are a well-known example of a cooperative function, and much interest has focused on the nature of phase transitions and magnetism in two dimensions. The number of possibilities is large, and considerably more research is needed to relate a specific film's structure to its functional properties.

The area of Langmuir-Blodgett films, monolayer structures transferred from a water surface to a substrate, has been receiving a great deal of attention. These films are appealing for study because of the facile manner in which a single monolayer or multilayers can be deposited. Such a capability brings to mind applications as organic superlattices created by the successive deposition of alternating layers of different molecules. Whether these materials could even find use is highly speculative, but they do serve as good model systems. One could imagine some utilization in a number of areas, including optics, sensors, and barrier films. Electron beam resists[1,2] and "self-healing" capacitor layers'[3] have been demonstrated in the laboratory. Functionalized phthalocyanines with attached molecular side groups to change or improve properties,

such as solubility, can be used to form LB films, and this is an important advance because they are among the most robust organic molecules known.[4] Topotactic polymerization reactions, dependent on the structural proximity and orientation of reactants, have been used to create poly(diacetylenes) that are crystalline and exhibit nonlinear optical properties.[5-7]

1.2 Applications and Challenges

The explosive growth of microelectronics technology since 1960 is well chronicled. According to some estimates, the "cost of computing" has decreased by several orders of magnitude during this time. Moreover, the value of the business has greatly increased, making this an attractive area for possible applications of new technology. We know of some specific cases where organic films are being successfully used. Already we have photoresists and electron beam resists for making patterns for very large scale integrated circuits (VLSI), organic photoconductors for printing and copying that compete directly with inorganic photoconductors, liquid crystals for displays, polymer films for insulation and packaging (various layers to encapsulate and protect a VLSI circuit from the environment), and attached molecules and chemically reactive sites to modify surfaces. A classic example of this controlled chemistry is illustrated by color film for photography; films consist of some 20 layers, some as thin as 1 μm, with numerous diffusion barriers.

All of this sounds exciting and promising, but we should be aware that there are still many unsolved problems. Organic thin films suffer from fragility, impurities, and defects. Consequently, their use has been limited by the ability to produce films with

good integrity, i.e., mechanical, thermal, and chemical stability, as well as with the desired properties. Also, they must be made with few defects, or some mechanism for repair must be found. Efforts to overcome some of these problems, and to find applications that even take advantage of them, are progressing well. For strength, films are being polymerized and cross-linked. Schemes are being developed to produce them with higher purity and, for polymeric films, with a narrower molecular weight range, and hence more uniformity. Weak interactions, e.g., van der Waals forces, acid-base and charge-transfer interactions, and certain covalent chemical bonding, could be used to modify organic thin films more easily and to make molecular engineering and design changes. That is, there are many ways to modify and make assemblies, but one of the key problems is to make an organized structure whose collective properties can be optimized for a desired goal. Today we have only scratched the surface, and, as stated above, we need more scientific understanding of the relationships not only of the component molecular species but also of the properties of an oriented and arranged array with the desired materials characteristics. This cannot be emphasized enough! If one were asked to make a thin organic film with a particular set of desired physical and chemical properties, generally an empirical approach would be taken. This process must definitely be shortened and put on a more rigorous scientific basis requiring better understanding of preparation and characterization methods.

The areas considered to be the most promising for technology are as follows:

- thin-film optics, optical layers and films exhibiting some special optical behavior, such as nonlinear optical effects for second harmonic generation, or switching, amplification, and modulation of optical signals;

- sensors and transducers, thin films for specific sensors, such as bio-logical sensors, as for coupling physical or chemical measurement probes to the film properties, e.g., electrochemical, mass, optical, and conductivity;
- protective layers, thin organic films impervious to deleterious species in the environment so as to prevent some contaminant from disrupting the operation or function of the other layers;
- patternable materials, photoresist and electron beam resists to create patterns at high packing density with greater resolution ($<<1\ \mu m$) than heretofore seen;
- surface preparation and modification, surface groups to enhance lubrication, adhesion, wetting, and biological response or to provide new paths for chemical reactions not found in solution or isotropic media;
- chemically modified electrodes, coatings on electrodes to give desired properties for new electrochemical reactions or analyses; and
- biomacromolecules, our understanding of protein films needs to be expanded for more effective utilization. Can we produce or mimic biological effects with artificial films, and how well can we do this?

Besides these technological uses for thin organic films there are also a number of scientific problems which must be addressed:

1 The relationships between structure of oriented and aligned arrays of molecules and their collective properties are not well understood. New chemical designs and unique architecture may be able to create systems capable of exhibiting novel properties.

2 Molecular films can serve as models for the tailoring of interfaces and surfaces. For example, surfactants and modified polymeric surfaces have been used for a long time, but an understanding of them that could lead to new chemistry at a surface or to fabricate a new electronic device without delamination at the interfaces is still in its infancy. Films also can be examples for theoretical models involving several interactions, e.g., more than two-body interactions and several molecule-molecule interactions, as well as molecule-surface interactions.

3 Thermodynamics and kinetics of films involving phase transitions, viscosity near a surface, elasticity, diffusion, and transport of ions, electrons, and molecular species across them are all important to their properties. The transition from solid to fluid-like behavior, through liquid crystal behavior, is a gradual process and an interesting phenomenon, which requires more investigation.

1.3 Self-Assembled Monolayers

In this research, we have chosen self-assembled monolayers as organic thin films to investigate some of the aspects that have been brought up in the preceding section. Self-assembled monolayers are chosen for the advantages they have over Langmuir-Blodgett (LB) films and thin polymeric films. SAMs are thermally and chemically more robust than LB films, and the structural and surface properties can be controlled more easily than thin polymeric films.

Self-assembled monolayers are molecular assemblies that are formed instantaneously when the surfactant molecules adsorb from the solution phase on to an appropriate substrate. Typically as surfactant is made up of three groups: (1) a head

group, which participates in bonding with the substrate, (2) a long hydrocarbon chain that participates in the weak interchain van der Waals interactions and (3) a surface or terminal group that dictates the surface properties. Classically three types of SAMs are studied:

- trifunctional silanes on hydroxylated surfaces
- long chain carboxylic acids on aluminium oxide surfaces, and
- long chain thiols on gold, copper or silver surfaces

The field of self-assembled monolayers (SAMs) has witnessed tremendous growth in synthetic sophistication and depth of characterization over the past 20 years. The field really began much earlier than is now recognized. In 1946 Zisman published the preparation of a monomolecular layer by adsorption (self-assembly) of a surfactant onto a clean metal surface.[8] At that time, the potential of self-assembly was not recognized, and this publication initiated only a limited level of interest. Early work initiated in Kuhn's laboratory at Gottingen, applying many years of experience in using chlorosilane derivative to hydrophobize glass, was followed by the more recent discovery, when Nuzzo and Allara showed that SAMs of alkanethiolates on gold can be prepared by adsorption of di-n-alkyl disulfides from dilute solutions.[9] Getting away from the moisture-sensitive alkyl trichlorosilanes, as well as working with crystalline gold surfaces, were two important reasons for the success of these SAMs. Many self-assembly systems have since been investigated, but monolayers of alkanethiolates on gold are probably the most studied SAMs to date.

The formation of monolayers by self-assembly of surfactant molecules at surfaces is one example of the general phenomena of self-assembly. In nature, self-assembly

results in supermolecular hierarchical organizations of interlocking components that provides very complex systems.[10] SAMs offer unique opportunities to increase fundamental understanding of self-organization, structure-property relationships, and interfacial phenomena. The ability to tailor both head and tail groups of the constituent molecules makes SAMs excellent systems for a more fundamental understanding of phenomena affected by competing intermolecular, molecular-substrates and molecule-solvent interactions like ordering and growth, wetting, adhesion, lubrication, and corrosion. That SAMs are well-defined and accessible makes them good model systems for studies of physical chemistry and statistical physics in two dimensions, and the crossover to three dimensions.

SAMs provide the needed design flexibility, both at the individual molecular and at the material levels, and offer a vehicle for investigation of specific interactions at interfaces, and of the effect of increasing molecular complexity on the structure and stability of two-dimensional assemblies. These studies may eventually produce the design capabilities needed for assemblies of three-dimensional structures.[11] However, this will require studies of more complex systems and the combination of what has been learned from SAMs with macromolecular science.

The exponential growth in SAM research is a demonstration of the change chemistry as a discipline has been going through. Chemistry has been moving away from traditional disciplines and into interdisciplinary areas, and chemists are engaged in research at the interface of chemistry with physics, biology, and engineering. The fabrication and manipulations of molecular assemblies, molecular recognition, biomineralization, hierarchical structure and function, and computational chemistry to

elucidate structure-function relationships have become central themes in modern chemistry. These important changes can find their origin partly in the areas of Langmuir-Blodgett and self-assembled monolayers, which continue to serve as major techniques for the fabrication of supramolecular structures.

The interest in the general area of self-assembly, and specifically in SAMs, stems partially from their perceived relevance to science and technology. In contrast to ultrathin films made by, for example, molecular beam epitaxy (MBE), and chemical vapor deposition (CVD), SAMs are highly ordered and oriented and can incorporate a wide range of groups both in the alkyl chain and at the chain termination. Therefore, a variety of surfaces with specific interactions can be produced with fine chemical control.[12] Due to their dense and stable structure, SAMs have potential applications in corrosion prevention, wear protection, and more. In addition, the biomimetic and biocompatible nature of SAMs makes their applications in chemical and biochemical sensing promising. Their high molecular order parameter in SAMs makes them ideal as components in electrooptic devices. Recent work on nanopatterning of SAMs suggests that these systems may have applications in patterning of GaAs and in the preparation of sensor arrays.[13] Figure 1.1 depicts some of the applications SAMs can be potentially used for.

1.4 Surface Engineering Using SAMs

Independent control of surface structure and chemical properties and the resulting structure-property relationships are both scientifically interesting and technologically important. For many applications, controlling the properties of interfaces is very important. However, in real-life circumstances, interfaces that contain at least one

polymer surface are typically irregular. Surface properties of polymers depend critically upon the chemical and physical details of molecular structure at the surface of the polymer. To control surface properties by manipulating surface structure, it is necessary to have an extensive database of detailed correlations between properties and structure for the polymer surface of interest. However, other than generalizations about simple behavior (e.g., wetting and chemical reactivity), very little definitive work has been reported on such structure-property correlations for polymer surfaces.

Since surface properties are generally considered to be controlled by the outmost 5-10 Å at a polymer film, a logical solution is to use self-assembled monolayers (SAMs) as model polymer surfaces.[14] To fully understand the breadth of surface interactions, one needs a portfolio of chemical functionalities so that different surface forces can be tailored at the molecular level. SAMs are especially suited for the studies of interfacial phenomena due to the fine control of surface functional group concentration. These surfaces can be produced to have surface energies, which span the range from "Teflon-like" surfaces (surface CF3 groups) to very high energy surfaces (surface OH or COOH groups), i.e., surface tensions of 10-70 dyne cm^{-1}.

For example, SAMs with variable lengths of alkyl chain can be used to screen the interactions of a polymer with an underlying substrate. Charged surface functionalities can be used to study the Debye screening length in processes such as protein adsorption. Polar surfaces, with groups such as cyano (CN), can be used to investigate the contribution of dipole-dipole interactions in surface adhesion. Surface OH groups can vary wetting behavior and provide insight into the importance of H-bonding in surface phenomena.

1.5 Outline of Research

In this research, we concentrated on self-assembled monolayers of trifunctional silanes formed on hydroxylated surfaces (precisely silicon surfaces). Though lot of research is being carried on self-assembled monolayers, there still remain several unresolved issues and, it is important both on fundamental and technological point of view to understand these various aspects that affect the structure and formation of the self-assembled monolayers.

1.5.1 Objective

The overall objective of this research is to gain fundamental understanding in the formation of self-assembled monolayers of silane or siloxane based. This research consists of three parts:

1.5.2 Structure and Packing density of SAMs

In the first part of research, discussed in chapter 3, we have investigated the effects of hydrocarbon chain length and terminal functional group on structure, orientation and packing density of the SAMs. The objective of this part is to study how the intermolecular interactions, mostly van der Waals interchain interactions, depend on the hydrocarbon chain length, and how these interactions in turn determine the structure, mechanism of formation, and also packing density of the monolayers. Similarly we looked into the aspects of the effect of terminal functional group, how the polarity of the

terminal group affects the inclination of the monolayer and the packing density of the monolayers. We have considered octadecyltrichlorosilane (OTS, 18 carbon chain with methyl termination), undecyltrichlorosilane (UTS, 11 carbon chain with methyl termination), 11-cyano undecyltrimethoxysilane (CUTMS, 11 carbon chain with cyano (C≡N) termination) and aminopropyltrimethoxysilane (APS, 3 carbon chain with amine (NH_2) termination) varying in chain length and terminal functional groups. Their structure, morphology, mechanism of formation and packing density have been investigated using series of complementary techniques such as FTIR, AFM, ellipsometer and contact angle measurements. We also looked into the temperature effects on the mechanism of the formation.

Self-assembled monolayers formation is initiated by three distinct growth regimes: (i) island-like growth regime below phase transition temperature (ii) homogeneous growth regime at high temperatures (above phase transition) and (iii) mixed regime at intermediate regimes. We have investigated the dependence of the phase transition temperature on hydrocarbon chain length.

1.5.3 Modification of self-assembled monolayers

In the second part of research, discussed in chapter 4, we have looked into surface modification (engineering) of SAMs. High reactivity of the electrophilic head group (trifunctional silane) limits the functional groups that can be incorporated on a siloxane based SAM. Due to this limitation, several useful functional groups such as alcohols, carboxylic acids, amines, amides, thiols, phosphines, enamines, enol ethers etc., cannot be prepared. In this part of research, we have used a simple in situ hydrolysis reaction

approach to transform terminal cyano (CN) group into useful carboxyl (COOH) group. We have investigated the reaction kinetics both by contact angle measurements and FTIR. COOH surface is very sensitive to the surrounding pH. As a result of this, we have studied the local structure, primarily the surface 2-D distribution of the COOH and COO^-, by varying pH. We also evaluated the molar absorptivities of COOH, COO^- and CN moieties from simple stoichiometric analysis.

1.5.4 Self-assembled monolayers as Model Membranes

The objective of this part of research is to investigate the sorption properties of various gas phase analytes on various monolayers in order to elucidate the governing interactions that govern the absorption process. We have investigated the sorption properties of acetone and hexane vapors, and are discussed in chapter 5.

Acetone vapors are chosen because of the sensitivity exhibited by the carbonyl group to the IR spectrum. Carbonyl group exhibits different IR vibrational frequencies depending on whether it exists in the state of hydrogen bonded, physisorbed or vapor. How the governing interactions of the acetone molecules depend on the properties of the underlying monolayer are investigated. The effects of partial pressure and surface tension of the monolayer on the absorption process are also studied. The absorption process is modeled by simple Langmuir and BET sorption models.

We are interested in absorption of hexane because it is one of the short chain alkanes, and alkanes, even though they are the simplest of the organic molecules, they often play an important role as building blocks in various organic materials such as surfactants, liquid crystals, and polymers. We investigated the effects of partial pressure

and the underlying monolayer properties on the absorption of hexane vapors. We also studied the alignment of absorbed hexane molecules on the underlying monolayers, and qualitatively modeled the alignment of hexane molecules on the OTS (methyl terminated) monolayer.

And finally we conclude with some directions for future work in chapter 6.

1.6 References

1. Barraud, A.; Rosilio, C.; Ruaudel-Teixier, A. *Thin Solid Films* **1980**, *68*, 99.

2. McCord, M. A.; Pease, R. F. W. *J. Vac. Sci. Technol., B* **1986**, *4*, 86.

3. Agarwal, D. K.; Srivastava, V. K. *Solid State Commun* **1972**, *11*, 1461.

4. Roberts, G. G.; Petty, M. C.; Baker, S.; Fowler, M. T.; Thomas, N. *J. Thin Solid Films* **1985**, *132*, 113.

5. Kajzar, F.; Messier, J.; Zyss, J.; Ledoux, I. *Opt. Commun.* **1983**, *45*, 13.

6. Chollet, P. A.; Kajzar, F.; Messier, J. *Thin Solid Films* **1985**, *132*, 1.

7. Sauteret, C.; Hermann, J. P.; Frey, R.; Pradere, F.; Ducuing, J.; Baughman, R. H.; Chance, R. R. *Phys. Rev. Lett.* **1976**, *36*, 956.

8. Bigelow, W. C.; Pickett, D. L.; Zisman, W. A. *J. Colloid Interface Science* **1946**, *1*, 513.

9. Nuzzo, R. G.; Allara, D. L. *J. Am. Chem. Soc.* **1983**, *105*, 4481.

10. Ulmann, A.; Kuhn, H. *Thin Films*; Academic Press: New York, 1995; Vol. 20.

11. Ball, P. *Designing the Molecular World*; Princeton University Press: Princeton, 1994.

12. Ulman, A.; Evans, S. D.; Shnidman, Y.; Sharma, R.; Eilers, J. E.; Chang, J. C. *J. Am. Chem. Soc.* **1991**, *113*, 1499.

13. Kumar, A.; Biebuyck, H. A.; Whitesides, G. M. *Langmuir* **1994**, *10*, 1498.

14. Allara, D. L. *Polymer Surfaces and Interfaces*; Wiley: Chichester, 1993; Vol. 2.

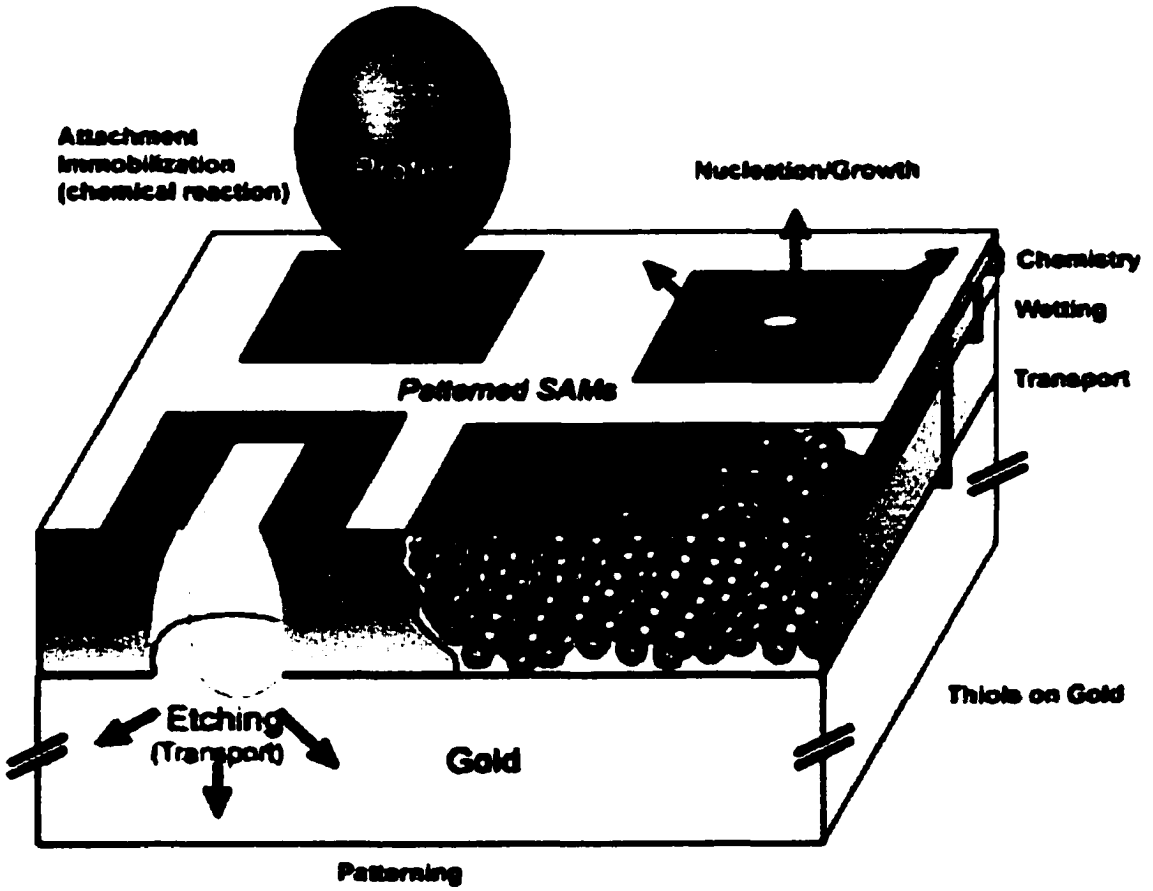

Figure 1.1: Cartoon depicting the potential applications of SAMs

Chapter 2

Background: A Brief Overview of Self-Assembled Monolayers

2.1 Introduction

In recent years, there has been an increasing interest in the study and development of molecularly thin films such as self-assembled monolayers (SAMs) and Langmuir-Blodgett films. SAMs provide a unique way of altering just the surface properties of a material, by modifying the terminal functional groups displayed on the surface without altering or affecting the bulk properties of the material. The ability to control the structure and properties of the SAMs gives rise to several technological applications such as protective coatings,[1] lubrication layers,[2] membranes for chemical and biochemical sensors,[3-7] templates for crystal growth,[8] fabrication of nanoparticles,[9-11,12] micropatterning,[13,14] and for molecularly thin transistors,[15] to name a few.

Self-assembled (SA) monolayers are molecular assemblies that are formed by spontaneous adsorption of the surfactant molecules (amphiphiles), present either in solution or vapor phase, on to the surface of an appropriate substrate. Three classical types of SA monolayers are: (i) trichloro or trialkoxy silanes on hydroxylated surfaces[16-23] (ii) alkanethiols on gold, copper or silver surfaces[18,1,24-27] (iii) long chain carboxylic acids on aluminum oxide surfaces.[28,29] The quality of the SA monolayer depends, including many other factors, on the head group, the hydrocarbon chain length,[1,30,31,20] the terminal functional group, solvent used,[32] amount of water present in the solvent[17] and temperature of preparation.[31,33,34,21]

The structure and properties of the organized molecular assemblies such as SA monolayers and LB films have been widely investigated. Extensive efforts have been made to study and understand completely the formation mechanisms and structural features. Various techniques have been employed like contact angle measurements,[25,35,24] Fourirer transform infrared spectroscopy (FTIR),[36,30,26,1] ellipsometer, x-ray reflectivity,[37] x-ray photoelectron spectroscopy (XPS),[37-41] atomic force microscopy (AFM)[17,33,34,42] have been used to study and understand completely the formation mechanism and structural features. In this chapter, a brief overview on self-assembled monolayers is given in the following sections.

2.2 Interactions involved in the formation of Self-Assembled Monolayers

Self-assembled monolayers are molecular assemblies that are formed spontaneously when certain surfactant molecules chemisorb from solution onto an appropriate solid substrate and form ordered assemblies on it. The first study on SAMs was reported in 1947 by Zisman,[43] who observed that dilute solutions of eicosyl alcohol in n-hexadecane did not wet the walls of the Pyrex, glass-stoppered, flask. This was an indication that the surface of the flask had been modified. However, it wasn't until the pioneering work done by Sagiv and his coworkers,[28,44,45,29,16] who studied OTS adsorption onto hydroxylated surfaces, that interest in SAMs exploded.

The formation of these SAMs is driven primarily by three energetic contributions.[46] First among these is the strong interaction of the surfactant head group with the adsorbing substrate resulting in chemisorption, the most exothermic process. These very strong molecular-substrate interactions result in an apparent pinning of the

head group to a specific site on the surface of the substrate. These interactions can be one of the following types:

- A covalent Si-O linkage in the case of alkyltrichlorosilanes on hydroxylated surfaces.
- A covalent, but slightly polar, Au-S bond in the case of alkyl thiols on gold
- An ionic $-CO_2^-Ag^+$ bond in the case of carboxylic acids on AgO/Ag or Al_2O_3.

The energy associated with chemisorption is of the order of tens of kcal/mol. As a result of the exothermic head group-substrate interactions, molecules try to occupy every available binding site on the solid surface, and in the process they push together molecules that are already on the surface. The second of these energy contributions is the van der Waals interaction of the alkyl chain, which is of the order of a few (<10) kcal/mole. These interactions play an important role in the orientation and in an indirect way on the packing of the surfactant molecules. The last of these energy contributions is due to the surfactant's terminal functionality, which in the case of a simple alkyl chain is just a methyl (CH_3) group. These groups are thermally disordered at room temperature. The energy (~0.7 kcal/mol) associated with this interaction is much smaller than the other contributions (of the order of a few kTs, k: Boltzman's constant; T: Absolute temperature). These forces are schematically represented in figure 2.1.

2.3 Mechanism of formation of siloxane self Assembled monolayers

Mechanism of formation of siloxane self-assembled monolayer is well understood, and it involves three steps. In the first step, the head group, consisting of either a trichlorosilane or a trialkoxy silane, undergoes hydrolysis in the bulk of the solution or at the interface of the substrate and the head group converts into hydroxyl

groups. The hydrolyzed surfactant molecules diffuse from the solution bulk phase to the interface of the substrate, and finally these hydrolyzed head groups react with the hydroxyl groups of the substrate to form stable monolayers. The molecules transported through the surface can undergo surface diffusion, depending on the presence of thin water layer on the substrate, and form a well packed uniform layer. The process is schematically shown in figure 2.2.

The formation of a siloxane self-assembled monolayers depend on several factors such as water in the solvent, which plays a prominent role in the bulk hydrolysis, water layer present (hydration state) on the substrate (will assist for surface hydrolysis and surface diffusion of the adsorbed molecules), solvent used, temperature, deposition time, hydrocarbon chain length, and terminal functional group. Thus, even though the formation of siloxane SAMs might be easy to prepare, it is very difficult to control the structure, orientation and morphology of the siloxane SAMs as they depend on several controlling parameters, which are sometimes difficult to control. Several researchers have looked into how these various parameters affect the final structure of the SAM formed, and we will look into some of the aspects in the following sections.

2.4 Effect of Solvent

Solvent plays a crucial role in the solution-based SAM formation. If we consider the adsorption of surfactant molecules from the solution to be of a Langmuir-type sorption, i.e., site specific, then the solvent molecules and the adsorbate (surfactant) molecules compete to adsorb on the surface of the substrate. Ideally speaking, the adsorption processes should not depend on the solvent used as long as the solvent is non-

competing with the surfactant molecules. However, due to various interactions ranging from strong polar-polar to weak van der waals interactions that are present between molecules, the solvent does play some role on the final SAM formation.

Depending on the competing nature of the solvent the kinetics of the SAM formation and also on the final structure of the SAM varies. Kessel et al have shown that it is difficult to form a uniform OTS monolayer using a polar, reactive solvent like THF (tetrahydrofuran).[47] THF being able to adsorb with the surface silanols, competes with the OTS molecules and thus disabling OTS molecules to form a uniform monolayer. However, with other non-competing solvents such as $CHCl_3$ and CCl_4, they were able to obtain a uniform monolayer. McGovern et al[48] have shown that the nature of the solvent used in the adsorption process has an effect on the time of formation, as well as the structure of the monolayer. The authors attributed the observed differences to the ability of the solvent to extract surface water into the bulk phase, where the OTS molecules undergo hydrolysis. In addition, when they used dioxane (a solvent with excess water) the authors observed that OTS molecules undergo extensive hydrolysis, which facilitates polymerization of the intermediate silanetriol, directly in competition with the surface adsorption of this triol.

Similar dependence on structure and monolayer formation is seen on the solvent used in the preparation of APS monolayers. In the formation of mixed monolayers, Fan et al have shown that the ratio of the monomer-surfactant molecules adsorbing on to the substrate can be controlled by controlling the solvent properties.

2.5 Effect of water content in solvent

As discussed in the mechanism of silane-based SAM formation, water acts an initiator in hydrolysis of trichloro and trialkoxy head groups. So the presence of excess or deficiency of water content affects the rate and also the structure of the SAM formed. Presence of excess water in the bulk solution results in the formation of oligomers in the bulk, and these oligomers diffuse to the interface of the substrate, instead of only monomers diffusing and reacting with the substrate. Oligomers diffusing to the surface results in a non-uniform structure. When the adsorption occurs from a low water content solvent, the surfactant species are predominantly monomeric. On the other hand, dehydrated solvent effectively inhibits the hydrolysis process, thus increasing the time for the surfactant molecules to form a uniform layer. The monolayer obtained is also not good because of the insufficient hydrolysis of the monomers. OTS formed a uniform, condensed layer if hydrated hexadecane is used, and formed a less crystalline structure if non-hydrated hexadecane is used.

2.6 Effect of Surface Hydration

The effect of the water present on the substrate has been investigated by several research groups[49-52]. Angst and Simmons[49] have also reported that the amount of water on the substrate surface is vital for the formation of a complete monolayer. They are able to obtain a tightly packed monolayer on a fully hydrated silicon wafer, whereas reaction with a dry silicon wafer gave a disordered monolayer with low surface coverage. In a study by Le Grange et al,[50] it is found that the OTS coverage increased with increase in hydration of the silica surface. However, the authors also report that a fully hydrated

surface is not required for complete coverage of the substrate indicating that not every silane group is bonded to the surface. Tripp et al[52] showed that the use of super saturated fumed silica as the substrate resulted in the formation of a polymerized OTS layer. Tripp et al[52,51] also showed that the in the case of dehydrated substrates they observed the absorption of bulk water, (i.e.) water dissolved in the solvent, by the substrate surface. Finklea et al report a study of OTS SAMs formation on gold, an oxide free surface, suggesting again that OTS SAMs can be obtained on a hydroxyl free surface. In a recent study by Allara et al. the authors proved that organosilane SAMs prepared on vastly different surfaces like hydrolyzed gold and oxidized silicon have similar IR spectra, and thus the SAM structure is the same irrespective of the presence or absence of siloxy links at the surface. The above studies seem to suggest an adsorption mechanism in which the first step in the adsorption of the SAM is adsorption of a water film. This is followed by the physisorption of the silane to this water film. The last step in this process is the chemical reaction on the water film linking the silanes together and anchoring the net to the film.

The mechanism of the formation at molecular level also varied on the amount of water present on the substrate. Kumar et al have shown that on a dry dehydrated substrate, OTS formed small dot like structures, and formed large fractal like structures on fully hydrated substrates, for low deposition times. The reason for this is because water assists in the lateral diffusion of the adsorbed molecules. On a dry surface, once the surfactant molecules are chemisorbed to the substrate, it becomes difficult for the molecules to migrate laterally in 2D to form fractal like structures. The AFM images of OTS monolayers on different surfaces, with respect to water content on the surface, are

shown in figure 2.3. Another way of looking at the picture is, at time t=0, the molecules near the surface of the substrate randomly anchor to the substrate. However, for the subsequent molecules coming to the surface have a choice. They can either attach to the nearest active site available for anchoring or migrate to the location where there are already anchored molecules (or molecule islands). Migration to the near by islands is facilitated by interchain interactions between the molecules, thus reducing the free energy of the system. Presence of water on the surface facilitates this surface migration.

2.7 Effect of Temperature on Mechanism of Formation

Temperature, too, sometimes plays a key role on the type and mechanism of SAM formation. Self-assembled monolayers can be initiated by three distinct mechanisms: island growth at low temperature, homogeneous growth at high temperature and a mixed regime at intermediate temperatures. The effects of temperature can be drawn from analogy between the 3D matter and 2D layers. In 2D (Langmuir film), similar to 3D, depending on the level of interaction between the neighboring molecules, molecules exist in gaseous state, liquid expanded (LE) state, liquid condensed (LC) state or liquid solid (LS) state. A typical π-A isotherm, showing all the states, of an OTS monolayer on water subphase is shown in figure 2.4.

By varying temperature, the state of the matter can be changed. At high temperatures, molecules tend to separate and go farther apart decreasing the enthalpy or intermolecular interactions. But, however, at high temperatures, the molecules have higher entropy or degrees of freedom to exist. Self-assembled monolayers at high temperatures show uniform growth due to decrease in intermolecular interactions and

increase in entropy. At low temperatures, due to enhancement in intermolecular interactions, the molecules form clusters, and show island-like growth structures. At intermediate temperatures they show mixed regime. Carraro et al have shown this phenomenon for OTS monolayers. The effect of temperature on growth mechanism of OTS monolayer was studied using AFM and is shown in Figuure 2.5 OTS molecules showed island-like growth for T<16°C (triple point or transition temperature), where the molecules existed in liquid condensed (LC)-gas phase equilibrium. OTS exhibited homogeneous growth for T>40°C, where the molecules existed in LC-LE phase equilibrium, and mixed regime at intermediate temperatures, where the OTS molecules existed in LE phase. The temperature range for these growth regimes, of course, depends on the hydrocarbon chain length and terminal functional group. Rondolez et al have predicted a 3.5 °C increase in the critical temperature for phase transition an additional methylene group in the carbon chain.

2.8 References

1. Jennings, G. K.; Munro, J. C.; Yong, T.-H.; Laibinis, P. E. *Langmuir* **1998**, *14*, 6130-6139.

2. Gennes, P. G. d. *Rev. Mod. Phys.* **1985**, *57*, 827.

3. Lahiri, J.; Isaacs, L.; Grzybowski, B.; D.Carbeck, J.; Whitesides, G. M. *Langmuir* **1999**, *15*, 7186-7198.

4. Ottova, A.; Tvarozek, V.; Racek, J.; Sabo, J.; Ziegler, W.; Hianik, T.; Tein, H. T. **1996**.

5. Piletsky, S. A.; Wulff, G.; Piletskaya, E. V.; Panasyuk, T. L.; Elskaya, A. V.; Levi, R.; Karube, I. *Macromolecules* **1998**, *31*, 2137-2140.

6. Rubinstein, I.; Steinberg, S.; Tor, Y.; Shanzer, A.; Sagiv, J. *Nature* **1988**, *332*, 426-429.

7. Schierbaum, K. D.; Weiss, T.; Velzen, E. U. T. v.; Engbersen, J. F. J.; Reinhoudt, D. N.; Gopel, W. *Science* **1994**, *265*, 1413-1415.

8. Lockhead, M. J.; Letellier, S. R.; Vogel, V. *J. Phys. Chem. B* **1997**, *101*, 10821-10827.

9. Jiang, P.; Liu, Z.-F.; Cai, S.-M. *Surface Science* **2001**, *486*, L507-L512.

10. Li, L. S.; Lianhua Qu, R. L.; 1, X. P.; Zhao, Y.; Li, T. J. *Thin Solid Films* **1998**, *327–329*, 408–411.

11. Li, L. S.; Jin, J.; Tian, Y. Q.; Zhao, Y. Y.; Li, T. J.; Du, Z. L.; Ma, G. H.; Zheng, N. *Supramolecular Science* **1998**, *5*, 475-478.

12. Zhang, L.; Shen, G.; Pan, Z.; Lu, Z. *Materials Chemistry and Physics* **1998**, *55*, 160-163.

13. Sugimura, H.; Ushiyama, K.; Hozumi, A.; Takai, O. *Langmuir* **2000**, *16*, 885-888.

14. Whitesides, G. M.; Aizenberg, J.; Black, A. J. *nature* **1998**, *394*, 868-871.

15. Schon, J. H.; Bao, Z. *Applied Physics Letters* **2002**, *80*, 847-849.

16. Sagiv, J. *Journal of American chemical Society* **1980**, 92-98.

17. Kumar, N.; Malderelli, C.; Steiner, C.; Couzis, A. *Langmuir* **2001**, *17*, 7789-7797.

18. Sabatani, E.; Rubinstein, I.; Maoz, R.; Sagiv, J. *J. Electroanal. Chem.* **1987**, *219*, 365-371.

19. Angst, D. L.; Simmons, G. W. *Langmuir* **1991**, *7*, 2236-2242.

20. Bierbaum, K.; Grunze, M.; Basaki, A. A.; Chi, L. F.; Schrepp, W.; Fuchs, H. *Langmuir* **1995**, *11*, 2143-2150.

21. Parikh, A. N.; Allara, D. L.; Azouz, I. B.; Rondelez, F. *The Journal of Physical Chemistry* **1994**, *98*, 7577-7590.

22. Silberzan, P.; Leger, L.; Ausserre, D.; Benattar, J. J. *Langmuir* **1991**, *7*, 1647-1651.

23. Wasserman, S. R.; Tao, Y.-T.; Whitesides, G. M. *Langmuir* **1989**, *5*, 1074-1087.

24. Creager, S. E.; Clarke, J. *Langmuir* **1994**, *10*, 3675-3683.

25. Bain, C. D.; Whitesides, G. M. *Langmuir* **1989**, *5*, 1370-1378.

26. Cheng, S. S.; Scherson, D. A.; Sukenik, C. N. *Langmuir* **1995**, *11*, 1190-1195.

27. Wang, J.; Frostman, L. M.; Ward, M. D. *Journal of Physical Chemistry* **1992**, *96*, 5224-5228.

28. Sagiv, J.; Iscovici, R.; Gun, J. *J of colloid and interface science* **1984**, *101*, 201-213.

29. Maoz, R.; Sagiv, J. *J. of Colloid and interface science* **1984**, *100*, 465-496.

30. Iimura, K.-i.; Nakajima, Y.; Kato, T. *Thin Solid Films* **2000**, *379*, 230-239.

31. Brzoska, J. B.; Azouz, I. B.; Rondelez, F. *Langmuir* **1994**, *10*, 4367-4373.

32. Kallury, K. M. R.; Macdonald, P. M.; Thompson, M. *Langmuir* **1994**, *10*, 492-499.

33. Carraro, C.; Yauw, O. W.; Sung, M. M.; Maboudian, R. *The Journal of Physical Chemistry B* **1998**, *102*, 4441-4445.

34. Carraro, C.; Yauw, O. W.; Sung, M. M.; Maboudian, R.; Kim, Y. *Journal of Physical Chemistry B* **2000**, *104*, 1556-1559.

35. Bain, C. D.; Whitesides, G. M. *Langmuir* **1989**, *5*, 1370-1378.

36. Kumar, V.; Krishnan, S.; Steiner, C.; Maldarelli, C.; Couzis, A. *J. Phys. Chem B* **1998**, *102*, 5152-5159.

37. Brandow, S. L.; Chen, M. S.; Aggarwal, R.; Dulcey, C. S.; Calvert, J. M.; Dressick, W. J. *Langmuir* **1999**, *15*, 5429-5432.

38. Dulcey, W. J. D. C. S.; Chen, M.-S.; Calvert, J. M. *Thin Solid Films* **1996**, *284-285*, 568-572.

39. Heiney, P. A.; Gruneberg, K.; Fang, J.; Dulcey, C.; Sashidhar, R. *Langmuir* **2000**, *16*, 2651-2657.

40. Hooper, A. E.; Werho, D.; Hopson, T.; Palmer, O. *Surface and Interface Analysis* **2001**, *31*, 809-814.

41. Sieval, A. B.; Linke, R.; Heij, G.; Meijer, G.; Zuilhof, H.; Sudholter, E. J. R. *Langmuir* **2001**, *17*, 7554-7559.

42. Doudevski, I.; Hayes, W. A.; Woodward, J. T.; Schwartz, D. K. *Colloids and Surfaces: A Physicochemical and Engineering Aspects* **2000**, *174*, 233-243.

43. Bigelow, W. C.; Pickett, D. L.; Zisman, W. A. *J. Colloid Interface Science* **1946**, *1*, 513.

44. Sagiv, J.; Gun, J. *J of Colloid and interface science* **1986**, *112*, 457-472.

45. Sagiv, J.; Cohen, S. R.; Naaman, R. *J. of physical chemistry* **1986**, *90*, 3054-3056.

46. Ulman, A. *J. of Materials Education* , *11*, 207-279.

47. Kessel, C. R. *Langmuir* **1991**, *7*, 532-538.

48. McGovern, M. E.; Kallury, K. M. R.; Thompson, M. *Langmuir* **1994**, *10*, 3607-3614.

49. Angst, D. L.; Simmons, G. W. *Langmuir* **1991**, *7*, 2236-2242.

50. Grange, J. D. L.; Markham, J. L. *Langmuir* **1993**, *9*, 1749-1753.

51. Tripp, C. P.; Hair, M. L. *Langmuir* **1995**, *11*, 1215-1219.

52. Tripp, C. P.; Hair, M. L. *Langmuir* **1992**, *8*, 1120-1126.

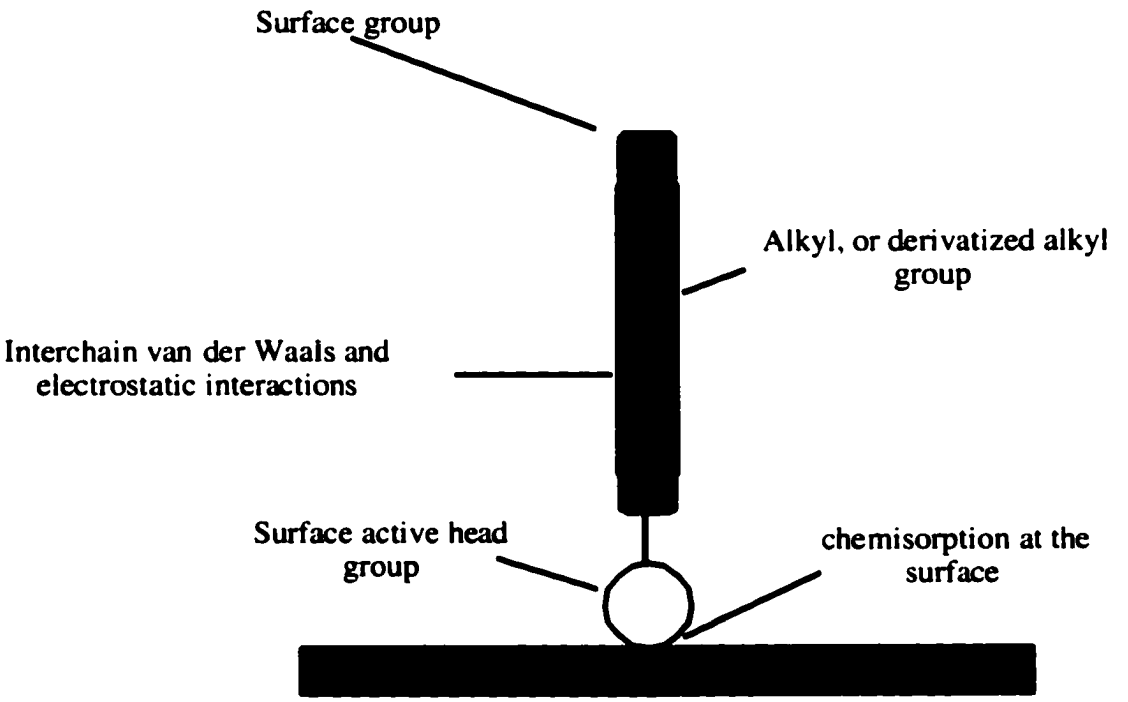

Figure 2.1: Cartoon of a surfactant molecule showing all the forces involved in the formation of a self-assembled monolayer

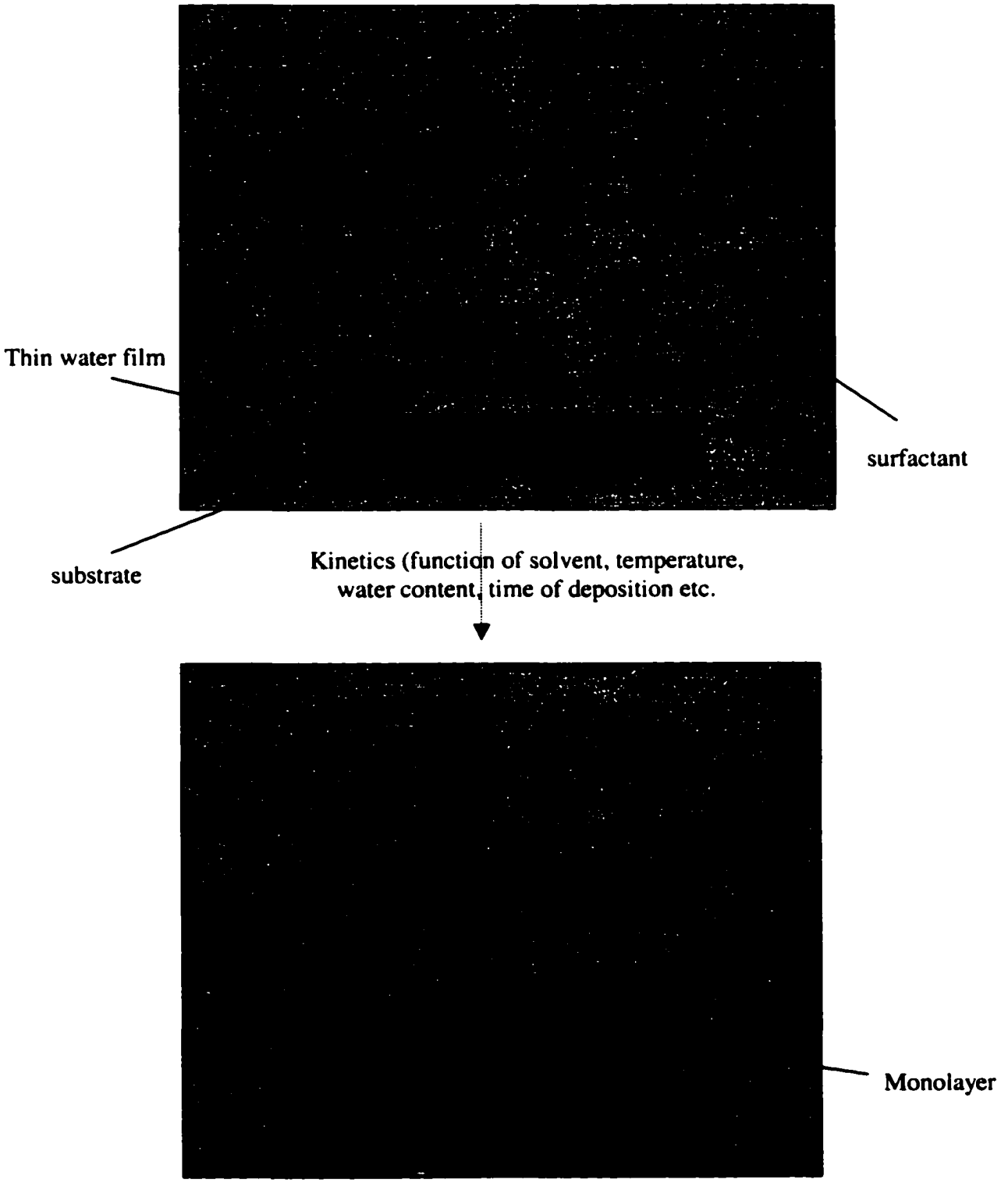

Figure 2.2: Cartoon depicting the mechanism of formation of self-assembled monolayer

(a) OTS monolayer on hydrated substrate

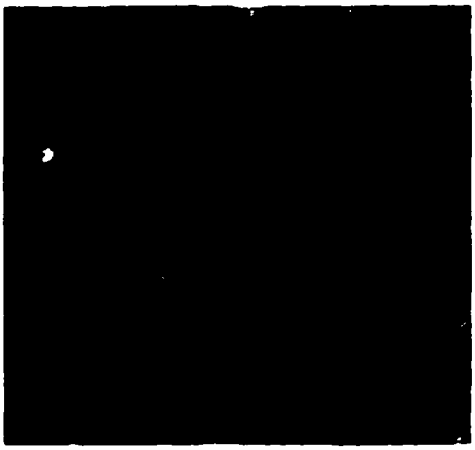

(b) OTS monolayer on partially hydrated substrate

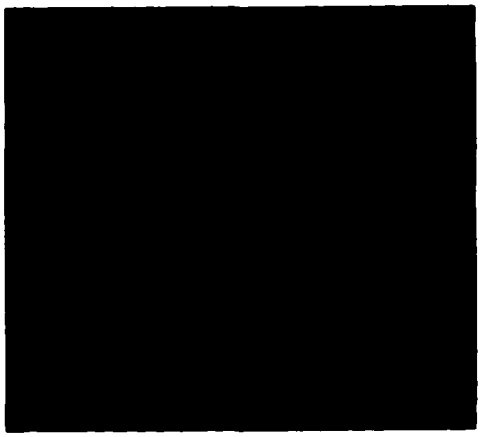

(c) OTS monolayer on dehydrated substrate

Figure 2.3: Effect of surface hydration of monolayer formation (a) on hydrated substrate OTS forms island-like fractal structures (b) on partailly hydrated substrate island size decreases and (c) on dehydrated substrate only dot-like structure are seen (courtesy Nitin et al)

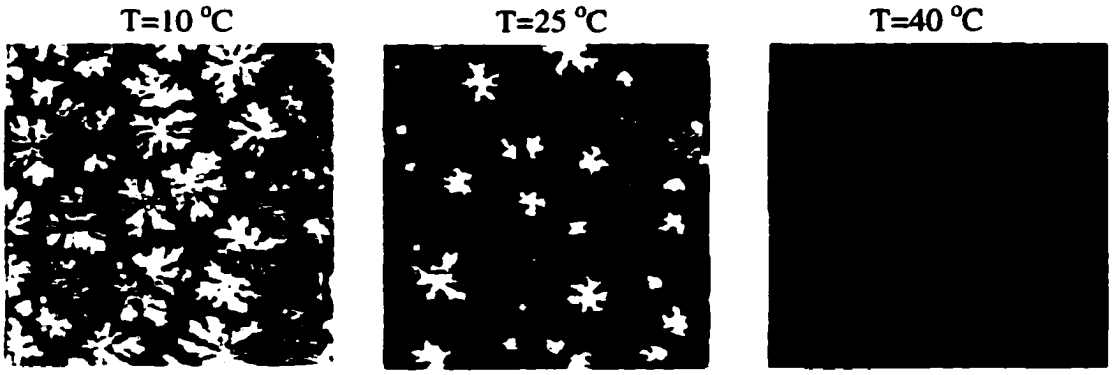

Figure 2.5: Effect of temperature on mechanism of formation of monolayers: OTS showing three different growth patterns depending on temperature of deposition (a) at low temperatures, below critical temperature, forms island-like structures (b) at T= 25 °C, forms less islands (c) above critical temperature, shows homogeneous growth pattern (courtesy Carraro et al)

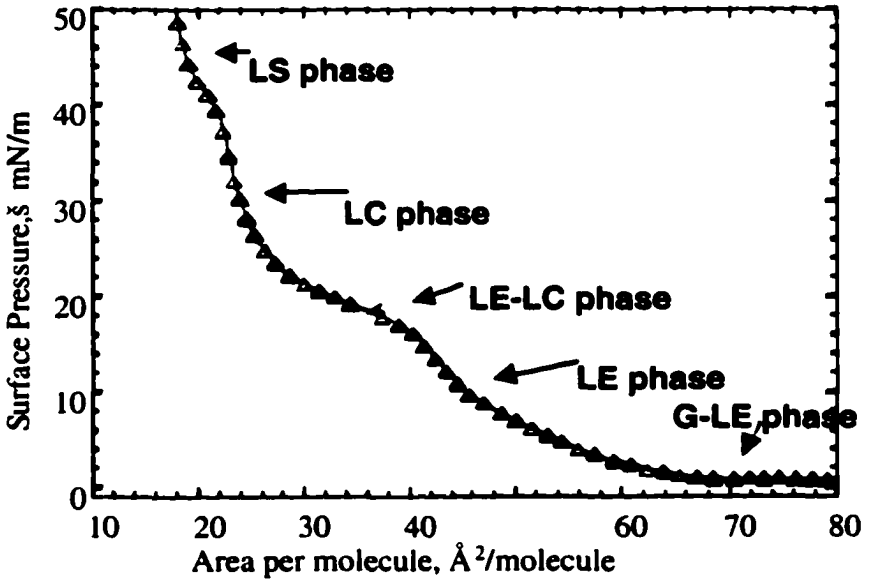

Figure 2.4: π-A isotherm of OTS molecules exhibiting different phases

Chapter 3

Effect of Chain Length and Terminal Functional Group on Structure, Morphology, Mechanism of Formation and Packing Density of the Self-Assembled Monolayers

3.1 Introduction

In the recent years, it has been found that SA monolayers with long chain hydrocarbon molecules form a very ordered and densely packed structures, with the methylene groups aligned mostly in an all trans conformation.[1,2] It has been also observed that the crystallinity in the structure of the monolayer formed increased with the increase in the hydrocarbon chain length. It is believed that reason for the increased crystallinity (or packing density) in the structure of the monolayer with increase in hydrocarbon chain length is because of the energetically favorable weak, intermolecular chain- chain interactions. Whereas, it has been observed that, short chain molecules formed disorder structures. The disorder in the monolayers is attributed to increase in the gauche conformations. Chain length also affects the mechanism of the formation of monolayers. For long chain molecules, the SA monolayers grow via islands (deposition nulceation and aggragation), in contrast, the short chain molecules show a uniform growth with no island formation.[3]

Iimura et al have studied SA monolayers of trichlorosilanes of varying hydrocarbon chain lengths using FTIR spectroscopy as a function of temperature.[1] In their studies they found that the silanes with chain length 16 or less always existed in

liquid state (disordered state) for all the temperatures above 0^0 C. They have attributed that the temperature at which the monolayers were prepared was above the phase transition temperature. In analogy with the 3-dimensional matter, the monolayer existed as crystalline (solid state) for temperatures below the critical transition temperature and, existed as disordered, liquid state for temperatures above the transition temperature. Independently, Laibinis et al in their studies with SA monolayers of alkanethiols on gold have noticed that the disorder in the structure increased with decrease in hydrocarbon chain length, when prepared at the same temperature.[2]

The packing density or the molecular coverage of the monolayers would decrease with increase in disorder. The disorder, in a way, means an increase in entropy, which in turn means that the molecules can exist in more possible states available for the molecule with in the constraints. For example, let us take a molecule freely dangling in space. This test molecule can be present, at a particular instant of time, in any one of the possible states available for the molecule in the 3-D space. However, now, if we consider the case where the test molecule is tethered at one end to the surface, with no surrounding molecules around it, then the number possible states, in which the molecule can be present at any particular instant, will be lesser than the freely dangling molecule. The decrease in the number of available states is because of the constraint induced in the system by tethering the molecule at one end. Based on similar arguments, the number of possible states available for the test molecule, tethered at one end and also surrounded by molecules, will be lesser than when the test molecule is only tethered, with no surrounding molecules. Of course, the above argument holds only if the surrounding molecules are present with in the radius of gyration of the test molecule (for a polymer)

or with in the distance of the chain length of the molecule (for molecules which do not fold). So, increase in disorder means increase in entropy, which in turn means, increase in the number of available states for the molecule to be oriented or in a way decrease in the packing density.

In this chapter, we will discuss the effects of chain length and terminal functional group of surfactant molecules on the structure, morphology, mechanism of formation and packing density of the self-assembled monolayers formed by these surfactant molecules. We have considered octadecyltrichlorosilane (OTS, 18 carbon chain with methyl termination), undecyltrichlorosilane (UTS, 11 carbon chain with methyl termination), 11-cyano undecyltrimethoxysilane (CUTMS, 11 carbon chain with cyano (C≡N) termination) and aminopropyltrimethoxysilane (APS, 3 carbon chain with amine (NH_2) termination). The structures of these molecules obtained from Chem-3D software are shown in figure 3.1.

3.2 Experimental Section

3.2.1 Materials

11-cyanoundecyltrimethoxysilane (CUTMS) is purchased from Gelest, Undecyltrichlorosilane (UTS) is purchased from United Chemical Technologies and Octadecyltrichlorosilane (OTS, 95% purity) and Aminopropyltrimethoxysilane (APS) are obtained from Sigma Aldrich Co. Chloroform, Toluene and Acetone are purchased from Fisher Scientific. Carbon tetrachloride and Hexadecane of anhydrous grade are purchased from Sigma Aldrich. Silicon wafers used are obtained from Montco Silicon Technologies (Pennsylvania). The silicon wafers used in our experiments are of thickness-450-500μm,

double sided polished and of orientation (111). Silicon Internal Reflection Elements (dimensions: 50x10x3 mm and orientation (111)) used for Infrared Spectroscopy are obtained from Harrick Scientific. Concentrated sulfuric acid is obtained from Fisher Scientific and the Nochromix crystals used for cleaning purposes is obtained from Godax Laboratories. All Chemicals are used as purchased without any further purification except Hexadecane, which is saturated with water by flowing water vapor under a hood for about 48 hours. Deionised water with a resistivity of 18MΩ cm from a Millipore System is used in all our experiments.

3.2.2 Cleaning Protocol

Silicon crystals are thoroughly cleaned before used. Rigorous cleaning is performed on the crystals that are reused just to make sure that the surface is clean from organic contamination. The crystals are first sonicated in a freshly prepared Nochromix solution for 30min. The Nochromix solution is prepared by dissolving the Nochromix crystals in sulfuric acid and stirring the solution until it became clear. The Nochromix treatment is followed by rinsing with water and subsequent sonication in water for 30 min. Then the crystals are further cleaned using Plasma Cleaner (Harrick Scientific Corp., model PDC-32G). The Plasma treatment is performed under argon environment at low pressures. After the Plasma treatment, the crystals are again cleaned with Nochromix and deionised water. Same procedure is followed for Silicon wafers also with the exception of Plasma treatment. Wetting tests (contact angle measurments) are performed, to make sure that the substrates (wafers or crystals) are clean from any contamination, before proceeding with the deposition experiments.

3.2.3 Monolayer Preparation

The cleaned substrates (crystals or wafer) are deposited in a solvent mixture of known concentration for a fixed amount of time. After the fixed amount of time, the substrates are thoroughly rinsed with chloroform to remove the physisorbed molecules from the substrate surface. The substrate with monolayer on it is taken from the solvent and dried under dry N_2. Then the monolayer is subjected to various complementary surface analytical techniques such as contact angle goniometer for contact angle measurements, ellipsometer for thickness measurement, FTIR for structure and orientation of the monolayer measurement and AFM for measurement of morphology of the monolayer formed. Figure 3.2 shows the schematic of the formation of a typical monolayer.

3.2.3.1 OTS Monolayer

For OTS monolayer, a mixture of hexadecane, carbontetrachloride and chloroform in the ratio of 30:5:3 by volume, respectively, is used in the OTS solution preparation. The substrate is deposited for 30 min in the above-prepared solution.

3.2.3.2 UTS Monolayer

For UTS monolayers, the concentration of the UTS silane solution is maintained between 4-5mM. Solvents used varied from Chloroform, Toluene and Hexadecane. The deposition time is varied from minutes to days. A stable uniform monolayer formed after about 8 hours.

3.2.3.3 CUTMS Monolayer

For CUTMS monolayers, the concentration of the CUTMS silane solution is maintained between 4-5mM. Solvents used varied from Chloroform, Toluene and

Hexadecane. The deposition time is varied from minutes to days. A stable uniform monolayer formed after 24 hours.

3.2.3.4 APS Monolayer

The concentration of surfactant is maintained at 1% by weight of solvent in the preparation of APS monolayers. Toluene is used as solvent.

3.2.3.5 LB Film of Stearic Acid

A 100μl of 1.34mg/ml of a solution of Stearic acid in Chloroform is spread on a subphase (deionised, Millipore water, 18 MΩ) maintained at 20^{0}C and a pH of 2.0 (by adding HCl) in a KSV 2000 dual compartment LB trough. The solution is allowed to stabilize for about 15min for the chloroform to evaporate. The trough barriers compressed the surface until the surface pressure reached the desired value of 30mN/m, at which time the transfer of the LB monolayer on to an OTS coated (hydrophobic) silicon crystal is performed. At that surface pressure, before transferring, the stearic acid layer is allowed to stabilize for another 30min to minimize any fluctuations. The transfer speed is maintained at 2.5mm/min. The structure and orientation information of the transferred film is then obtained from IR measurements.

3.2.4 Contact Angle Measurements

Contact Angle goniometer is used to characterize the monolayers prepared. A 2 μl drop of deioinsed water is placed on the sample surface and the contact angle is measured with in 2 minutes after the drop is placed to reduce errors caused by evaporation of water drop. The measurements are taken at different locations of the sample. All the values reported are an average of 5-6 measurements.

3.2.5 Ellipsometry

The thickness information of the monolayer is obtained from Variable Angle Null Ellipsometer (Rudolph Instruments). A He-Ne laser beam, corresponding to wavelength of 632.8nm, is incident on the substrate. The thickness and refractive index of the monolayer is evaluated from the changes in the polarization and the reflectivity of the incident parallel and perpendicular polarized light beams. Principally, the ellipsometer is supposed to evaluate both the refractive index and thickness of the thin film simultaneously, but due to the instrument limitations in obtaining data for thin films, the refractive index of the film is assumed and thickness is obtained. Organic films have a refractive index of about 1.46, and we have assumed this value as the refractive index for all our monolayers.

3.2.6 IR Measurements

IR spectra are measured using a Bio-Rad FTS 175 spectrometer. Spectra are collected as interferograms with a resolution of $4cm^{-1}$ and Fourier transformed with triangular apodization. Monolayer spectra are obtained in Attenuated Total Internal Reflection mode (ATR) with scans averaging between 100-200. Spectra of liquid samples are obtained in transmission mode using NaCl windows. For quantitative analysis, the peaks are fit with a Lorentzian function. The fit is done using an in-built software of the Bio-Rad. The area under the concerned peak is taken as the Absorbance value. However, the readers have to be cautioned that the Absorbance Value (or peak area) is very sensitive to

the type of fit used and baseline selection. For consistency in the results, one has to maintain the same procedures through out the quantitative analysis.

3.2.7 AFM Imaging

Atomic force microscopy images are obtained using Nanoscope III (Digital instruments, Inc,). Silicon nitride sharpened tips with a force constants of 0.58N/m, (purchased from Digital Instruments, Inc.) are used for height and friction images in contact mode. A normal force of approximately 116nN is used in the contact mode experiments. Tapping mode images are obtained using silicon tips. At least three images are acquired for each sample at various locations. Height and friction differences between the various phases on the samples are obtained by taking cross sections at random locations. The surface area coverage is calculated using the bearing analysis mode of AFM software.

3.3 Results and Discussions

3.3.1 Structure and Properties of the Monolayers

Fourier Transform Infrared Spectroscopy (FTIR) in attenuated total internal reflection (ATR) mode is used to study the structural and orientational properties of the monolayers. A typical spectrum of various monolayers of interest, formed on a silicon substrate, is shown in Figure 3.3. (Clean silicon substrate is used a background in obtaining the spectrum). Some of the important vibrational modes pertaining to methyl and methylene symmetric and asymmetric stretching modes for the various monolayers

are shown in Table 3.1. Asymmetric stretching mode of the methylene group reveals a great deal of information on the local molecular order and packing.[4,5] How this information is used to get the packing density and coverage is discussed later. One interesting aspect is, lower the wavenumber of the Methylene asymmetric stretching mode, the higher the crystallinity (order) in the corresponding monolayer and higher the wavenumber, greater is the disorder in the corresponding monolayer.

OTS monolayer, with CH_2 asymmetric stretching peak at 2919 cm^{-1}, forms a well-ordered, crystalline structure and the crystallinity decreases gradually with UTS, CUTMS and APS, respectively. UTS monolayer shows the asymmetric stretching peak at 2924 cm^{-1} indicating that it forms a disordered monolayer. The difference between the OTS and UTS is attributed to the differences in the chain length of the monolayers. Interchain van der waals interactions become prominent in the OTS molecules, consisting of 18 carbon chain. The order in the molecules depends on the hydrocarbon chain length. The molecules try to maximize the interaction between the neighboring molecules in the process of minimizing the over all free energy of the system. As the hydrocarbon chain length increases, because of the increased hydrophobicity, the molecules align perpendicular to the substrate surface decreasing the energetically unfavorable hydrophobic-hydrophilic interactions. This increases the packing density of the long chain carbon molecules. This, on the other hand, also increases the energetically favorable hydrophobic-hydrophobic interactions. However, the molecules pay an entropic penalty because of the order in the system. So the difference between the enthalpic and entropic energies determines the final structure and order of the monolayers. The system tries to minimize the Gibbs Free Energy of the system.

$$\Delta G = \Delta H - T\Delta S$$

These hydrophobic-hydrophobic (HH) interactions are also present in the short chain molecules such as UTS also. However, energy gain because of the favorable HH interactions for short chains is comparatively less when compared to long chains because of more number of interactions. So, to minimize the free energy of the system, the molecules decrease the entropic penalty by increasing disorder. Iimura et al have studied the effect of chain length on the molecular crystallinity.[1] In their studies, they reported a liquid-like or a disordered structure for chain lengths less than 16 prepared at temperatures above 0^0 C. Laibinis et al found that the disorder of the molecular structure increased with decrease in chain length in their studies with alkanethiols on copper.[2] Hence, UTS, with an 11-carbon chain, forms a disordered structure on the substrate.

The disorder in the structure increases as we move from UTS to CUTMS monolayers. The difference in the structure between these two monolayers is attributed to the difference in the terminal functional group. Cyano group, being a more polar group than methyl, shows higher affinity towards the hydrophilic substrate. This inclination in the tethered CUTMS molecule towards the substrate increases the disorder in the monolayer. APS molecule, a short chain carbon with a polar amino terminal functional group, on similar arguments, forms the most liquid-like or disordered monolayer structure and is clearly evident from the asymmetric methylene stretching frequency at 2928 cm^{-1}. In the case of APS monolayer, amino-substrate interactions play a prominent role in the final monolayer structure.

Column 2 of table 3.1 shows the contact angle measurements of water on these various monolayers. OTS and UTS exhibit contact angles of 110° and 105°, respectively,

indicating that the monolayers are hydrophobic, exposing primarily the methyl groups to the monolayer surface. The hydrophilicity of the monolayers increased with CUTMS and APS, with the monolayers showing contact angles of 55° and 35°, respectively.

Column 3 of table 3.1 shows the thickness of the monolayers obtained using ellipsometer. The thickness values agreed reasonably with the theoretical thickness of the end to end distance of the monomer molecules calculated using Chem 3D software, except for the case of APS layer. The thickness of the APS monolayer varied from 8-18 A° depending on the method of preparation, whereas the theoretical thickness calculated is about 8A°, indicating that APS is forming multilayers. More evidence for the formation of multilayers by APS is shown in the next section.

3.3.2 Packing density

How does structure and orientation of the monolayer effect the packing density or coverage density? Depending on whether the monomer molecule is lying flat to the substrate, or aligned perpendicular to the substrate or inclined at some random angle to the substrate, the packing density of the monolayer changes. For instance, consider the case where the monomer molecules are aligned perpendicular to the substrate occupying only one active site while tethering to the substrate, and leaving the rest of the active sites exposed and equally probable for the additional monomer molecules to come and attach to the substrate. In this case, the monolayer has high packing density because monomer molecules occupy all the active sites. Now consider the other extreme case, where the molecules are lying flat to the surface. These molecules apart from tethering to an active site of the substrate, by lying flat, they block the other active sites, disallowing other

molecules to come and attach to the surface. In this case, the packing density will be considerably less compared to the first case, and will be a strong function of the length of the molecule lying flat. Now consider the case, when the molecules are inclined at an angle to the surface. Then the packing density will be some value bounded by the extreme cases of when the molecules are (1) aligned perpendicular to the substrate and (2) the molecules are lying flat. Of course, the packing density, for an inclined case, is a function of angle of inclination and also the chain length of the molecule. The angle of inclination in turn depends on the terminal functional group and chain length of the tethering molecule apart from other factors. In the simple qualitative analysis, we have assumed that the molecules do not have any tendency to overlap and form multilayers. Thus, the hydrocarbon chain length and the terminal functional group of the monomer molecule affect the packing density, in a way.

For calculating packing density of SAMs, evaluation of molar absorptivity (ε) is necessary. We have used Beer-Lambert's law

$$log(\frac{I}{I_o}) = \varepsilon_{bulk} C t \qquad (3.1)$$

where I is the intensity of the reflected or absorbed beam, I_o is the intensity of the incident beam, C is the concentration of the species and t is the thickness of the medium (cell).

Equation 3.1 transforms into

$$log(\frac{I}{I_o}) = N\varepsilon_{monolayer}\Gamma \qquad (3.2)$$

where N is the total number of reflections (which is equal to 18 for our experimental set-up from geometrical conditions) and Γ is the surface coverage.

Equation 3.2 has 2 unknowns in the form of $\varepsilon_{monolayer}$ and Γ and one equation. ε_{bulk}, can be evaluated using equation 3.1, and can be used as $\varepsilon_{monolayer}$, to a first-order approximation. One important aspect is molar absorptivity, ε is characteristic of the chemical moiety and the value differs from one chemical moiety to the other. In the analysis, we have used asymmetric stretch of the methylene group.

From equation 3.1, ε_{bulk} is evaluated to be 2.31×10^6 cm/mole/CH_2. The methyl and methylene peaks are fit using a Lorentzian function and the area under the asymmetric CH_2 peak is taken as the absorbance value (or $log(\frac{I}{I_o})$). A typical spectrum used for the Lorentzian fit is shown in figure 3.4. Figure 3.5 shows the linear fit used to evaluate the ε_{bulk}.

Using ε_{bulk} in equation 3.2 gives coverage of 4-5 A^{o2}/molecule for OTS monolayer. This value is physically not possible as the cross-sectional area of the head group of an OTS molecule is about 20 A^{o2}/molecule. The reason for the discrepancy is because of the difference in the values of ε_{bulk} and $\varepsilon_{monolayer}$. In the evaluation of ε_{bulk}, the molecules are present in dilute concentrations in the solvent (carbontetrachloride) and the molecules do not interact with each other. However, in the case of monolayer, the molecules are relatively densely packed, and hence the molecules interact with the surrounding molecules. This additional interaction parameter causes the change in ε_{bulk} and $\varepsilon_{monolayer}$ values.

In order to evaluate $\varepsilon_{monolayer}$, we have used Langmuir-Blodgett film of Stearic acid. The strearic acid film is transferred on to the OTS coated silicon crystal at transfer pressure of 30 mN/m and surface coverage of 18 A^{o2}/molecule. The other conditions at

which the transfer is performed are given in experimental conditions. Assuming that the surface coverage does not change while LB transfer, the $\varepsilon_{monolayer}$, using equation 3.2, is evaluated to be 4.12×10^6 cm/mole/CH_2. Using this value of $\varepsilon_{monolayer}$, the OTS coverage density is found to be 22.5 A^{o2}/molecule, and this value agreed reasonably both the cross-sectional area of the molecule and also with the values reported in the literature. The coverage densities for UTS, CUTMS and APS are evaluated to be 30, 45-60, and 13.5 A^{o2}/molecule, respectively.

As can be seen, though OTS and UTS have same terminal functional group, OTS has higher coverage density because of the hydrophobic-hydrophobic interactions between molecules (due to longer chain length). This also reveals that the UTS molecules are inclined to the substrate. Similarly, the effect of terminal group on the coverage can be seen by comparing the CUTMS and UTS monolayers. CUTMS, has lower coverage indicating that the molecules are inclined further towards the substrate. The increase in the inclination is due to the affinity of polar CN group to the hydrophilic substrate. On the other hand APS has molecular coverage of 13.5 A^{o2}/molecule, which is lower than the cross-sectional area of the APS molecule head group. This indicates that APS forms multilayers. This also confirms with the ellipsometric data obtained. A simple cartoon depicting the structure of the various monolayers is shown in figure 3.6.

3.3.3 Effect of Temperature on Mechanism of Formation

Similar affects of temperature, as discussed in background section 2.7, are seen for CUTMS monolayer. CUTMS monolayer showed uniform growth mechanism at room

temperatures, which is above the phase transition temperature for the short 11-carbon chain. Figure 3.7 shows the AFM image obtained in contact mode of the CUTMS monolyer formed at room temperature. The image is uniform with no features, indicating homogeneous growth regime. At low deposition temperatures (T=0°C), the CUTMS monolayer showed mixed regime growth, indicating the existence of LC-LE phase equilibrium. Figure 3.8 shows the spectrum of CUTMS monolayer formed at 0°C. The peak split of CH_2 asymmetric and symmetric stretches indicate the existence of two phases in equilibrium.

3.4 Conclusions

The structure and properties of the SAMs greatly depended on the chain length and terminal functional group. Long chain molecules (OTS) formed a well-packed, ordered, crystalline structure and the order decreased with decrease in the hydrocarbon chain length. For same carbon chain length molecules also, the structural properties depended on the terminal functional group. CUTMS formed a more disordered structure than UTS because of the hydrophilic nature of the CN terminal group of CUTMS. APS, the shortest carbon chain molecule studied formed a disordered structure. The packing density of the monolayers is also evaluated, and the coverages of these monolayers are determined to be 22.5, 30, 45-60 and 13.5 A^{o2}/molecule for OTS, UTS, CUTMS and APS respectively. The differences in the coverages are attributed to the differences in hydrocarbon chain length and terminal functional group. APS formed multilayers. CUTMS showed homogeneous growth at room temperatures and mixed growth regime at low temperatures (T=0°C).

3.5 References

1. Iimura, K.-i.; Nakajima, Y.; Kato, T. *Thin Solid Films* **2000**, *379*, 230-239.

2. Jennings, G. K.; Munro, J. C.; Yong, T.-H.; Laibinis, P. E. *Langmuir* **1998**, *14*, 6130-6139.

3. Bierbaum, K.; Grunze, M.; Basaki, A. A.; Chi, L. F.; Schrepp, W.; Fuchs, H. *Langmuir* **1995**, *11*, 2143-2150.

4. Parikh, A. N.; Allara, D. L.; Azouz, I. B.; Rondelez, F. *The Journal of Physical Chemistry* **1994**, *98*, 7577-7590.

5. Parikh, A. N.; Liedberg, B.; Atre, S. V.; Ho, M.; L.Allara, D. *J. Physical Chemistry* **1995**, *99*, 9996-10008.

OTS (octadecyltrichlorosilane)
18-carbon chain
methyl (CH_3) termination

UTS (undecyltrichlorosilane)
11-carbon chain
methyl (CH_3) termination

CUTMS (11-cyanoundecyltrimethoxysilane
11-carbon chain
cyano (CN) termination

APS (aminopropyltrimethoxysilane)
3-carbon chain
amine (NH_2) termination

Figure 3.1: Cartoon depicting the surfactant molecules considered for studying the effects of hydrophobic chain length and terminal functional group

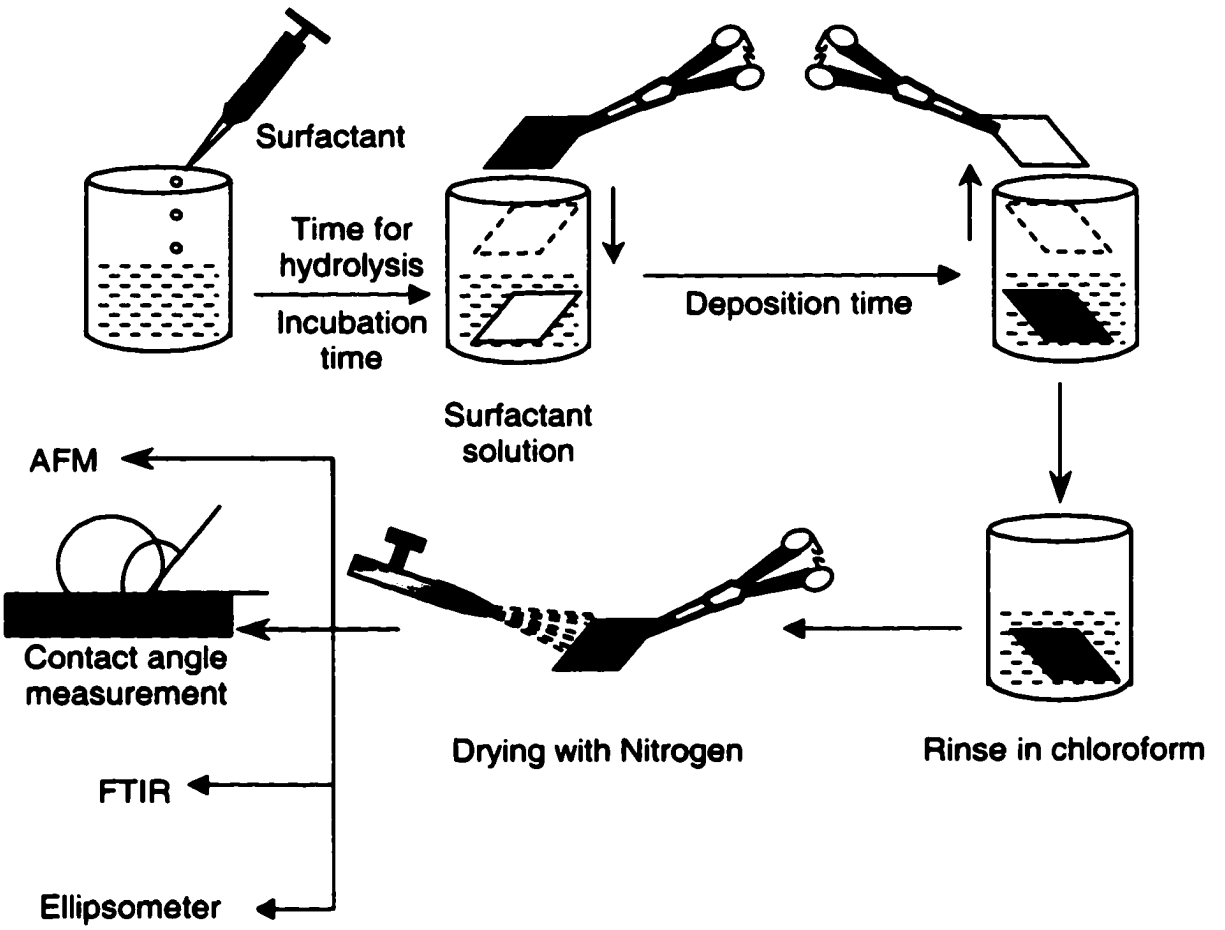

Figure 3.2: Cartoon depicting the procedure for preparation of self-assembled monolayers

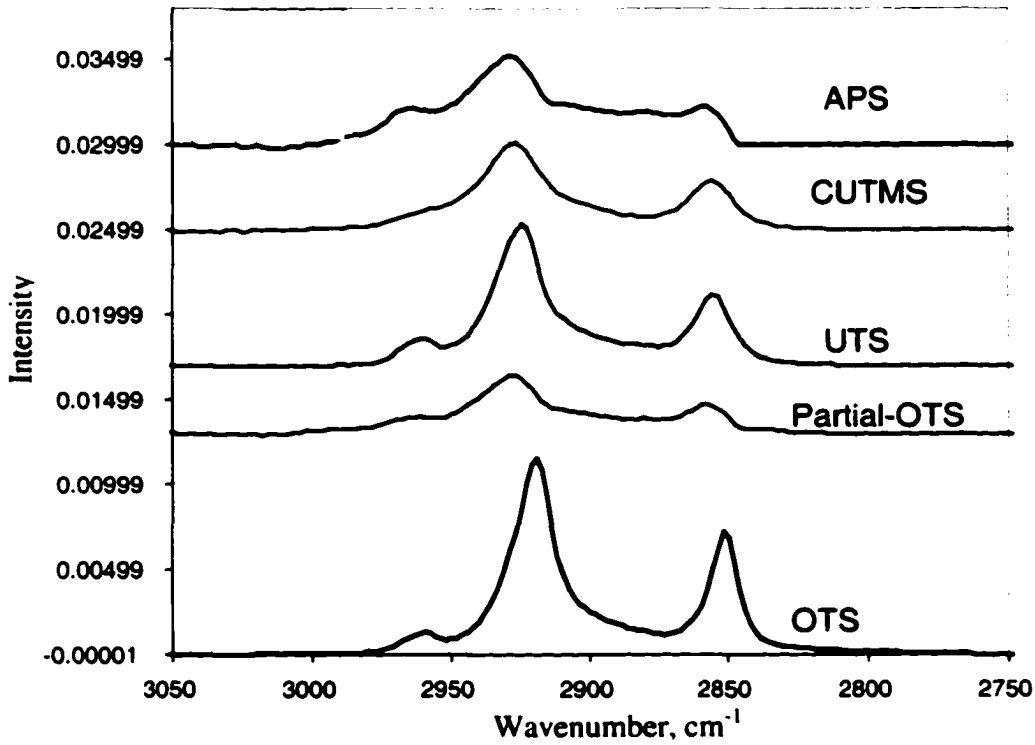

Figure 3.3: IR Spectra of different monolayers formed on silicon crystal

Monolayer	Contact Angle with Water	Ellipsomter Thickness, A °	CH_2 Asymm, cm^{-1}	CH_2 Symm, cm^{-1}	CH_3 Asymm, cm^{-1}
OTS	110°	25	2919	2851	2960
Partial-OTS	70°	21	2928	2857	2962
UTS	105°	~11-14	2924	2854	2960
CUTMS	55°	~10-14	2927	2856	2960
APS	35°	~8-18	2928	2859	2964

Table 3.1: Showing the methylene and methyl stretches of the spectra shown in figure 3.3. Also shows the contact angle and ellipsometer measurements for all the monolayers

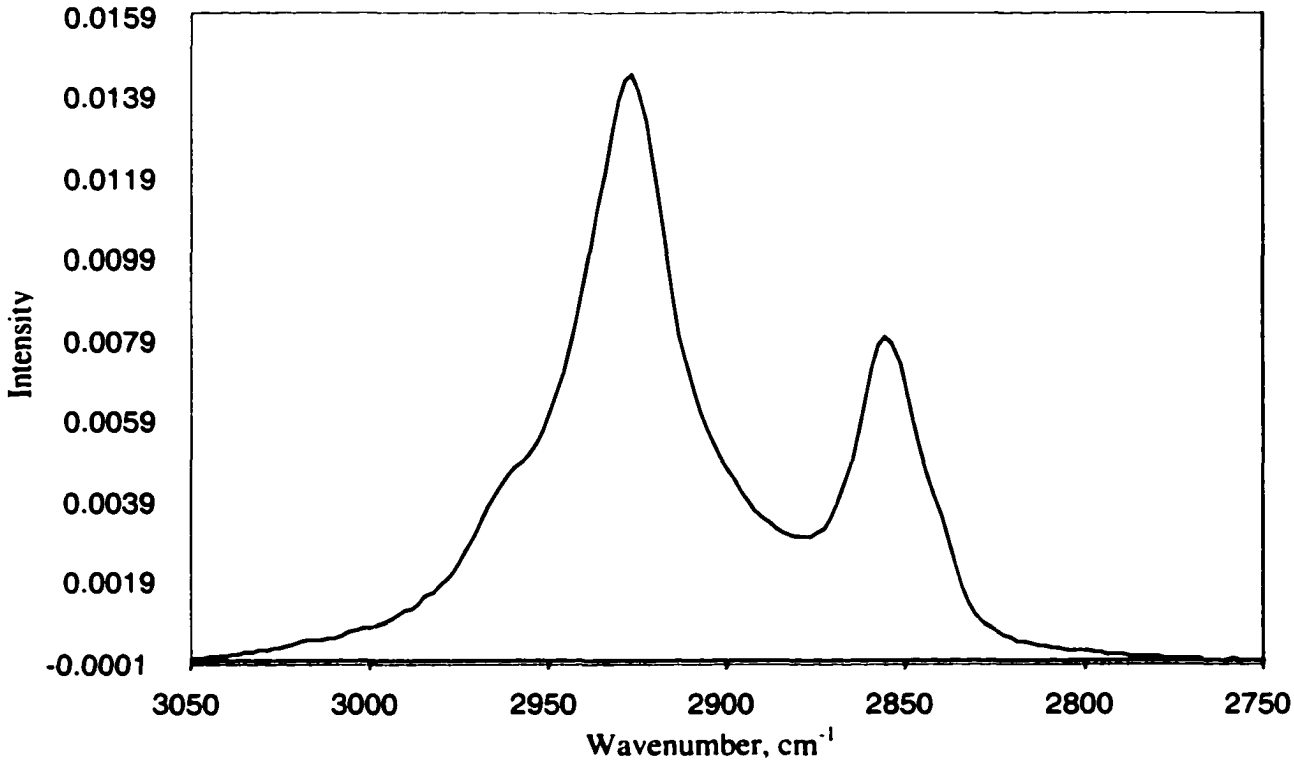

Figure 3.4: Sample spectrum of a monolayer, showing methylene and methyl asymmetric and symmetric vibrations, used for peak fit during packing density measurements

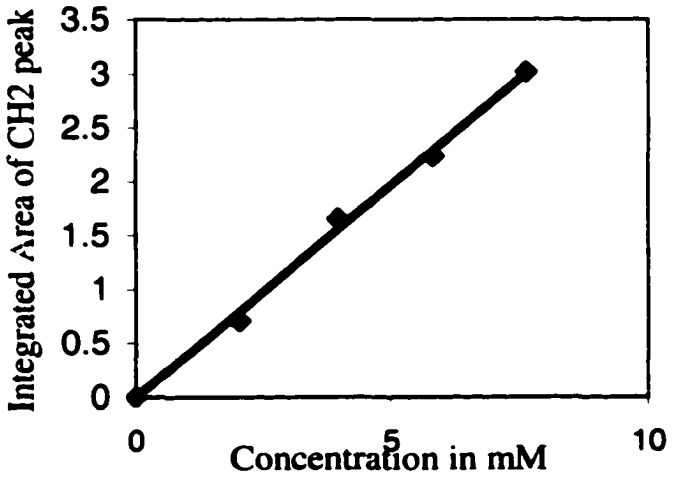

Figure 3.5: Calibration curve, showing the linear variation in area of asymmetric methylene stretching frequency with the concentration of OTS surfactant concentration, for obtaining ε_{bulk}

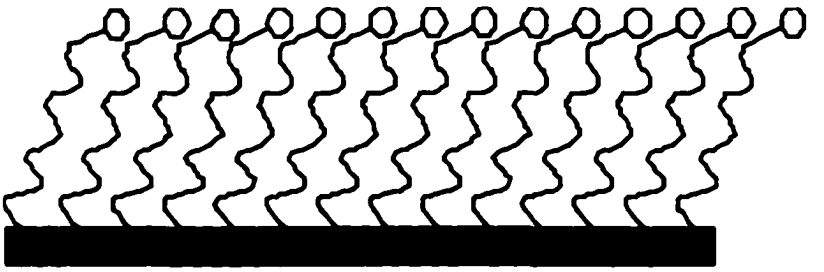

(a) Schematic of OTS monolayer; Molecules are aligned perpendicular to the substrate

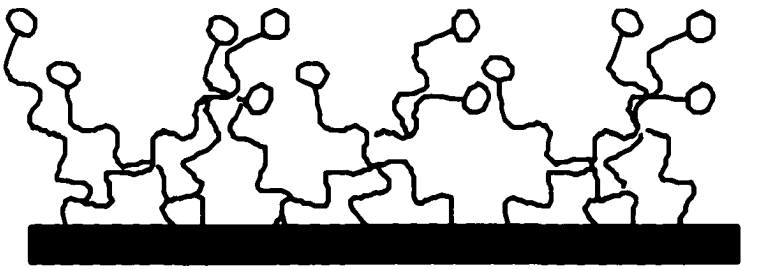

(b) Schematic of UTS and CUTMS monolayers; Molecules are randomly arranged on the surface

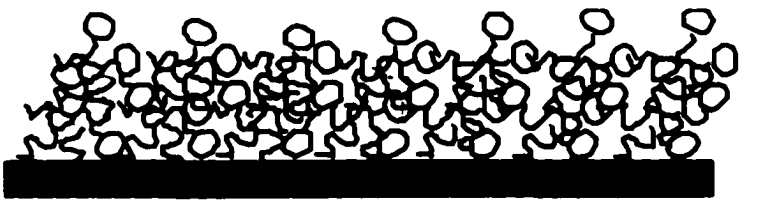

(c) Schematic of APS monolayer; Molecules are randomly arranged on the surface and they form multilayers

Figure 3.6: Schematic of various monolayers

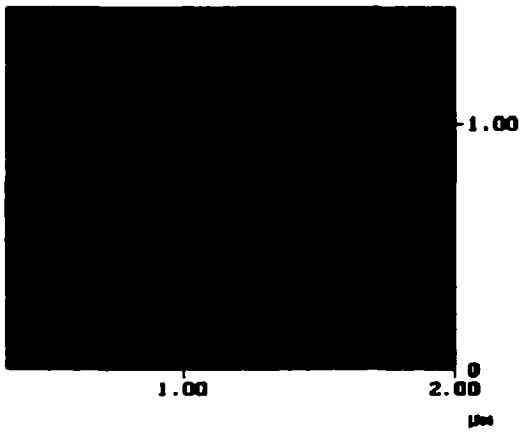

Figue 3.7: AFM image of CUTMS monolayer formed at room temperatures taken in contact mode. Absence of islands indicates homogenous growth regime at room temperatures

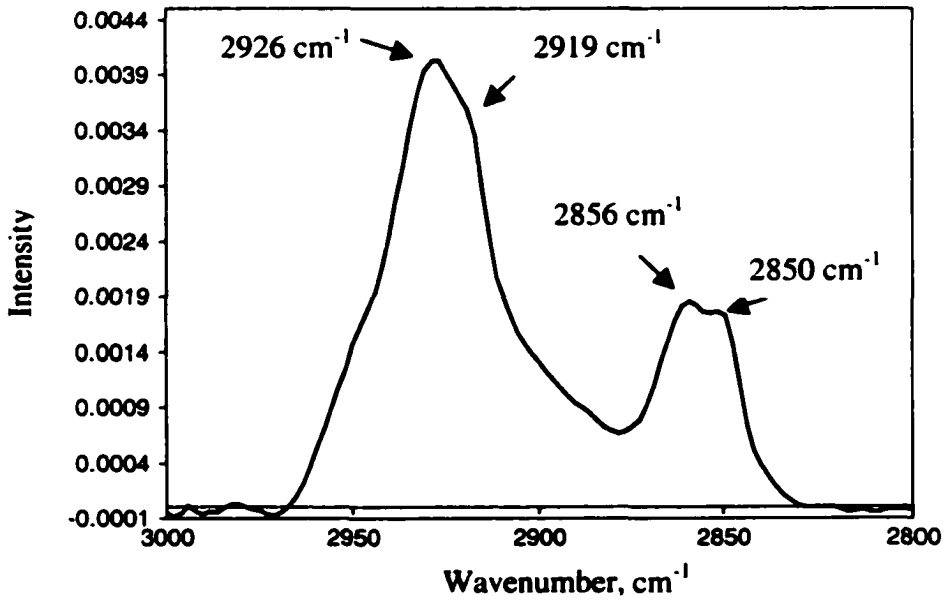

Figure 3.8: Spectrum of CUTMS monolayer formed at 0°C. Peak splits for methylene asymmetric and symmetric stretches indicate the existence of LC-LE phases in equilibrium

Chapter 4

Modification of Self-Assembled Monolayers: Conversion of CN Terminal Functional Group to COOH Group

4.1 Introduction

Independent control of surface structure and chemical properties and the resulting structure-property relationships are both scientifically interesting and technologically important. For many applications such as protective coatings,[1] lubrication layers,[2] membranes for chemical and biochemical sensors,[3-7] templates for crystal growth,[8] fabrication of nanoparticles,[9-11·12] micropatterning,[13,14] and for molecularly thin transistors,[15] controlling the properties of interfaces is very important. SAMs provide a unique way of altering just the surface properties of a material, by modifying the terminal functional groups displayed on the surface without altering or affecting the bulk properties of the material.

While SAM formation is well studied, the field of synthetic elaboration of SAM surfaces has received only limited attention. Chemical modification of organic monolayers is often carried out through common solution-phase or gas-phase methods. Such methods have several potential limitations for the preparation of useful devices. Solution-phase reactions with the surface can result in absorption of reactant material into the bulk of a sample, and many common condensed-phase reactions do not occur at surfaces. Vapor-phase reactions are more controlled and eliminate the need for solvent remediation, yet even fewer reaction types are available for gas-phase treatment than for solution-phase treatment because of vapor pressure requirements and the absence of

catalysts. The primary drawback to these general reaction routes, however, is that, in themselves, they do not provide spatial control of the reaction at the surface.

When compared to siloxane-based SAMs, alkanethiol SAMs on gold surfaces are widely studied because of the ease by which they can be prepared. [16,1,17-20] Thiol monolayers are formed via the covalent linkage between the surface gold atom and the sulfur atom of the alkanethiol molecule. [16,1,17-20] Due to the lack of reactivity between the various terminal functional groups and the sulfur surface binding group, alkanethiol surfactants with different terminal functionalized groups can be prepared a priori to the adsorption process and monolayer formation. Thus, making it convenient to prepare thiol-based monolayers with varying functionalized groups. Thiol-based monolayers can also be modified by simple synthetic approaches. Several researchers have successfully converted thiols of one functional group to another.[21,22] However, these thiol-based SAMs are relatively fragile both thermally and chemically, which restricts the conditions that can be employed for subsequent surface modification.[23-25]

Contrary to thiol-based SAMs, silane-based SAMs are thermally and chemically robust. Silane-based SAMs are thermally stable even at temperatures approaching 600 K in an inert nitrogen environment.[26,27] However, due to the high reactivity of the eletrophilic trifunctionalsilane group, the functional groups that can be incorporated on a silane SAMs are restricted. Due to this limitation, several useful functional groups such as alcohols, carboxylic acids, amines, amides, thiols, phosphines, enamines, enol ethers etc., must either be protected in non-nucleophilic form or introduced subsequent to the monolayer assembly. In addition to this, any functional group present on the alkyl tether

must be sterically small enough to allow a close-packed well-ordered SAM to form on a hydroxylated surface.

Due to the reasons mentioned above, several researchers have been investigating ways of modifying the silane-based SAMs to form monolayers of various terminal functional groups. Sukenik et al. have successfully demonstrated the transformation of Br, CN, SCN and $SCOCH_3$ functionalities to N_3, NH_2, SH, SO_3H, SCH_2CH_2, $SO_2CH_2CH_2$ by nucleophilic substitution using various reagents and reacting conditions.[28-32] Fryxell et al. have shown, by nucleophilic displacement DMED (N-N-dimathylethylenediamine) amidation, hydroxylamine amidation and hydrazine amidation.[33] Calvert et al have demonstrated the nucleophilic displacement reactions on benzyl halide SAMs.[34] Kakkar et al have used simple acid-base hydrolytic chemistry approach to form SAMs of long chain alcohols terminated with alkyl, phenyl and acetylene groups.[35,36] Nealey et al have chemically modified the SAMs of inert or hydrophobic nature to reactive or hydrophilic state by exposing the monolayers to soft X-rays in air.[37] Graham et al have converted the hydroxyl-terminated SAMs to ester or ether-terminated by using low-energy collisions of polyatomic cations.[38] Table 4.1 shows the conditions at which various transformations are possible.

In this chapter, we present the results of the modification of the CN terminal functional group of 11-cyanoundecyltrimetjoxysilane (CUTMS) monolayer to COOH terminal group by a simple hydrolysis reaction. SAMs with a COOH terminal group are technologically interesting, as the ionization state of these groups is sensitive to the pH of the surrounding environment.[19,18,39] By varying the pH of the surface, the terminal groups are transformed from all COOH (at low pH) to all COO^- (at high pH) or a mixture

of COOH and COO^- (at intermediate pH values). By controlling the pH, the ratio of number densities of COOH to COO^- groups is controlled, which in turn determines the local structure and arrangement of the surface groups. Thus, in an indirect way, the structure and arrangement of the COOH and COO^- groups on the surface is fine-tuned by just controlling the pH of the system. We also demonstrate this inter converitibility of COOH $\leftrightarrow$ COO^- by controlling the pH using both modified CUTMS monolayer and LB film of stearic acid. From quantitative analysis of the infrared spectra of COOH and COO^- groups, the number densities of these groups present on the surface has been independently determined. This also provides a tool to determine the extent of reaction or conversion of the cyano groups to carboxyl groups.

4.2 Experimental Section

4.2.1 Materials

11-cyanoundecyltrimethoxysilane (CUTMS) is purchased from United Chemical Technologies and Octadecyltrichlorosilane (OTS, 95% purity) is obtained from Sigma Aldrich Co. Concentrated Sulfuric acid, Chloroform and Toluene are purchased from Fisher Scientific. Anhydrous grade of Hexadecane is purchased from Sigma Aldrich. Stearic Acid is brought from Fluka. Silicon wafers used are obtained from Montco Silicon Technologies (pennsylvania). The silicon wafers used in our experiments are of thickness-450-500μm, double sided polished and of orientation (111). Silicon Internal Reflection Elements (dimensions: 50x10x3 mm and orientation (111)) used for Infrared Spectroscopy are obtained from Harrick Scientific. Nochromix crystals used for cleaning

purposes is obtained from Godax Laboratories. All Chemicals are used as purchased without any further purification. Deionised water with a resistivity of 18MΩ cm from a Millipore System is used in all our experiments.

Cleaning Protocols: Described in chapter 3.

Monolayer Preparation: Described in chapter 3.

4.2.2 Modification of CUTMS Monolayer

The CN terminal groups of the CUTMS monolayer prepared as mentioned above are transformed into COOH groups by simple hydrolysis reaction. The CUTMS monolayer is kept in a 50:50 (v/v) solution mixture of 15% Hydrochloric acid and deinoised water maintained at 75^0 C. Before modifying the CUTMS monolayer, the substrates are annealed at 150^0 C for about 2 hours. Monolayer is not stable for the above-mentioned reaction conditions unless it is annealed. The monolayer molecules desorbed if the substrate is kept for durations more than 1 and half-hours.

4.3 Results and Discussions

4.3.1 Formation of CUTMS monolayer

The structure and properties of CUTMS self-assembled monolayer are discussed in brief in chapter 2. Here, some of the aspects like the hydrolysis and the kinetics of the formation of monolayer formation are discussed in detail. A typical spectrum of a CUTMS monolayer formed on a silicon substrate, after a deposition time of 24hrs, is shown in figure 4.1. Some of the important vibrational modes pertaining to methyl and methylene symmetric and asymmetric stretching modes are shown in table 4.2.

Asymmetric stretching mode of the methylene group reveals a great deal of information on the local molecular order and packing.[40,41] How this information is used to get the packing density and coverage is already discussed. Methylene asymmetric stretching mode for the CUTMS monolayer appears at ~2927 cm^{-1} and that of symmetric stretching mode appears at 2856 cm^{-1}. These values correspond to a liquid-like structure. The spectrum is compared with the solution spectrum of CUTMS in anhydrous chloroform, obtained independently using NaCl windows in transmission mode. The details of the spectral features are shown in table 4.2. The asymmetric and symmetric peaks of CH_2 match close to that of the CUTMS monolayer. The slight differences in the spectra of the molecules at the surface and in the solution are attributed to the small degree of ordering as the molecules are being anchored to the substrate by one end.

As discussed in chapter 2, formation of self-assembled monolayers of silanes on silicon substrates is a three-step process. Initially the trichloro or trimethoxy groups of the silanes are hydrolyzed either in the solution, due to the presence of trace amounts of water in the solvent, or near the surface of the substrate, where a thin water film of 2-3 monolayers of film is present. Secondly, these hydrolyzed silanes react with the surface hydroxyl groups and get chemically adsorbed on the surface. Finally as the monomers adsorb on the surface due to the weak, van der Waals chain-chain interactions, the molecules order and arrange themselves.

There is a possibility of these hydrolyzed monomers reacting in the solvent and forming oligomers in the bulk itself, before actually adsorbing on to the surface.[42,43] The process of polymerization (oligomerization) depends on several factors such as amount of water present in the bulk solution, the incubation time of the silane solution

before the deposition process and also on the susceptibility of the trichloro or trimethoxy silanes to be converted to hydroxyl groups.[44-46] Figure 4.1 shows a peak at 2961.8 cm^{-1} corresponding to the CH_3 asymmetric stretch of the methoxy group attached to the silicon head group. This clearly indicates that the hydrolysis of the CUTMS monomers is not complete. Trichloro silanes are more susceptible to change to hydroxyl groups. As the reaction of chloro (Cl) to hydroxyl (OH) proceeds, hydrochloric acid is liberated, which in turn acts as catalyst for the reaction, thus enhancing the reaction rate. The reaction rate for a methoxy (OCH_3) or ethoxy (OC_2H_5) on the other hand is relatively very slow when compared to chlorosilanes. The CH_3 peak could be seen even after long deposition times, thus emphasizing on the low reactivity rates of the methoxy groups. After a uniform layer of CUTMS is formed, the total amount of the molecules adsorbed on the surface did not increase even with increase in deposition time. The total amount adsorbed is qualitatively discerned from the total absorbance value. The details of the actual qualitative analysis are given later. The plausible reason for the methoxy groups not able to convert to hydroxyl groups could be because of the low water content in the solvent used in the experiments. Kessel et al, in their studies with alkoxy silanes, had to perform the hydrolysis reaction of the alkoxy groups in a water rich THF solvent before using the silanes for monolayer formation.[43] The other possible reason could be that, the monomer molecules present near the surface (which has a very thin water layer) adsorb at the surface instantaneously with one of the alkoxy group hydrolyzing and forming an anchor. But it will be difficult for the other two non-anchoring alkoxy groups of the anchored-molecule to get hydrolyzed since the water is present in very low concentrations in the solution, and also because of the diffusion limitations for the water molecules once the

monolayer of partially hydrated silanes is formed.[47,48] Experiments with saturated solvent also had alkoxy groups on the surface thus enhancing credibility to our presumption that hydrolyzation of alkoxy groups is inhibited because of the slow diffusion process.

Figure 4.1 also shows peaks at 2248 cm^{1} and 1725 cm^{-1} corresponding to the cyano (C≡N) and carbonyl (C=O) stretching bands. The peak at 2248 cm^{-1} is understandable due to the presence of the cyano groups in the monomer, however we believe that the presence of C=O peak is because of the transformation of some of the CN groups to carboxylic acid (COOH) groups because of hydrolysis. Similar phenomenon of acetylchlorides transforming to carboxylic acid groups, during the monolayer formation, is observed by the Sukenic et al.[19] They reported that "the rapid hydrolysis of acid chloride to carboxylic acid is likely due to the presence of thin water film of adsorbed water on the surface of the ATR element and the relatively high local concentration of HCl formed during the establishment of the siloxane network." The effect of solvent on the monolayer formation was studied. Table 4.3 shows the details of all the important spectral features observed under different solvent conditions. The solvents used are Chloroform, Toluene and Carbontetrachloride. As can be seen, there are no considerable differences in the spectral features under different solvent environments. However, we presume that the kinetics of the monolayer formation would be slightly, if not considerably, different in these environments because of the solvent effects.

The kinetics of the CUTMS monolayer formation is studied from the contact angle measurements. Figure 4.2 shows the variation of the contact angle with deposition time. The solution used is chloroform. The measurements were taken within 10 minutes

after the removal of the sample from the solution. However to guarantee that the monolayer formation process is complete, we have used for all our experiments a deposition time of at least 24 hours. The equilibrium contact angle of 55^0 is less than the reported value of 65^0 Sukenic et al for surfaces formed by 1-cyano-16-trichlorosilyl hexadecane.[29] One reason for this contact angle difference is the formation of COOH groups as the monolayer formation proceeds as we have described earlier. The other plausible reason for this difference is the difference in the packing densities of the monolayers formed by the two surfactants. We have used an 11-carbon chain length surfactant while Sukenic et al have used a 16-carbon chain length of surfactant. As discussed in chapter 2, the packing density of the CUTMS monolayer will be lesser compared to 16-carbon chain length surfactant used by Sukenic et al. Upon heating to 150 ^{0}C for a few hours, the contact angle reached a steady state value of 70^0. The value is very stable and is independent of the heating time.

The thickness of the film is found to vary from 10-14 $A^0 \pm 2\ A^0$. The length of the fully extended CUTMS monomer is calculated to be ~14 A^0 using the CACHE software. The thickness obtained is reasonable, since in a disordered structure, the molecules will be inclined at an angle to the surface normal instead of being fully extended. Simple geometrical calculation gives an angle of inclination to the surface normal to be as large as 55^0. The molecules are oriented in all possible angles from 0^0 to 55^0 to the surface normal. Even the densely packed monolayers of OTS on hydroxylated surfaces and Alkanethiols on gold surfaces are found to be inclined to the surfaces from dichroic measurements. However, the difference in both of them lies in the order and the packing. Cartoon in figure 3.6 (chapter 3) depicts the idea of the molecular order and direction. In

the densely packed monolayers, all the molecules are aligned in the same direction or, in other words, the molecules have a net order parameter value, which is non-zero. However, the molecules in the CUTMS monolayer, though inclined, are not aligned in a particular direction. The order parameter, if one can be defined, will be lesser than that for the densely packed monolayers. Dense packing, caused by weak Vander Waal's interactions between chains, brings in local order of the molecules arranged on the surface.

4.3.2 Conversion of CN to COOH group

The terminal groups of the CUTMS monolayers are modified to COOH groups by a simple hydrolysis reaction as described in the experimental section.

$$-CN + 2H_2O \xrightarrow{\text{Acid, } H^+} -COOH + NH_3$$

The kinetics of the reaction is followed by contact angle and IR measurements. The changes in the contact angle with reaction time are shown in figure 4.3. The contact angle reached an equilibrium value of ~32^0 after approximately 45 minutes. A contact angle of 30-40^0 on monolayers with COOH terminal groups is reported by Whitesides et al.[49] This clearly indicates that the terminal groups have converted to COOH groups. The mole fraction of CN and COOH groups present on the surface, as the reaction proceeds, are calculated using Cassie Equation:

$$\cos(\theta_{avg}) = f_{cooh}\cos(\theta_{cooh}) + f_{cn}\cos(\theta_{cn})$$

where f_{cooh} and f_{cn} correspond to the mole fraction of COOH and CN terminal groups respectively. θ_{cooh} and θ_{cn} correspond to the equilibrium contact angle, when the whole monolayer is filled with either COOH or CN groups respectively. θ_{avg} is the contact

angle on the surface containing a mixture of COOH and CN groups. The variation of f_{cooh} and f_{cn} is shown in figure 4.4. (θ_{cooh} was taken as 32^0 and θ_{cn} was taken as 65^0)

The changes in the COOH and CN peak intensities are also followed by IR. A typical spectrum is shown in figure 4.5. The spectrum clearly indicates the decrease in CN peak (2253 cm^{-1}) and an increase in COOH peak (1702 cm^{-1}). The decrease in CN peak intensity is plotted in Figure 4.6.

4.3.3 pH Depedence

One interesting phenomenon is that the COOH groups are highly sensitive to pH changes, and the COOH $\leftrightarrow$ COO^- can be interchangeably converted back and forth by changing the pH. Figure 4.7 shows the spectra of the modified COOH surface at different pH values. At low pH values of ~2 (any value below pKa value), the surface is covered with COOH groups. The peak at 1718 cm^{-1} confirms that. When the same sample is immersed in a solution of higher pH value (any value greater than pKa value), the groups are converted to COO^- groups. The Figure 4.7(b) shows a peak split. The peak at 1590 cm^{-1} corresponds to COO^- stretching. The broad peak between 1650 and 1725 cm^{-1} correspond to the unconverted COOH and the surface bound water. Sukenik et al have calculated the pKa values of the monolayer from the changes of COOH and COO^- peaks and found that value to be 5.4.[19].

4.3.4 Calculation of Molar Absorptivities for evaulation of Number density

In the following section we tried to quantitatively measure the molecular coverage of the molecules from the molar absorptivity. The procedure is discussed in chapter 2.

In this study, we have used the LB film of the Stearic Acid to estimate the ε_{CH2} and ε_{COOH} and ε_{COO^-}. Calculation of these values provides a tool to quantitatively measure the molecular coverage, extent of conversion and the relative coverage of the COOH and COO^-. The LB film of Stearic Acid was transferred on to a silicon substrate coated with the OTS monolayer using the method described in the experimental section. The IR spectrum of the transferred LB film is shown in Figure 4.8. The details of the prominent peaks for the OTS monolayer and the LB film of stearic acid are given in table 4.4. The peaks at 2917 cm^{-1} and 2850 cm^{-1} corresponding to CH_2 asymmetric and symmetric stretching bands respectively, indicates that the LB film is crystalline and uniform. The peak at 1702 cm^{-1} corresponds to the C=O stretching band of the COOH groups. When the COOH groups are far apart, the COOH groups exist as monomers and the peak is seen between 1720 and 1740 cm^{-1}. However, when the molecules are closely packed, then the neighboring COOH molecules interact with each other (hydrogen bonding) and exist as dimers. Crooks et al have seen the similar phenomenon in the carboxylic acid terminated thiol self-assembled monolayers.[50] A shoulder at 1692 cm^{-1} confirms the strong inter molecular interactions between the neighboring molecules.

The sensitivity of the COOH groups to pH of the surrounding environment was proved by immersing the substrate containing LB film covered with COOH groups in a $CaCl_2$ solution of pH 11.5 for about 30 minutes. Figure 4.8 (b) shows the spectrum of the resulting substrate. As can be seen, the peak at 1702 cm^{-1} vanished and a very small peak, corresponding to the COOH groups existing as monomers, appeared at 1737 cm^{-1}. Two peaks appeared at 1577 cm^{-1} and 1541 cm^{-1} corresponding to free COO^- groups and the bonded COO^- groups respectively. The interchangeability of the COOH and COO^- groups

was proved by immersing the above sample in deionised water of pH 2.4 for about 30 minutes. Figure 4.8 (c) shows the spectrum of the same. As can be seen, the two distinct peaks appear at 1703 cm^{-1} and 1583 cm^{-1}. These two peaks correspond to the COOH existing as dimers and COO^- existing as free monomers respectively. There is also a shoulder at 1735 cm^{-1} corresponding to the free monomers of COOH groups. If the immersion time is increased, the spectrum would look identically like spectrum of figure 4.8 (a). Thus COOH dimers, monomers and COO^- monomers coexist on the surface. Figure 4.8 (d) shows the spectrum when the sample was immersed again in a solution of high pH of 10.5 for about 20 min. The spectral features of Figure 4.8(b) and (d) are qualitatively very similar. The difference in the quantities arises from the difference in the deposition times and also the pH. Cartoon in figure 4.9 (a) & (b) depicts the whole process in short.

Whitesides et al have hypothesized that the COOH and COO^- groups will be randomly arranged with no well-defined spatial arrangement. However, from our IR results, we believe that there is some degree of spatial arrangement of the surface groups. We hypothesize this from figure 4.8. If the groups are far apart, that means, when the influence of one molecule is not felt by the other, then we can presume that there is no local spatial order. However, if the neighboring molecules tend to interact with each other, then the molecules would arrange themselves such as to minimize the free energy. Also there will be spectral shifts only if the presence of one molecule has some influence on the surrounding molecule. The extent of spectral shift are shown in the figure 4.8 (a,d,c,d). From these we strongly believe that there is some local order and arrangement corresponding to a unique lattice arrangement of these various groups on the surface. The

uniqueness of the lattice arrangement depends on the number density of the various groups present on the surface. Cartoon 10 (c) depicts the spatial arrangement of COOH and COO^- surface groups.

For the quantitative analysis, the packing density of the stearic acid LB film is set at 18 $Å^2$/molecule. This assumption is drawn from the π-A isotherm of the strearic acid LB film obtained on a subphase of pH 2. The absorbance values for the CH_2 asymmetric and symmetric stretching bands are obtained by fitting the data with a Lorentzian peak. All the spectra are baseline corrected before the peak fitting analysis is done. For COOH, COO^- and CN peaks, the peaks are not fit and the absorbance values are evaluated by calculating the area between 2 wavenumbers. The details of the absorbance values for CH_2, COOH and COO^- and calculated molar absorptivities for the respective groups are given in table 4.5. Using $A_{CH2} = N\,\varepsilon_{CH2}(\Gamma)^*\,\Gamma_{CH2}$, where N is the number of reflections in the ATR element (N is geometrically determined to be 18) and Γ is the molecular coverage of the stearic acid monolayer expressed in moles/cm^2, ε_{CH2} is found to be 4.12×10^6 cm/mole/CH_2 group.

Since the vibrational frequencies for COOH and COO^- differ by a considerable amount, we have assumed the values of ε_{COOH} and ε_{COO^-} to be different. However, we did not differentiate between the freely existing and bounded COOH and COO^- groups. From Figure 4.8 (b), since the total number of COOH and COO^- should be constant and equal to the molecular coverage of the monolayer, one can write

$$A_{COOH}/\varepsilon_{COOH} + A_{COO^-}/\varepsilon_{COO^-} = \Gamma = A_{COOH}/\varepsilon_{COOH}$$

(From figure 4.8 b) (figure 4.8 a)

Which allows us to determine the ratio of the molar emissivities of the charged and the uncharged carboxylates, $\varepsilon_{COO^-}/\varepsilon_{COOH}$, to be 1.48. The data from figure 4.8(c) is used for a consistency check and the values agreed.

4.4 Conclusions

We have used contact angle measurements, ellipsometry and IR reflection measurements to characterize the structure of a cyano terminated monolayer formed by the adsorption of CUTMS on a silicon substrate. We have characterized the structure of the monolayer before and after hydrolysis of the terminal cyano group. CUTMS forms a monolayer film that has a liquid-like, disordered structure. The coverage of the CUTMS molecules was found to be approximately between 45-60 $Å^2$/ molecule. The -CN terminal groups of CUTMS monolayer were converted to COOH terminal groups by a simple hydrolysis reaction. The kinetics of the reaction was followed using IR and contact angle measurements. COOH groups are very sensitive to the pH of the surrounding environment and can be reversibly ionized by changing the pH of the wetting solution. LB film experiments revealed that there is some local spatial arrangement of the COOH and COO^- groups if they coexist on the surface at intermediate pH values. The spatial arrangement, of course, depends on the number densities of COOH and COO^- groups coexisting on the surface. We are looking at these aspects. The molar absorptivites, ε for CH_2, COOH and COO^- are evaluated. COOH and COO^- have different vibrational frequencies, which in turn implies different energies to activate these dipole moment transitions. We presumed different ε values for COOH and COO^- groups and from experiments the ratio of $\varepsilon_{COO^-}/\varepsilon_{COOH}$ was found to be 1.5.

4.5 References

1. Jennings, G. K.; Munro, J. C.; Yong, T.-H.; Laibinis, P. E. *Langmuir* **1998**, *14*, 6130-6139.

2. Gennes, P. G. d. *Rev. Mod. Phys.* **1985**, *57*, 827.

3. Lahiri, J.; Isaacs, L.; Grzybowski, B.; D.Carbeck, J.; Whitesides, G. M. *Langmuir* **1999**, *15*, 7186-7198.

4. Ottova, A.; Tvarozek, V.; Racek, J.; Sabo, J.; Ziegler, W.; Hianik, T.; Tein, H. T. **1996**.

5. Piletsky, S. A.; Wulff, G.; Piletskaya, E. V.; Panasyuk, T. L.; Elskaya, A. V.; Levi, R.; Karube, I. *Macromolecules* **1998**, *31*, 2137-2140.

6. Rubinstein, I.; Steinberg, S.; Tor, Y.; Shanzer, A.; Sagiv, J. *Nature* **1988**, *332*, 426-429.

7. Schierbaum, K. D.; Weiss, T.; Velzen, E. U. T. v.; Engbersen, J. F. J.; Reinhoudt, D. N.; Gopel, W. *Science* **1994**, *265*, 1413-1415.

8. Lockhead, M. J.; Letellier, S. R.; Vogel, V. *J. Phys. Chem. B* **1997**, *101*, 10821-10827.

9. Jiang, P.; Liu, Z.-F.; Cai, S.-M. *Surface Science* **2001**, *486*, L507-L512.

10. Li, L. S.; Lianhua Qu, R. L.; 1, X. P.; Zhao, Y.; Li, T. J. *Thin Solid Films* **1998**, *327–329*, 408–411.

11. Li, L. S.; Jin, J.; Tian, Y. Q.; Zhao, Y. Y.; Li, T. J.; Du, Z. L.; Ma, G. H.; Zheng, N. *Supramolecular Science* **1998**, *5*, 475-478.

12. Zhang, L.; Shen, G.; Pan, Z.; Lu, Z. *Materials Chemistry and Physics* **1998**, *55*, 160-163.

13. Sugimura, H.; Ushiyama, K.; Hozumi, A.; Takai, O. *Langmuir* **2000**, *16*, 885-888.

14. Whitesides, G. M.; Aizenberg, J.; Black, A. J. *nature* **1998**, *394*, 868-871.

15. Schon, J. H.; Bao, Z. *Applied Physics Letters* **2002**, *80*, 847-849.

16. Sabatani, E.; Rubinstein, I.; Maoz, R.; Sagiv, J. *J. Electroanal. Chem.* **1987**, *219*, 365-371.

17. Creager, S. E.; Clarke, J. *Langmuir* **1994**, *10*, 3675-3683.

18. Bain, C. D.; Whitesides, G. M. *Langmuir* **1989**, *5*, 1370-1378.

19. Cheng, S. S.; Scherson, D. A.; Sukenik, C. N. *Langmuir* **1995**, *11*, 1190-1195.

20. Wang, J.; Frostman, L. M.; Ward, M. D. *Journal of Physical Chemistry* **1992**, *96*, 5224-5228.

21. Lukkari, J.; Kleemola, K.; Meretoja, M.; Ollonqvist, T.; Kankare, J. *Langmuir* **1998**, *14*, 1705-1715.

22. Tillman, N.; Ulman, A. *Langmuir* **1989**, *5*, 101-111.

23. Delamarche, E.; Michel, B.; Kang, H.; Gerber, C. *Langmuir* **1994**, *10*, 4103.

24. Benesebaa, F.; Ellis, T. H.; Badia, A.; Lennox, R. B. *Langmuir* **1998**, *14*, 2361.

25. Tam-Chang, S.-W.; Biebuyck, H. A.; Whitesides, G. M.; Jeon, N.; Nuzzo, R. G. *Langmuir* **1995**, *11*, 4371.

26. Sung, M. M.; Kluth, G. J.; Yauw, O. W.; Maboudian, R. *Langmuir* **1997**, *13*, 6164-6168.

27. Sung, M. M.; Kluth, G. J.; Maboudian, R. *Langmuir* **1997**, *13*, 3775-3780.

28. Lee, Y. W.; Reed-Mundell, J.; Sukenik, C. N.; Zull, J. E. *Langmuir* **1993**, *9*, 3009-3014.

29. Balachander, N.; Sukenik, C. N. *Langmuir* **1990**, *6*, 1621-1627.

30. Barness, Y.; Gershevitz, O.; Sekar, M.; Sukenik, C. N. *Langmuir* **2000**, *16*, 247-251.

31. Collins, R. J.; Sukenik, C. N. *Langmuir* **1995**, *11*, 2322-2324.

32. Grisaru, H.; Cohen, Y.; Aurbach, D.; Sukenik, C. N. *Langmuir* **2001**, *17*, 1608-1619.

33. Fryxell, G. E.; Rieke, P. C.; Wood, L. L.; Engelhard, M. H.; Williford, R. E.; Graff, G. L.; Campbell, A. A.; Wiacek, R. J.; Lee, L.; Halverson, A. *Langmuir* **1996**, *12*, 5064-5075.

34. Koloski, T. S.; Dulcey, C. S.; Haralson, Q. J.; Calvert, J. M. *Langmuir* **1994**, *10*, 3122-3133.

35. Kakkar, A. K.; Yitzchaik, S.; Roscoe, S. B.; F., K.; Allan, D. S.; Marks, T. J. *Langmuir* **1993**, *9*, 388-390.

36. Yam, C. M.; Tong, S. S. Y.; Kakkar, A. K. *Langmuir* **1998**, *14*, 6941-6947.

37. Kim, T. K.; Yang, X. M.; Peters, R. D.; Sohn, B. H.; Nealey, P. F. *J. Phys. Chem. B* **2000**, *104*, 7403-7410.

38. Wade, N.; Gologan, B.; Vincze, A.; cooks, R. G.; Sullivan, D. M.; Bruening, M. L. *Langmuir* **2002**, *18*, 4799-4808.

39. Bain, C. D.; Whitesides, G. M. *Langmuir* **1989**, *5*, 1370-1378.

40. Parikh, A. N.; Allara, D. L.; Azouz, I. B.; Rondelez, F. *The Journal of Physical Chemistry* **1994**, *98*, 7577-7590.

41. Parikh, A. N.; Liedberg, B.; Atre, S. V.; Ho, M.; L.Allara, D. *J. Physical Chemistry* **1995**, *99*, 9996-10008.

42. Peters, R. D.; Nealey, P. F.; Crain, J. N.; Himpsel, F. J. *Langmuir* **2002**, *18*, 1250-1256.

43. Vallant, T.; Brunner, H.; Mayer, U.; Hoffmann, H.; Resch, R.; Grasserbauer, M.; Friedbacher, G. *J. Phys. Chem. B* **1998**, *102*, 7190-7197.

44. Kessel, C. R.; Granick, S. *Langmuir* **1991**, *7*, 532-538.

45. Oostendorp, D. J.; Bertrand, G. L.; O.Stoffer, J. *Silanes and Coupling Agents* **1992**, 159-179.

46. Osterholtz, F. D.; Pohl, E. R. *Silanes and other coupling agents* **1992**, 119-141.

47. Maoz, R.; Sagiv, J. *Langmuir* **1987**, *3*, 1034-1044.

48. Sagiv, J.; Gun, J. *thin solid films* **1985**, *132*, 135-151.

49. Wasserman, S. R.; Tao, Y.-T.; Whitesides, G. M. *Langmuir* **1989**, *5*, 1074-1087.

50. Crooks, R. M.; Sun, L.; Kepley, L. J. *Langmuir* **1992**, *8*, 2101-2103.

Monolayer (silanes)	Reagent	In situ Transformation
$(CH_2)_{16}Br$	$NaSCN$	$(CH_2)_{16}SCN$
$(CH_2)_{16}Br$	NaN_3	$(CH_2)_{16}N_3$
$(CH_2)_{16}SCN$	$LiAlH_4$	$(CH_2)_{16}SH$
$(CH_2)_{16}SCOCH_3$		$(CH_2)_{16}SH$
$((CH_2)_{16}S)_2$		$(CH_2)_{16}SH$
$(CH_2)_{16}CN$	$LiAlH_4$ or BH_3	$(CH_2)_{16}NH_2$
$(CH_2)_{16}N_3$	$LiAlH_4$ or $SnCl_2$	$(CH_2)_{16}NH_2$
$(CH_2)_{16}Br$	Na_2S	$((CH_2)_{16})_2S$
$(CH_2)_{16}Br$	Na_2S_2	$((CH_2)_{16}S)_2$
$((CH_2)_{16})_2S$	H_2O_2	$((CH_2)_{16})_2SO_2$
$(CH_2)_{16}SH$		$(CH_2)_{16}SO_3H$
$(CH_2)_{16}SH$	Br_2	$((CH_2)_{16}S)_2$
$(CH_2)_{16}X$	CH_3COONa	$(CH_2)_{16}OH$
$(CH_2)_{16}OH$	CXH_2COX	$(CH_2)_{17}COOX$
$(CH_2)_{16}X$	$C_6H_4CH_2XCH_2X$ (α, α' dibromo p-xylene)	$(CH_2)_{16}C_6H_4CH_2X$
$(CH_2)_{16}COOH$	$LiAlH_4$ or BH_3	$(CH_2)_{16}CH_2OH$
$(CH_2)_{16}CH_2OH$	$RCOCl$	$(CH_2)_{16}CH_2OCOR$
$(CH_2)_{16}COOH$	PCl_5	$(CH_2)_{16}COCl$
$(CH_2)_{16}COCl$	ROH	$(CH_2)_{16}COOR$

$(CH_2)_{16}COCl$	RNH_2	$(CH_2)_{16}CONHR$
$-C_6H_4CH_2X$	Li-EDA	$-C_6H_4CH_2NHCH_2CH_2NH_2$
$-C_6H_4CH_2X$	Li-PYR	$-C_6H_4CH_2C_5H_4N$
$(CH_2)_{16}CH=CH_2$	HX (peroxide)	$(CH_2)_{16}CH_2CH_2X$
$(CH_2)_{16}CH=CH_2$	$KmnO_4$ or HCO_2OH	$(CH_2)_{16}CHOHCH_2OH$
$(CH_2)_{16}Br$	$^-SCH_2CHNH_2C00^-$	$(CH_2)_{16}$ $SCH_2CHNH_2C00^-$
$((CH_2)_{16}CO_2CH_2CF_3)_2$	$NH_2(CH_2)_2N(CH_3)_2$	$((CH_2)_{16}CO)_2$ $N(CH_2)_2N(CH_3)_2$
$((CH_2)_{16}CO_2CH_2CF_3)_2$	NH_2OH	$(CH_2)_{16}CONHOOC(CH_2)_{16}$
$((CH_2)_{16}CO_2CH_2CF_3)_2$	NH_2NH_2	$(CH_2)_{16}CONHNHOC(CH_2)_{16}$

Table 4.1 : In situ transformation of monolayers into different functional groups

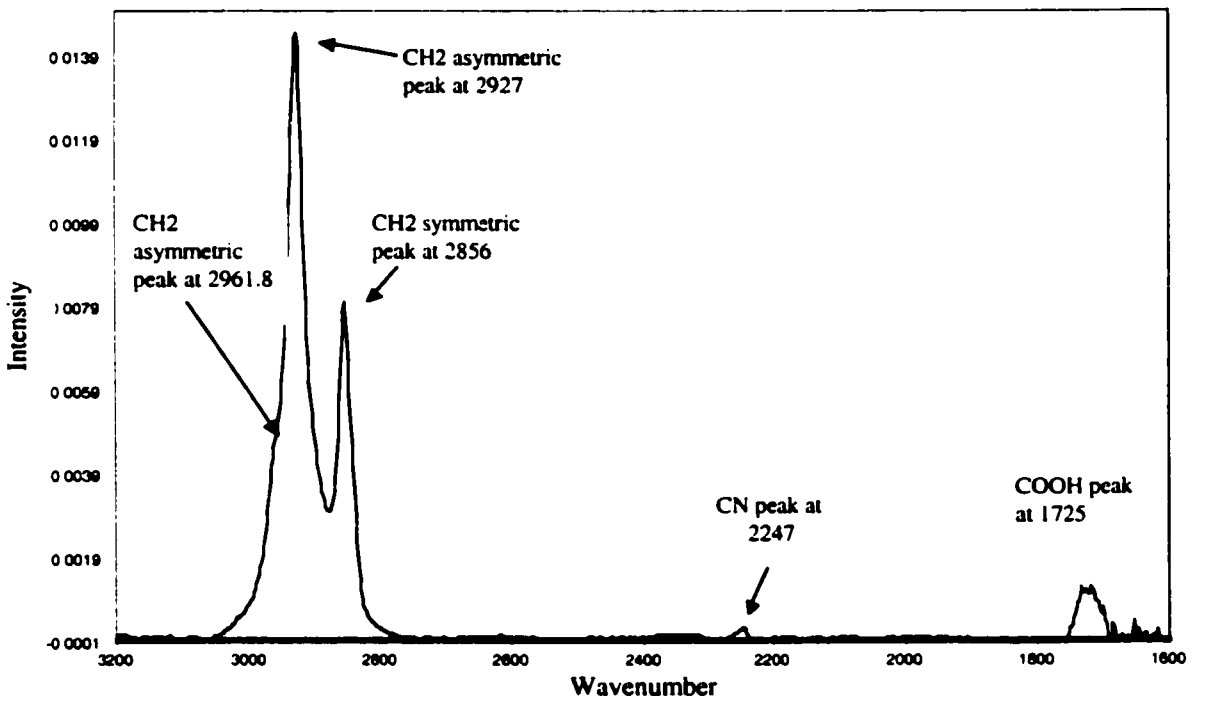

Figure 4.1: Typical spectrum of CUTMS monolayer formed on a Silion crystal

	CH_2 asymmetric	CH_2 symmetric	CN	COOH
Liquid CUTMS	2930	2857	2250	-
CUTMS monolayer	2927	2856	2248	1725

Table 4.2: Peak positions of important vibrations of between CUTMS liquid and monolayer spectra. The difference in spectral values is not considerably different, indicating that the monolayer formed resembles a liquid-like structure.

Solvent Used	CH_2 asymmetric	CH_2 symmetric
Chloroform	2927	2856
Hexadecane	2928	2857
Toluene	2927	2856

Table 4.3: Peak Positions of methylene symmetric and asymmetric vibrations of CUTMS monolayer prepared in different solvents. Data shows that there is no considerable effect of solvent on the monolayer structure of CUTMS.

	CH_2 asymmetric	CH_2 symmetric
OTS Self-assembled Monolayer	2919	2850
Stearic Acid LB Film	2917	2949.6

Table 4.4: Peak positions of methylene symmetric and asymmetric vibrations for OTS self-assembled monolayer and Stearic acid LB film. Both of them form a densely packed, crystalline structure.

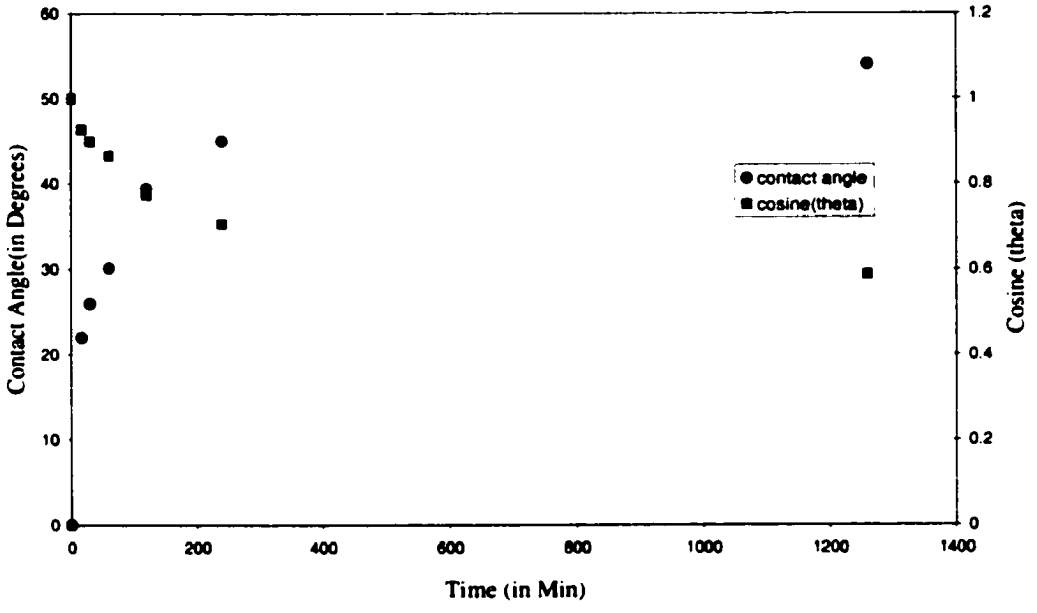

Figure 4.2: Variation in contact angle of the CUTMS monolayer with increase in deposition time.

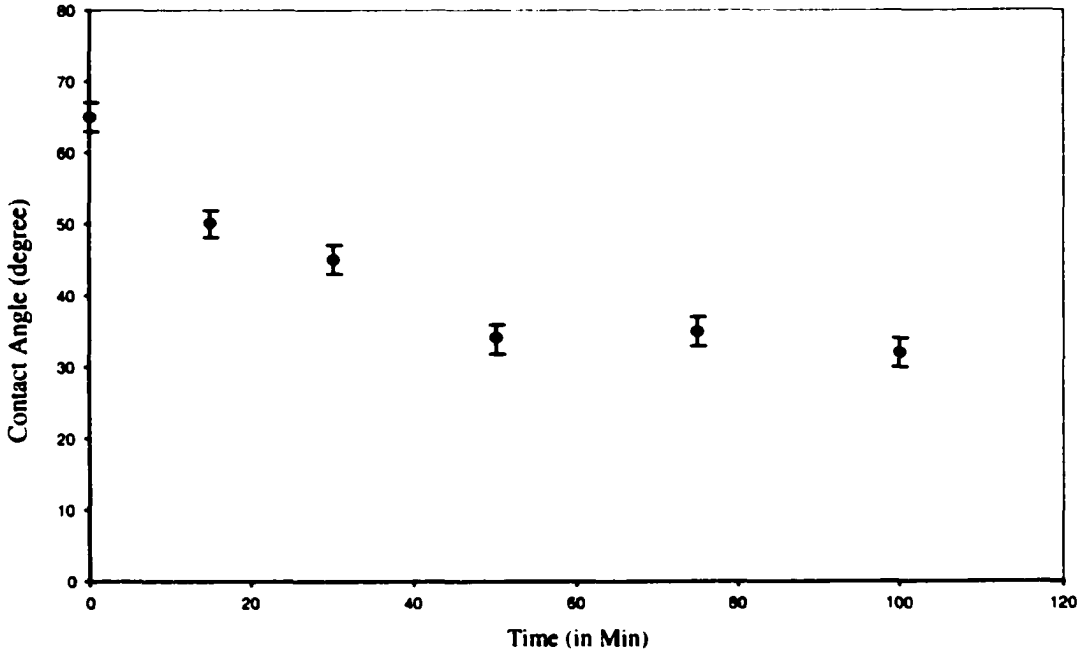

Figure 4.3: Variation in contact angle as reaction proceed

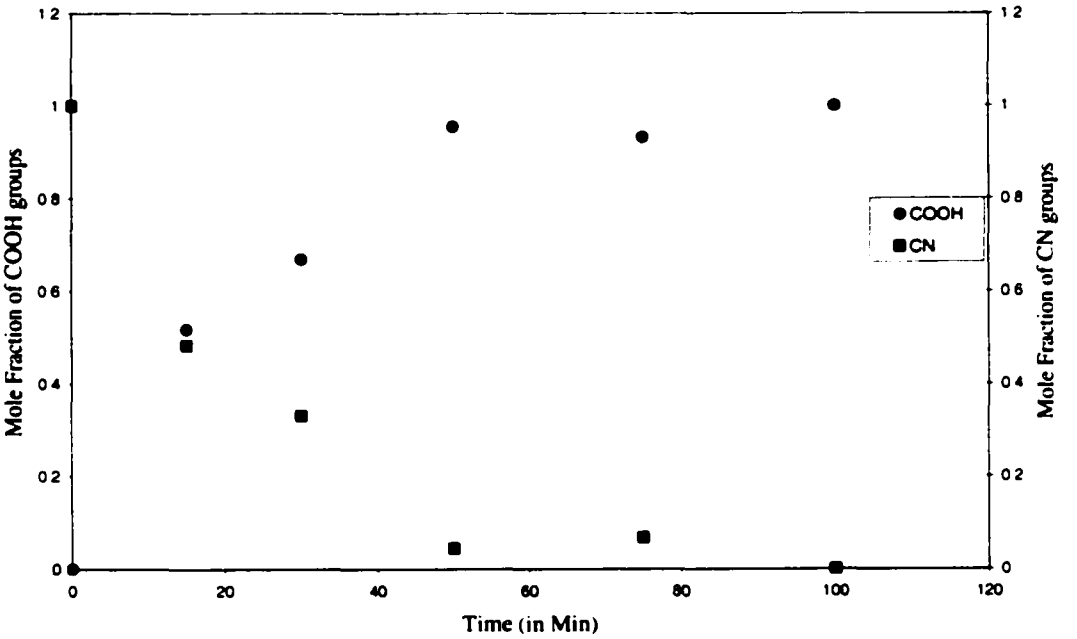

Figure 4.4: Fraction of COOH and CN groups present on the surface as the reaction proceeds (calculated using Cassie Eqn)

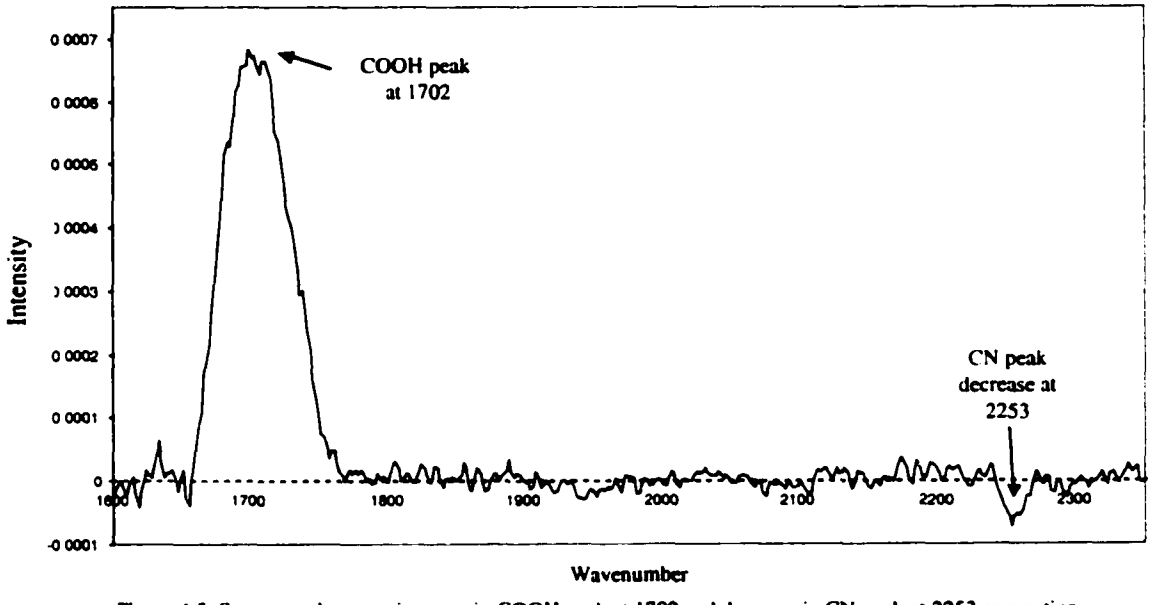

Figure 4.5: Spectrum shows an increase in COOH peak at 1702 and decrease in CN peak at 2253 as reaction proceeds

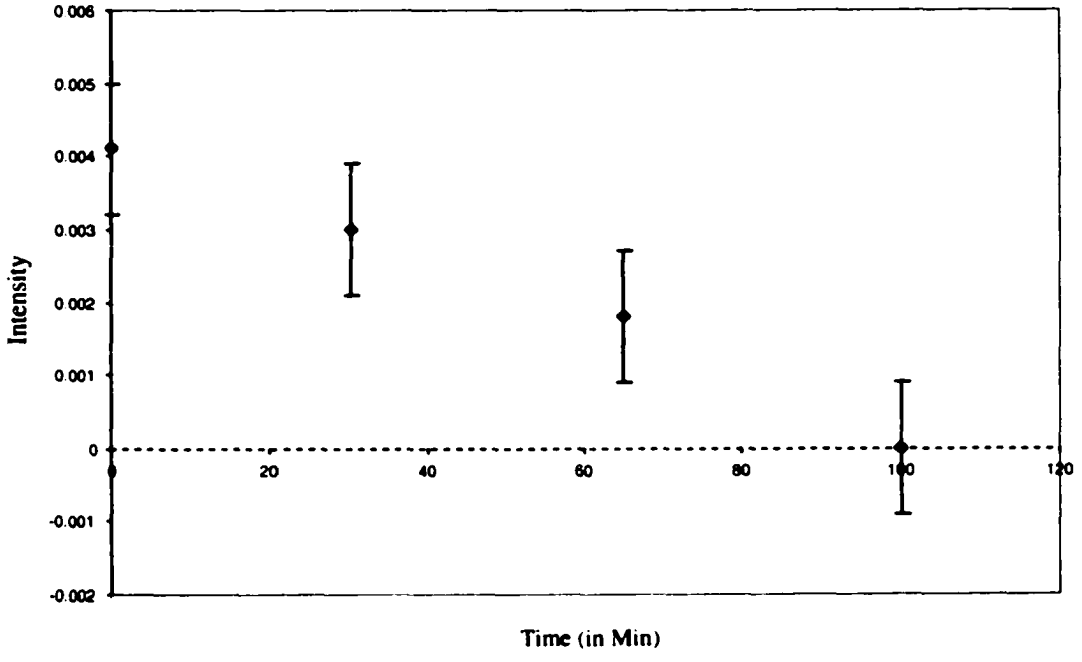

Figure 4.6: Decrease in CN peak intensity as reaction proceeds

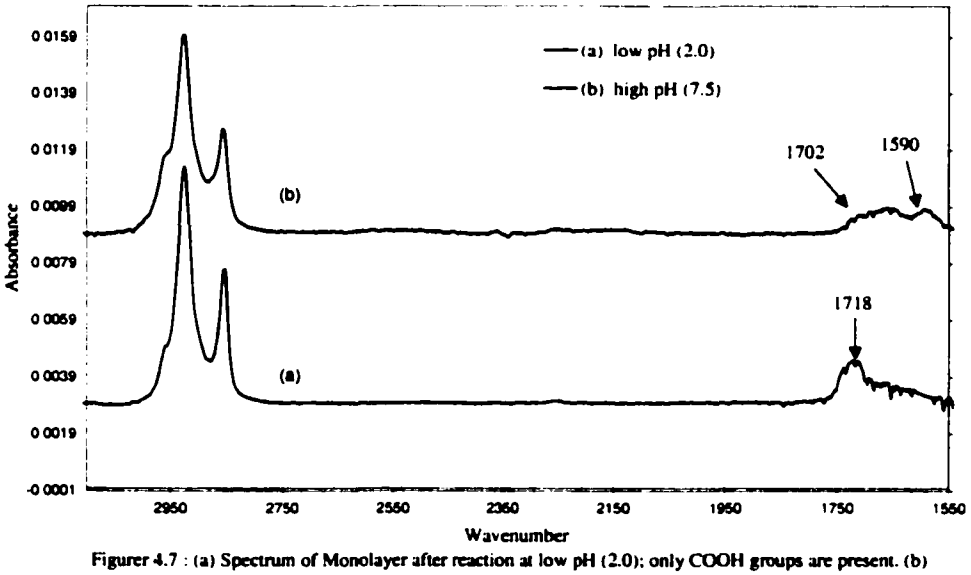

Figurer 4.7 : (a) Spectrum of Monolayer after reaction at low pH (2.0); only COOH groups are present. (b) spectrum of monolayer at pH 7.5 after reaction; both COOH and COO- exist

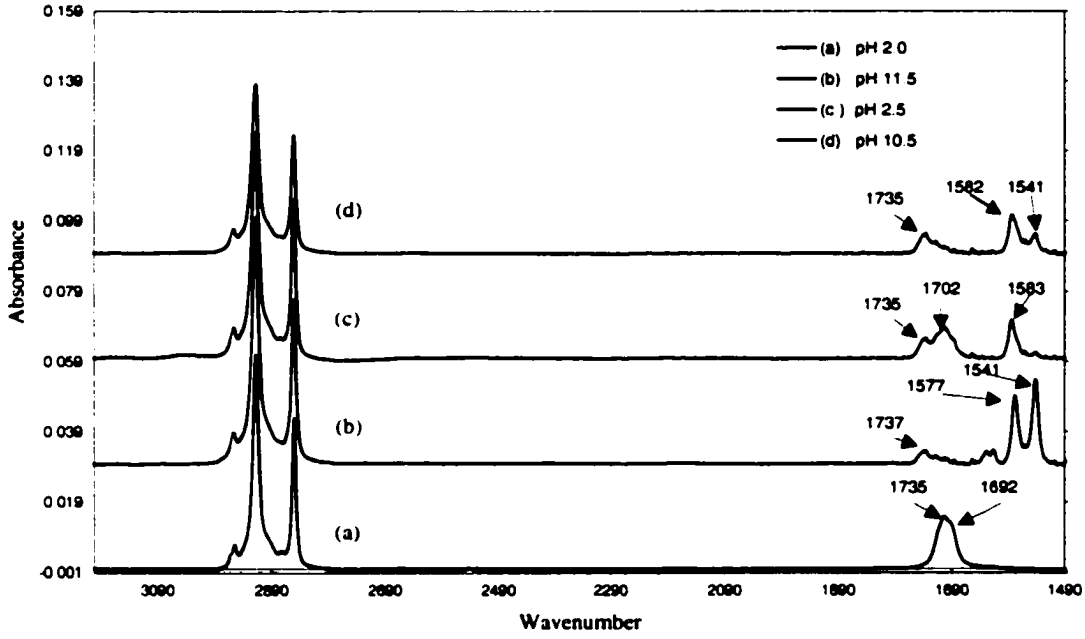

Figure 4.8: (a) LB Film of stearic acid at pH 2.0 (b) LB film immersed in calcium chloride solution of pH 11.5 (c) LB Film again immersed in a solution pH of 2.5 (d) again immersed in a sodium hydroxide solution of 10.5

	COOH		A_{COOH}	COO^-		A_{COO^-}
	Unbound monomers	Bounded dimers		Unbound monomers	Bounded dimers	
pH at 2.0	-	1702 & shoulder at 1692	0.5260			-
pH at 11.5	1737	-	0.0695	1577	1541	0.678
pH at 2.4	1735	1702	0.4229	1583		0.159
pH at 10.5	1735	-	-	1582	1541	-

Table 4.5: Peaks of COOH and COO^- (bounded and unbounded) of stearic acid LB film at various pH values. Integrated absorbance values are also given in the table. No differentiation was drawn between bounded and unbounded COOH and COO^- in the calculation of the integrated absorbance values.

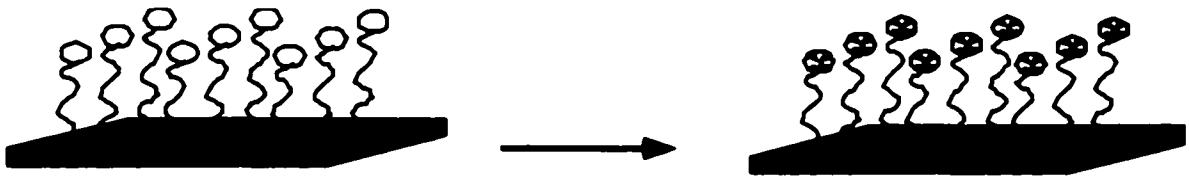

Assuming 100% converrsion and low pH

Figure 4.9 (a) : Cartoon of a CN terminated monolayer modified to COOH terminal groups. Conditions: 1:1 (v/v) of 15% HCl and Water at a temperature of 75^{o} C.

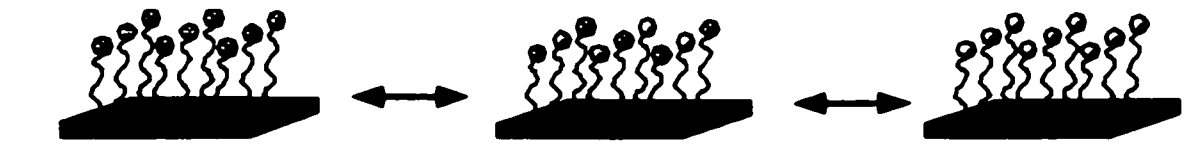

Figure 4.9 (b): Schematic showing the dependence of COOH terminal groups on pH of the environment. At low pH the surface is only covered with COOH groups and at high pH the surface is covered with COO^{-} groups., whereas at intermediate pH values, the surface is covered with both COOH and COO^{-} groups

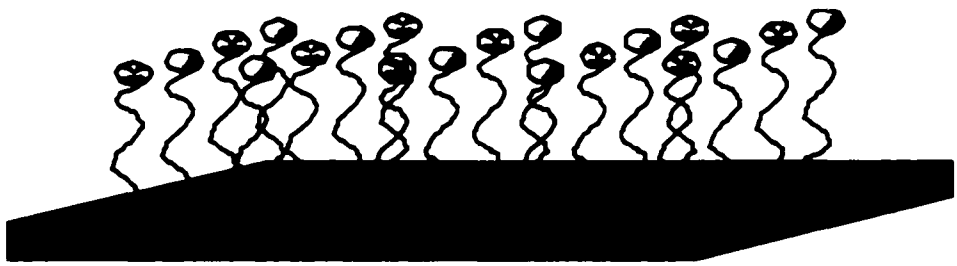

Is there any Spatial Arrangement if COOH and COO^{-} groups coexist?

Figure 4.9 (c) : Shematic showing the spatial arrangement of COOH and COO^{-} for a particular intermediate pH value. The spatial arrangement will be a strong function of pH as the ratio of $COOH/COO^{-}$ varies with pH of the surrounding environment.

Chapter 5

Self-Assembled Monolayers as Model Membranes: Absorption of Acetone and Hexane Vapors on Different Monolayers

5.1 Introduction

In the recent years there has been a considerable interest in designing material that can be used in membrane based separation applications as well as chemical sensing.[1-9] Such applications require simultaneously high mass transport throughput (permeability) and high component specificity (selectivity). Traditionally thick polymeric films have been used in such applications. The component selectivity is primarily derived from the specific interactions[10] between the probe and the film and permeability depends on the chemical structure, morphology, degree of polarizability, inter-chain forces, crystallinity to name a few. By increasing the thickness of the membrane, the separation process becomes primarily limited by slow diffusion process and high selectivity is achieved via the differences in relative transport rate through the membrane material. Never the less, since the process is diffusion limited, the permeability is affected considerably. Thin polymeric films offer the alternative by reducing the diffusion length scales and thus enhancing the permeability at the expense of selectivity. Hence, in most of the polymeric films used for separation or sensing processes, selectivity and permeability are inversely proportional, and a trade off has to be drawn between selectivity and permeability. For this purpose, there has been a growing interest in fabricating surfaces that can maximize both these properties simultaneously.

To this extent, self-assembled monolayers (SAMs) and Langmuir-Blodgett (LB) films offer as an excellent alternative as they are extremely thin, of the order of nanometers, and also for the ease with which they can be fabricated. The selectivity can also be fine tuned to the specifications by incorporating groups in the film that selectively interact with the molecule that has to be sensed or probe molecule. Moreover, by controlling the hydrocarbon chain length, the head group and the terminal functional group, the structure, morphology and packing density of both SAMs and LB films can be easily controlled. The terminal groups of these films can be modified into other functional groups by simple chemical transformations with out affecting the structural and packing properties of the SAMs and LB films. Thus these films provide us a tremendous tool by which the selectivity and permeability can be independently controlled without altering the other. Also, these films can be used as excellent model systems to study and investigate the specific interactions such as polar-polar, dispersive etc, which govern the selectivity. Specific groups to enhance selectivity can be incorporated in the thin polymer films also, but however, incorporation of these groups comes at the expense of the structural properties.

Researchers have been studying transport through LB films as early as when LB films gained prominence. But most of the initial studies were limited by the techniques available for analyzing the interactions at the molecular level. Transport properties of CO_2, N_2 and He gases through supported LB films were reported by Rose and Quinn.[11,12] The authors formed LB multilayers of stearic acid on a permeable membrane (experimental silicone copolymer XD-1) and determined the transfer coefficients of the gases by applying pressure gradient across the film. They observed

higher mass transfer coefficient for CO_2 despite its larger size when compared to N_2 and He. These studies showed that the transport through thin films is not just size-selective, but it also depends on the structure and the properties of the film and its interaction with the permeate. They also studied the effects of film structure and functional groups by looking into the permeabilities of oleic acid and cholestanol multilayers. They found the permeabilities of cholestanol to be comparable to those of stearic acid whereas oleic acid values were at least an order of magnitude larger. They also observed higher permeabilities in these LB films when compared to high-density polyethylene polymers. But there is one fundamental problem in these experiments. The flow of the molecules is driven by pressure difference applied across the film. Thus transport properties evaluated are affected by the inherent pinholes present in the film.

More recently, transport properties of water and pentane in LB films was reported by Vanderlick et al.[13] The authors formed multilayers of arachidic acid on the quartz crystal and investigated the transfer properties, using QCM, by monitoring the change in fundamental frequency of the crystal with increase in mass of the film, upon exposure to vapor as a function of pressure. In addition, surface adsorption and solubility were measured by examining films of different thicknesses. They also studied the effect of both aging and annealing of LB films on vapor penetration, and noticed that the vapor penetration depended on the state of the film. The differences observed in the transport properties of water and pentane vapors were attributed to the chemical nature and structure of the monolayer. They reported, water, being polar, resided near the polar terminal group (COO-) of the arachidic acid. But they left to speculation about the pentane vapors interactions. Diffusivity of these vapors was calculated from the rate of

uptake. Fickian diffusion coefficients for water and pentane were found to be $4x10^{-12}$ cm^2/s and $1x10^{-12}$ cm^2/s, respectively. Diffusion coefficient of bulk water in calcium stearate was estimated by Marshbanks et al[14] using FTIR-ATR technique. They found the value to be in the range between $1x10^{-10}$ cm^2/s to $1x10^{-13}$ cm^2/s. Value of $1.7x10^{-11}$ cm^2/s for diffusion coefficient of water in the polymer, polyvinylalcohol, was reported by Long and Thompson.[15] However, the value for diffusivity of water through polymer, cellulose acetate, reported by Perrin et al[16] varied by three orders of magnitude to those reported by the above authors. These studies indicate that the diffusivities depend on the membrane characteristics.

Contradictory reports can be widely seen in the literature pertaining to the penetrability of vapors through the monolayers. Lot of researchers contest whether the molecules actually penetrate through the monolayer or just adsorb at the surface.[17-19] For example, carefully prepared monolayers of saturated long-chain fatty acids (C_{17} to C_{20}) at the water-air interface were reported to reduce the rate of water evaporation by factors as high as 10^4 relative to that from the free water surface,[20] and built-up films of cadmium arachidate of six monolayers thick were found to block completely access of water to the underlying surface,[21] while, on the other hand, relatively large molecules were reported to diffuse without difficulty through a large number of monolayers in LB built-up films of same or similar surfactants.[13,18,19]

Performance of SAMs as barrier layers for corrosion protection of copper was investigated by Laibinis et al.[22] The copper metal with protective layer on it was exposed to oxygen at 100% relative humidity, and the efficiency of these layers as a function of monomer chain length was studied. Penetration of O_2 decreased linearly with increased

chain length. Greater resistance to penetrability of O_2 with increased chain length was attributed to crystalline characteristics exhibited by long chain alkanethiols due to enhanced van der Waals interactions. The monolayers lost their crystallinity due to the restructuring of the hydrocarbon chains during extended exposures to O_2. These studies clearly demonstrate that the penetration through monolayers depends on the crystalline state of the monolayers.

Schierbaum and co-workers[7] have observed selective molecular recognition of perchloroethylene by self-assembled monolayers of cavitand receptors using QCM. The authors attributed this to host/guest interactions. Selective adsorption of optical isomers, which have identical physical and chemical properties in a non-chiral environment, was also observed by modified self-assembled monolayers.[23] The authors were able discriminate the enantiomers by creating a non-chiral environment by modifying the polysiloxane surface. Very recently, Ricco et al[24] have used FTIR- ERS (Fourier Transform Infrared -External Reflection Spectroscopy) to get the chemical information during the sorption process. However in this mode, the spectra of both vapor phase probes and surface-confined probes present in the cell are obtained simultaneously during probe dosing.

Adsorption of vapors of various organic components, ranging from polar, apolar and aromatic, on metal and modified interfaces was investigated by Karpovich et al.[19] The authors formed SAMs of octadecanethiol and 11-mercapto-1-undecanol on gold surfaces and investigated the sorption properties using QCM, BET and Ellipsometer techniques. They observed penetration of certain vapors through octadecanethiol but none through 11-mercapto-1-undecanol. They concluded that penetration of vapors in

monolayers is not just size-selective, but it also strongly depends on dipolar properties of the vapors.

One of the aims of this work is to gain insight into the molecular interactions that govern the absorption processes, and to that extent, we are interested in looking into the absorption of various organic vapors ranging from polar, non polar to aromatic vapors. In this regard, we have used Fourier Transform Infrared spectroscopy (FTIR) in Attenuated Total Internal Reflection (ATR) mode to study and investigate the sorption properties of vapors of acetone and hexane on self-assembled monolayers varying in hydrocarbon chain length and terminal functional group. FTIR spectroscopy is a very good experimental technique for sorption studies as it reveals information, simultaneously, on the structural changes that occur in the film, as absorption process proceeds, and also on the probe molecule. From the absorption frequencies of the probe molecule and structural changes in the film, qualitative information on the mechanism of the absorption process, and the interactions that play a prominent role can be easily discerned. Moreover, this technique could safely be used for quantitative analysis also. We have considered, in this study, SAMs of octadecyltrichlorosilane (OTS), undecyltrichlorosilane (UTS), 11-cyanoundecyltrimethoxysilane (CUTMS) and aminopropyltrimethoxysilane (APS) formed on silicon substrates. The above mentioned SAMs vary in structure, thickness, packing density and also terminal functional groups, as discussed in chapter 3, thus providing the information on the effects of each of these properties on the absorption processes. As control experiments, adsorption of volatile organic vapors is also carried on clean Si crystal to study the effects of the presence of a thin film on the crystal.

In this chapter we report the results of the sorption of vapors of acetone and hexane on the above mentioned SAM surfaces. Acetone is chosen for the sensitivity offered by the carbonyl (C=O) group of the acetone molecule. Stretching frequency of carbonyl group of acetone molecule depends on physical state in which it is present, for example, whether it exists in the vapor, liquid, hydrogen bonded or solid form (state). For instance, C=O of acetone present in vapor, liquid or solid (adsorbed or hydrogen bonded) state exhibits vibrational frequencies at 1740, 1720 or 1702 cm^{-1} respectively. The adsorbed state in turn has two subdivided states (i) whether the C=O is hydrogen bonded to two neighboring molecules for which case the vibrational frequency is at 1690 cm^{-1} or (ii) hydrogen bonded to one adjacent molecule for which the frequency is at 1702 cm^{-1}.[25] In general, the stretching frequency decreases with increase in the rigidity of the form, i.e., carbonyl group exhibits lower frequency while it exists in solid form and higher frequency while it exists in vapor form. The schematic in figure 5.1 depicts this. This phenomenon of carbonyl group will provide an insight into the state in which the acetone molecule is present in the SAM matrix, the important interactions that govern the absorption process, and also whether the molecules diffuse and penetrate through the monolayer or just adsorb at the surface.

We have chosen hexane vapors for multiple reasons. First of all, hexane is non polar and would like to understand how the polarity of the adsorbate affect the absorption process. Secondly, hexane is one of the short chain alkanes, and alkanes, even though they are the simplest of the organic molecules, they often play an important role as building blocks in various organic materials such as surfactants, liquid crystals, and polymers. The physico-chemical properties of these organic materials are influenced by

including alkyl chains, and in particular cases, these properties are dominated by those alkyl chains. Thirdly, as discussed in chapter 3, the molecular orientation, structure and morphology of the monolayers formed depend on the alkyl chain length. We would like to investigate, apart from the sorption properties, whether the orientation of these hexane vapors can be controlled by the structure of the underlying monolayer.

5.2 Experimental Section

5.2.1 Materials

11-cyanoundecyltrimethoxysilane (CUTMS) is purchased from Gelest, Undecyltrichlorosilane (UTS) was purchased from United Chemical Technologies and Octadecyltrichlorosilane (OTS, 95% purity) and Aminopropyltrimethoxysilane (APS) are obtained from Sigma Aldrich Co. Chloroform, Toluene, Acetone and Hexane are purchased from Fisher Scientific. Carbon tetrachloride and Hexadecane of anhydrous grade are purchased from Sigma Aldrich. Silicon wafers used are obtained from Montco Silicon Technologies. The silicon wafers used in our experiments are of thickness-450-500μm, double sided polished and of orientation (111). Silicon Internal Reflection Elements (dimensions: 50x10x3 mm and orientation (111)) used for Infrared Spectroscopy are obtained from Harrick Scientific. Concentrated sulfuric acid is obtained from Fisher Scientific and the Nochromix crystals used for cleaning purposes is obtained from Godax Laboratories. All Chemicals are used as purchased without any further purification except Hexadecane, which is saturated with water by flowing water vapor

under a hood for about 48 hours. Deionised water with a resistivity of 18MΩ cm from a Millipore System is used in all our experiments.

Cleaning Protocol: Described in chapter 3.

Monolayer Preparation: Described in chapter 3.

5.2.2 Flow Conditions

The experimental set up for flow experiments is shown in figure 5.2. Dry N_2 gas is passed through the bubbler, containing volatile organic solvent (acetone or hexane), to generate saturated acetone vapors. N_2 gas is passed through the drierite in order to remove any trace amounts of water vapor present in the N_2 gas as IR spectroscopy is very sensitive to water vapors and may interfere with the C=O stretching frequency bands. Saturation of organic vapors is assured by using multiple bubblers, with spargers, in series. Spargers are used to generate small bubbles, thus increasing the area of contact between the solvent and gas bubble and allowing the solvent and gas bubble to reach equilibrium easily. These saturated organic vapors are passed over the flow cell in the FTIR instrument containing silicon substrate coated with a monolayer. Kinetics of the sorption process was studied by collecting spectra at regular intervals. A second stream of dry N_2 is used to control the partial pressure of the vapor. The two streams are mixed before the vapors entering the flow cell of the experimental set up. For partial pressure experiments, we started the flow conditions for the lowest partial pressure of interest and gradually increased the partial pressure in steps until reaching saturated vapor conditions. In all the experiments, the vapors are flown for exactly 20min for each partial pressure

and thus controlling the affects of time for which vapors are flown on the results. We chose 20min because in the kinetic studies, we realized that the absorption process reached equilibrium with in 20 minutes on all monolayers under study.

5.2.3 Quantitative Prediction of Molecular Coverage

In all the quantitative analysis in this chapter, the total amount of acetone and hexane absorbed on monolayers is considered proportional to the integrated area under wavenumbers 1622.53-1827.03 cm^{-1} and 2820-3020 cm^{-1}, respectively. We have assumed same molar absorptivity (ε) value for carbonyl group (C=O) of acetone molecule present in various states. We also assumed the molar absorptivity (ε) values of CH_2 symmetric and asymmetric peaks and also of CH_3 symmetric and asymmetric peaks of hexane molecules to be independent of the orientation, conformation and molecular coverage of the hexane molecules. Technically, as described and argued in chapter 3, the molar absorptivity (ε) coefficient depends on the physical state, orientation and molecular coverage and, ε value might vary considerably depending on the intermolecular interactions. However, since we are only interested in the relative absorption values of acetone vapors on different monolayers, we believe that our assumption will not lead to any serious errors in our final qualitative analysis and conclusions.

5.3 Results and Discussions

5.3.1 Structure, Morphology, Orientation and Packing density of OTS, UTS, CUTMS and APS Monolayers

The sorption properties of gases or vapors greatly depend on the structure, morphology, orientation and packing density of the film apart from the void fraction,

polymer (monolayer)-penetrant (vapor probe) interactions. So it is essential to know the structure, morphology, orientation and packing density of the monolayers under study before we try to analyze the sorption and diffusion properties of the penetrants. The above properties of the self-assembled monolayers under study are discussed in great detail in chapter 2.

5.3.2 Absorption of Acetone Vapors on Monolayers

In the following section, absorption of acetone vapors on fully characterized monolayers of OTS, UTS, CUTMS, APS and on clean Silion crystal are discussed. For quantitative analysis, the area of C=O peak between 1622.53 and 1827.03 cm^{-1} wavenumbers is used in all the experiments for consistency.

Typical adsorption kinetics of acetone vapor on a clean silicon crystal is shown in figure 5.3. With in 20 minutes, as can be seen from figure 5.3, the adsorption process reached equilibrium. Similar kinetic pattern is observed for absorption of acetone on other SAM surfaces under investigation. However, the amount of acetone absorbed depended on the adsorbing surface as can be seen from figure 5.4. Acetone showed higher affinity for the polar surfaces and vice versa. We shall discuss this, in detail, later in the chapter. The state of the binding of acetone vapor molecules strongly depended on the structure of the monolayer, the terminal functional group of the monolayer and, of course, on the packing density of the monolayer. All these factors also play an important role in the total amount of acetone absorbed on the monolayers. Figure 5.5 shows the IR spectra of carbonyl group of absorbed saturated vapors of acetone on the different surfaces after equilibrium is attained. (The IR spectra of figure 5.5, and also for the

spectra shown from henceforth, are obtained with the background as the spectrum of the corresponding monolayer, on which the absorption is carried out). The C=O stretching frequencies of the adsorbed acetone on the various surfaces is shown in table 5.1. The shifts in the carbonyl stretching frequency of the adsorbed acetone vapor on different surfaces indicate the dependence of the binding state underlying monolayer.

On clean silicon surface the C=O stretching frequency appears at 1703 cm^{-1} indicating that acetone molecules hydrogen bond with the hydrophilic hydrated silicon surface. It is believed that a thin layer, about 3-4monolayers thick of thin water film, exists on the hydrated silicon surface. The acetone molecules hydrogen bond with the OH groups of the exposed water layer on the silicon surface. Even on dehydrated silicon surface, the acetone molecules tend to hydrogen bond with the exposed OH groups of the silicon surface. The shoulder at 1718 cm^{-1} indicates the presence of the physically absorbed or condensed acetone molecules. The shoulder at the 1737 cm^{-1} is due to the acetone molecules present in the bulk vapor phase. Even though the IR in ATR mode gives information at the interface of the ATR element, the evanescent wave of the internally reflecting IR wave has a penetration depth, d_p , in the order of microns (μ) and it is a function of the wavelength. However, the thickness of all the surfaces under study are of angstroms, order of magnitude lesser than the penetration depth, which is equivalent to the sampling length. Thus, in all our experiments, we obtain some information from the bulk, pertaining to the vapor phase of the acetone molecules. The mechanism involved is quite simple. Initially, the acetone molecules present in vapor phase adsorb on to the OH groups present on the Si substrate. Once the OH group sites

are filled, the acetone vapors physically adsorb on the surface until the chemical coefficients for acetone present in the vapor and adsorbed phase become equal.

A similar phenomenon is observed on CUTMS monolayers, which are hydrophilic in nature to an extent. As can be seen from the figure 5.5(a), the IR spectum of acetone absorbed on CUTMS monolayer, the peak is centered at 1716 cm^{-1} indicating the prominence of physical sorption to chemical sorption (hydrogen bonding). A small shoulder at 1704 cm^{-1} indicates that some amount of hydrogen bonding takes place between the CUTMS monolayer and the acetone molecules. As described in chapter 3 and 4, CUTMS forms a liquid-like, disordered structure, indicating that surfactant molecules align in a random manner to the normal of the surface of the silicon substrate. Thus exposing the hydrogen of the methylene groups, present adjacent to the terminal CN groups, to hydrogen bond with the absorbing acetone molecules. APS is identical to that observed on CUTMS monolayer except for the fact that more amount of acetone is absorbed on APS surface owing to the higher hydrophilicity of it's surface compared to CUTMS monolayer. Also NH_2 terminal groups of APS surface can directly hydrogen bond with the absorbing acetone molecules. One can also envision the methylene groups, present adjacent to the terminal amine groups, to participate in hydrogen bonding as in the case of the CUTMS monolayer as APS also forms a disordered structure as discussed in the chapter 2. However, it is difficult to predict from the experimental data and also from the experimental set up what fraction of acetone is hydrogen bonding with the amine groups and what fraction hydrogen bonding with the adjacent methylene groups.

From Figure 5.4, the amount of acetone absorbed on OTS is considerably less when considered to that of adsorbed on clean Silicon substrate indicating that acetone

shows preferable affinity towards polar surfaces. As discussed earlier, OTS surface is exposed with hydrophobic methyl groups, which are incapable of forming hydrogen bonding. This can be clearly seen from the figure 5.5(b) showing the spectrum of acetone absorption on OTS monolayer. Peak at 1726 cm^{-1} corresponds to the physically adsorbed acetone molecule on OTS monolayer due to non-specific van der Waals interactions. Peak at 1738 cm^{-1} corresponds to the acetone vapors present in the overhead space of the flow cell. OTS monolayer is a densely packed monolayer and is difficult for acetone molecules to diffuse through the monolayer. Absence of hydrogen-bonded acetone confirms the impermeability of OTS monolayer to the acetone molecules. However, sometimes the absorption behavior of acetone molecules is quite contradictory to what is anticipated. Acetone showed absorption frequencies about 1704 cm^{-1} indicating the formation of hydrogen bonding. This we believe is because of the presence of pit holes or inhomogeneity in the OTS monolayer preparation. The spectrum of acetone absorbed on the OTS surface greatly depended on the structure and morphology of the OTS monolayer itself. Any presence of pit holes resulted in the formation of hydrogen bonding of absorbing acetone molecules on the uncovered silicon substrate.

We confirmed this fact by conducting absorption experiments on partially coated OTS monolayers. OTS formed island-like fractal structures for low deposition times and for temperatures below the transition temperatures. At these conditions, the OTS formed inhomogeneous, partially coated monolayer with molecules concentrated in small pockets covering only fraction of the silicon substrate, and rest of the area being uncovered by the OTS molecules. The fractional coverage of the OTS molecules, of course, depended on the deposition time. In our experiment, the temperature is maintained below the transition

temperature and deposition time of 1 min. The contact angle for the resultant partially coated monolayer is observed to be 60°, indicating the presence of mixture of OTS and clean surface. The fractional molecular coverage is calculated to be 10% of the uniform monolayer coverage. Method described in chapter 3 for calculation of monolayer coverages is used for calculation of fractional coverage of the OTS molecules in a partially coated monolayer. The spectrum of acetone absorbed on partially coated acetone molecules showed hydrogen bonding giving confidence to our premise of presence of pit holes causing formation of hydrogen bonds on the OTS monolayer. Other interesting result is that amount of acetone absorbed on partially coated OTS monolayer agreed reasonably well with the mixing rule

$$A_{partial} = f_{si}A_{si} + f_{ots}\,A_{ots} \qquad (5.1)$$

Where $A_{partial}$ is the amount absorbed on partially coated monolayer; A_{si} is the total amount of acetone absorbed on clean Silicon substrate; A_{ots} is the total amount of acetone absorbed on uniform OTS monolayer; f_{si} and f_{ots} are the fraction of clean Si surface and OTS surface available for acetone absorption.

Apart from this, even though it is difficult to visualize the diffusion of acetone molecules through densely packed OTS monolayers considering the packing density arguments, still some experiments showed evidence of acetone molecules actually penetrating the OTS monolayers. The evidence is again from the IR spectra. IR spectrum of carbonyl stretching frequency appeared at 1690 cm^{-1} indicating the formation of strong bonding. One plausible explanation could be the acetone molecule actually penetrating the OTS molecule through the monolayer and forming hydrogen bonds with the siloxane network present at the interface of the substrate and the monomer molecules forming

monolayer. The hydrogen bonding and the additional spatial constraint of acetone molecules being trapped in the monolayer adds rigidity or reduces the degree of freedom for the trapped-hydrogen bonded molecules, thus causing additional reduction in it's vibrational frequency. Similar observation of penetration of acetone molecules though OTS monolayers is made by karpovich et al adding confidence for our observed results and premises.

On the other hand, UTS monolayer, which has a lower packing density than the OTS monolayer showed some permeability to the acetone molecules. The evidence is drawn from the spectrum of acetone on UTS monolayer shown in figure 5.5 (c). Figure 5.5 (c) shows two peaks at 1719 cm^{-1} and 1738 cm^{-1} again corresponding to the physically adsorbed (due to non-specific van der Waals interactions) and vapor phase states of acetone respectively. Surface of UTS is also highly hydrophobic exposing methyl groups, but however, the physically adsorbed acetone on OTS and UTS monolayers differ by almost 7 cm^{-1} wavenumbers indicating that adsorption process is different for both the monolayers. Also physical adsorption of acetone molecules in presence of UTS monolayer is relatively stronger than in OTS monolayer. (This conclusion is drawn from the shift of vibrational frequency to lower wavenumbers). The plausible reason, we believe, for this shift in wavenumbers could be because of the acetone molecules being trapped inside the monolayer.

5.3.2.1 Effect of Partial Pressure

We have performed the sorption of acetone on various monolayers as a function of partial pressures to obtain the sorption isotherms and also to understand the type of

sorption that occurs on these systems. The equilibrium amount of vapor sorbed by a polymer versus external vapor activity (or pressure) at a particular temperature forms a sorption isotherm. It illustrates the thermodynamic equilibrium of the system and it also depends on the relative strengths of the interactions between the penetrants (sorbed molecules) and the polymer or between the penetrant themselves. Five types of sorption isotherms have been identified in polymer systems and they are: (i) Henry's law sorption, (ii) Langmuir-type sorption (iii) Flory-Huggins sorption (iv) BET-type sorption and (v) Dual-mode sorption.

The chemical nature of the penetrant and the chemical structure and morphology of the polymer play important roles in the mode of sorption. Henry's law sorption is an ideal solution behavior and may occur if there are no site-specific interactions between a penetrant and the polymer, or if the penetrant is evenly distributed in the polymer, or if the sorption amount is relatively small (<0.2%), and or if the dimension of the polymer matrix is not altered significantly by the sorbed penetrant. Langmuir-type sorption resulted from the site-specific interaction between a penetrant and the polymer when the number of sites is limited, such as hydrogen bonding formed between a polar penetrant and the hydroxyl end groups in some polymers and preferential sorption of gases in the cavity of a glassy polymer. Flory-Huggins sorption usually takes place in a rubbery polymer in which a penetrant can significantly plasticize the polymer matrix, the penetrant-penetrant interaction is strong enough to induce further sorption once a penetrant enters the polymer, and the sorption amount is relatively large so that the dimension of polymer matrix may increase, i.e., swelling. Usually Langmuir-type sorption does not exist alone without other types of sorption in polymer materials. BET-

type sorption is a combination of Langmuir-type and Flory-Huggins and the dual mode sorption is a combination of Langmuir-type sorption and Henry's law sorption.

Figure 5.6 shows the integrated intensity of the acetone vapors absorbed on clean silicon crystal with time. In the experiment, the flow is started with partial pressure of 0.05 and gradually increased in steps until it reached saturated vapor pressure. The flow is carried for 20 minutes for each partial pressure. As can be seen from figure 5.7, the absorption reached plateau after every 20 minutes, before the partial pressure of the acetone vapors is increased to next higher value. This indicates that absorption is reaching equilibrium for each partial pressure in our partial pressure flow experiments. Similar trends are seen for absorption of acetone vapors on other surfaces. Figure 5.7 shows the sorption isotherms of acetone vapors on all the surfaces. The sorption isotherms follow a linear curve until partial pressure of about 0.25 and after partial pressure of 0.3, the absorption attained plateau. However there is a sharp deviation from the plateau at saturated vapor pressures on all the surfaces. This sharp increase in the absorption is due to the dominance of physical absorption or condensation of acetone vapors at saturated pressures. The curves seem to indicate that the sorption isotherms resemble Langmuir-type sorption. We will discuss this in detail in the next section. Before that let us discuss a little bit more on the molecular interactions that play prominent role at various partial pressures on these surfaces.

Figures 5.8-5.13 show the spectra of acetone absorption at different partial pressures at various surfaces. The results qualitatively agree with those discussed already in the earlier section. However, some insights into the interactions can still be drawn at low vapor pressures by following the IR spectra. As can be seen, the vibrational

frequency of C=O bond of absorbed acetone molecules shift from lower wavenumbers to higher wavenumbers (i.e. from right to left in the spectrum). This indicates that at low partial pressures, only the specific interactions such as hydrogen bonding dominate the absorption process and, with increase in partial pressure physical sorption becomes prominent. At low partial pressures, the concentration of acetone is less, so there is abundance of specific sites available for absorption of acetone vapors and acetone molecules participate in hydrogen bonding. However, once all the specific sites are occupied at high acetone vapor concentrations then, penetrant-penetrant interactions, in our case, acetone-acetone interactions or in a more generic way, physical sorption or condensation regains dominance. Specific interactions dominate the initial absoOrption process if the specific sites are easily accessible for absorption, if not then non-specific interactions dominate the initial absorption process. Since, in all our experiments, the frequency values shift from lower to higher, we believe that the specific sites for hydrogen bonding of acetone molecules are easily accessible on all the surfaces. This mechanism is observed for all the surfaces.

5.3.2.2 Langmuir Sorption Model

Irving Langmuir devised a simple model involving a thermodynamic equilibrium to predict the fraction of solid surface covered by an adsorbate as a function of its gas pressure.[22] This was later extended to liquid systems, where the equilibrium involved concentrations in solution. In this model adsorbate molecules adsorb on sites on the adsorbent surface (monolayer).

Model equation:

$$x/v = x/v_m + 1/kv_m \quad (5.2)$$

where $x = p/p_o$ is the partial pressure, p is the inlet vapor pressrue and p_o is the saturated vapor pressure, v_m = monolayer coverage, and k = rate of condensation/ rate of evaporation.

5.3.2.3 Assumptions in the Langmuir Model

Langmuir had to make several assumptions in order to derive an (admittedly over-simplified) adsorption expression:

- all surface sites have the same adsorption energy for the adsorbate (and a similar statemt for the solvent)
- adsorption (of either solvent or adsorbate) at one site doesn't affect the availability of (block) the next site to adsorb solvent or adsorbate
- adsorption (of either solvent or adsorbate) at one site doesn't affect the energy of adsorption of the neighboring sites (as they adsorb either solvent or adsorbate)
- the activity of the adsorbate is directly proportional to its concentration (and a similar statement for the solvent)

These assumptions are not satisfied for many real-life cases. However, the simplified version gives insight into the dependence of surface coverage on concentration in solution. The driving force for adsorption on the surface is proportional to the concentration of the species in solution. The driving force for desorption from the surface is proportional to the fractional surface coverage of the species on the surface.

The langmuir parameters, k and v_m are evaluated by fitting the linear regime of the experimental data with the model. The fit is shown in figure 5.14 (a) and the estimated parameter values are shown in table 5.2. The model and experimental data

agree well as shown in figure 5.14 (b). The model tends to deviate at saturated vapor pressures where the physical sorption becomes prominent. As described, langmuir model does not take into consideration the affects of physical sorption and also formation of multilayers. Monolayer coverage, v_m increases monotonically with the hydrophilicity of the adsorbent.

5.3.2.4 BET Model

BET model is related to Langmiur except that sorption may occur at multiple layers. In this model, each layer is modeled by Langmuir isotherm and assumed that the second layer may form before first is saturated. In general, the n^{th} layer can start forming before the saturation of the $(n-1)^{th}$ and the layers below that. It is assumed, in this model too, that the sorption occurs at fixed sorption sites.

BET model equation:

$$x/[v(1 - x)] = 1/v_m c + (c-1)/ v_m cx \qquad (5.3)$$

$x = p/p_o$, partial pressure of the adsorbate

v = volume of vapor adsorbate sorbed

p = equilibrium pressure of the adsorbate

p_o = saturation pressure of adsorbate

v_m = volume of gaseous adsorbate absorbed when the entire surface is covered with a complete monolayer

c = constant related to heat of sorption

The BET parameters, c and v_m are evaluated by fitting the linear regime of the experimental data with the model. The fit is shown in figure 5.15 (b) and the estimated

parameter values are shown in table 5.3. The model deviates considerably from the experimental data indicating that the formation of multilayer is not the essential mode of absorption of acetone on these surfaces.

5.3.2.5 Effect of Surface Tension on Absorption

Interfacial tension plays an important role for processes occurring at micron, nano and molecular level. In this section we will discuss how the interfacial tension or the polarity of the absorbing surface correlates with the amount of absorption of acetone on these surfaces.

The surface tension of a solid polymer cannot be measured directly, as reversible formation of its surface is difficult. Many indirect methods have been proposed, including the liquid homolog (molecular weight dependence) method, polymer melt (temperature dependence) method, equation of state method, harmonic-mean method, geometric mean method, critical surface tension method, and others. We have used Geometric mean (GM) method and Harmonic mean (HM) method for evaluation of surface tension of the monolayers. Both GM and HM methods use the contact angles of two testing liquids and respective mean equations. The equations are given below:

Harmonic Mean Equation:

$$(1+ \cos(\theta_1)) \gamma_1 = 4\{ \gamma_1^d \gamma_s^d / (\gamma_1^d + \gamma_s^d) + \gamma_1^p \gamma_s^p / (\gamma_1^p + \gamma_s^p) \} \quad (5.4)$$

$$(1+ \cos(\theta_2)) \gamma_2 = 4\{ \gamma_2^d \gamma_s^d / (\gamma_2^d + \gamma_s^d) + \gamma_2^p \gamma_s^p / (\gamma_2^p + \gamma_s^p) \} \quad (5.5)$$

Geometric Mean Equations:

$$(1+ \cos(\theta_1)) \gamma_1 = 2\{ (\gamma_1^d \gamma_s^d)^{0.5} + (\gamma_1^s \gamma_s^s)^{0.5} \} \quad (5.6)$$

$$(1+ \cos(\theta_2)) \gamma_2 = 2\{ (\gamma_2^d \gamma_s^d)^{0.5} + (\gamma_2^s \gamma_s^s)^{0.5} \} \quad (5.7)$$

where $\gamma = \gamma^p + \gamma^d$ and subscripts 1 and 2 are for the testing liquids 1 and 2, respectively. If γ_i^p and γ_i^d, the polar and dispersive components of the testing liquids (i = 1 and 2) are known, then by solving the equations (5.4) and (5.5) or (5.6) and(5.7), the polar and dispersive components of the monolayer surface can be obtained. θ_1 and θ_2 are the contact angles of the testing liquids on the surface. We have used water and methylene iodide as the testing liquids in our surface tension measurements. The values estimated from the equations (solved using Maple software) are shown in table 5.3.

The absorption of acetone increased monotonically with the increase in surface tension of the surface as shown in figure 5.16 (a). Also, the absorption increased monotonically with the polar component of the surface tension of the surfaces, however, the absorption showed scattered relation with the dispersive component of the surface tension of the surfaces as shown in figure 5.16 (b), indicating that the absorption of acetone is primarily driven by the specific interactions.

5.3.3 Absorption of Hexane Vapors on Monolayers

In the following section, absorption of acetone vapors on fully characterized monolayers of OTS, UTS, CUTMS, APS and on clean Silion crystal are discussed. For quantitative analysis, the area under specific wavenumbers (2820-3020 cm^{-1}) containing CH_2 and CH_3 asymmetric and symmetric peaks is considered in all the experiments for consistency.

The amount of hexane absorbed depended on the adsorbing surface as can be seen from figure 5.17. Contrary to expectations, hexane showed higher absorption on polar surfaces and lower absorption on non-polar surfaces, such as OTS and UTS monolayers.

We will discuss the reason for this anomaly later in the chapter. The state of the binding, packing and aligning of hexane vapor molecules strongly depend on the structure of the monolayer, the terminal functional group of the monolayer and, of course, on the packing density of the monolayer. All these factors also play an important role in the total amount of hexane absorbed on the monolayers. Figure 5.18 shows the IR spectra of hexane vapors absorbed at saturated pressures on the different surfaces after equilibrium is attained. (The IR spectra of figure 5.18, and also for the spectra shown from henceforth, are obtained with the background as the spectrum of the corresponding monolayer, on which the absorption is carried out). The stretching frequencies of CH_2 symmetric, asymmetric peak and CH_3 asymmetric peaks of the adsorbed hexane vapors on the various surfaces are shown in table 6.1. The apparent shifts and the different intensities in the vibrational frequencies of methyl and methylene stretches clearly indicate the strong dependence of the aligning and binding characteristics of absorbed hexane vapors on the underlying monolayer.

On clean silicon crystal, the absorbed hexane vapor showed methylene peak at 2932 cm^{-1}, indicating that the hexane formed a disordered like structure on the surface.((CH_2) asymmetric peak position is an indirect measure of the alignment of the molecule with the surface normal of the substrate). Moreover, the HHDP (half height distance between the peak) is broader indicating that the molecules of the absorbed hexane are not ordered. Hexane is a non-polar molecule and it can participate only in non-specific vander waals interactions. Silicon crystal though it has lattice order, the lattice structure cannot be induced on the absorbed hexane as silicon crystal does not have any specific active or binding sites for hexane molecules to adsorb that can control the structure of the

absorbed hexane. Thiol monolayers on gold or siloxane monolayers on silicon surfaces showed structure because of the specific interactions that take place between the head groups of the surfactant molecules and the substrate. Even with the presence of specific interactions, the structure depended on, apart from other factors, on the chain length of the surfactant molecule. In general, short chains formed a disorderd, liquid-like structure. So, hexane molecules, with the absence of any specific interactions with the silicon crystal formed a disordered structure. Similar experiments of adsorption of hexane on gold surfaces, revealed that the backbone of the alkyl chain of the absorbed hexane molecules are aligned almost parallel to the surface, and our results concur with that in the literature.[23]

On APS monolayer, hexane showed some order compared to that on clean silicon crystal. The shifts in methylene asymmetric and symmetric peaks towards lower wavenumbers confirm the gain in order in the structure of the absorbed hexane. APS monolayer, as described in chapter 2, even though formed a disordered, liquid-like structure, it still has some structure imparted to it by the lattice arrangement of the silicon crystal. As far as hexane is concerned, APS monolayer has some structure to it when compared to clean silicon crystal, and thus the absorbed hexane molecules showed some structure associated with the structure of underlying APS monolayer. Similar observations are made for the absorbed hexane on the CUTMS monolayers. The induced structure on hexane absorbed on CUTMS is slightly more ordered than that on APS owing to the greater order in CUTMS monolayer structure compared to APS monolayer. On UTS and OTS monolayers, hexane vapors formed an all trans configuration with the

hydrocarbon chain aligned perpendicular to the surface of the monolayers. (Evidence obtained from the IR spectra).

In general, the structure of the absorbed hexane vapors is greater than the corresponding monolayers on which the vapors are being absorbed. This is an interesting phenomenon, which can be exploited for technological purposes where the structure can be induced on to the absorbing molecules.

5.3.3.1 Effect of Partial Pressure

We have performed the sorption of acetone vapors on acetone molecules on various monolayers as a function of partial pressures to obtain the sorption isotherms and also understand the type of sorption that occurs on these systems.

Figure 5.19 shows the integrated intensity of the hexane vapors absorbed on clean silicon crystal with time. In the experiment, the flow is started with partial pressure of 0.05 and gradually increased in steps until it reached saturated vapor pressure. The flow is carried for 20 minutes for each partial pressure. As can be seen from figure 5.19, the absorption reached plateau after every 20 minutes, before the partial pressure of the acetone vapors is increased to next higher value. This indicates that absorption is reaching equilibrium for each partial pressure in our partial pressure flow experiments. Similar trends are seen for absorption of acetone vapors on other surfaces. Figure 5.20 shows the sorption isotherms of acetone vapors on all the surfaces. The sorption isotherms follow a linear curve until partial pressure of about 0.25 and after that deviations from the straight line can be seen. One aspect, which is found in all the experiments, contrary to expectations, is decrease in absorbed intensity at saturated vapor

pressures when compared to the flow partial pressure of 0.7. We believe that this is because of loss in hexane vapor due to condensation on the tygon tubing used for flow experiments. Let us first discuss a little bit more on the molecular interactions and how the structural and aligning properties get induced on the absorbed hexane vapors at various partial pressures on these surfaces.

Figures 5.21-5.25 show the spectra of hexane absorption at different partial pressures on various surfaces. The results qualitatively agree with those discussed already in the earlier section. However, some insights into the molecular alignmnet can still be drawn at low vapor pressures by following the IR spectra. As can be seen, the vibrational frequencies of methylene and methyl stretches of the absorbed hexane molecules shift slightly from higher wavenumbers to lower wavenumbers (i.e. from left to right in the spectrum). This indicates that at low partial pressures, the absorbed molecules are more disordered and with increase in packing density or the absorbed molecules on the surface, the alignment or structure in the absorbed molecules increases. This phenomenon is observed for all the surfaces. However, the extent of rearranging with increase in partial pressure varies slightly from surface to surface.

The extent of structure inducement on the hexane vapors absorbed by the monolayer can clearly be seen from figure 5.26. Figure 5.26 shows the plot between the methylene asymmetric vibrational frequencies of the hexane vapors absorbed (x-axis) and the vibrational frequencies of the corresponding monolayer on which the vapors are absorbed (y-axis). This indicates that there is a strong correlation between the structure of the hexane vapors absorbed and the structure of the corresponding monolayer. In the graph 5.26, though the clean silicon surface does not have any methylene peaks, we have

assumed it to have peak at 2932 cm^{-1} same as that of hexane vapors absorbed on the silicon surface. This assumption is made to just plot the graph, with no particular inferences drawn.

5.3.3.2 Langmuir Model

The langmuir parameters, k and v_m are evaluated by fitting the linear regime of the experimental data with the model. The fit is shown in figure 5.27 (a) and the estimated parameter values are shown in table 5.5. The model and experimental data agree well for low pressures and disagree considerably at high partial pressures, with model under predicting, as shown in figure 5.27 (b). The plausible reason for the disagreement could be the possible formation of multilayers, which the Langmuir model does not take into consideration.

5.3.3.3 BET Model

The BET parameters, c and v_m are evaluated by fitting the linear regime of the experimental data with the model. The fit is shown in figure 5.28 (a) and the estimated parameter values are shown in table 5.6. The model deviates considerably from the experimental data. This is because the model takes into consideration the formation of infinite layers, and it might not be the case.

5.3.3.4 Model Prediction of the structure of hexane vapors on OTS and methyl terminated surfaces

The film growth of organic molecules on a metal substrate is not straight forward, depending on the substrate temperature, deposition speed, and so on. Here, we will discuss the growth mode of thin films with a simplified thermodynamic model, assuming the layer-by-layer growth and neglecting the kinetic factors. The growth mode of thin films is generally determined by the solid-solid and solid-vacuum interfacial free energies. When "A"-terminated surface is covered by a monolayer with "B"-terminated surface, the free energy change $\Delta\gamma$ is described as follows

$$\Delta\gamma_{A\rightarrow B} = \gamma_B + \gamma_{A\text{-}B} - \gamma_A \qquad (5.8)$$

where γ_A and γ_B are surface free energies of the A-terminated and the B-terminated surface, respectively, and $\gamma_{A\text{-}B}$ is a A/B interfacial energy mainly arising from strains at the A/B interface. If $\Delta\gamma_{A\rightarrow B} < \Delta\gamma_{A\rightarrow A}$, the B terminated surface is formed on the A-terminated surface. Because $\Delta\gamma_{A\rightarrow A}$ is zero, the condition for growth of a monolayer of which the surface is different from that of the underlying monolayer is

$$\Delta\gamma_{A\rightarrow B} < 0 \qquad (5.9)$$

Let us consider the three cases of the n-alkane film growth on the OTS monolayer: (1) hexane vapors forming a disordered structure with the molecules randomly oriented, (2) f hexane molecules lying flat, primarily exposing the methylene (CH_2) groups to the surface, and (3) hexane molecules standing up, primarily exposing the methyl (CH_3) groups.

- Hexane molecules randomly oriented : For a disordered structure formed, the equation 1 transforms to

$$\Delta\gamma_{CH3\rightarrow d} = \gamma_d + \gamma_{CH3\text{-}d} - \gamma_{CH3} \qquad (5.10)$$

where γ_d is the surface energy of the disordered phase of the hexane molecules absorbed and $\gamma_{CH3\rightarrow d}$ is the CH_3-disordered interfacial energy. γ_d and $\Delta\gamma_{CH3\rightarrow d}$, to a first order approximation, is assumed to be the surface energy of liquid hexane (γ_l) and CH_3-liquid interfacial energy ($\gamma_{CH3\rightarrow l}$), respectively.

Thus, eqn 5.10 transforms into

$$\Delta\gamma_{CH3\rightarrow l} = \gamma_l + \gamma_{CH3\text{-}l} - \gamma_{CH3} \qquad (5.11)$$

From surface tension studies,[24] the value of γ_l = 17.9 mN/m at room temperature (25°C) for hexane and $\gamma_{CH3\text{-}l}$ = 7.9 mN/m [25]

γ_{CH3} = 24.9 mN/m, calculated using contact angle method (Geometric and Harmonic Mean Method).

From equation 5.11 $\Delta\gamma_{CH3\rightarrow d} \sim \Delta\gamma_{CH3\rightarrow l} > 0$, thus making the process energetically unfavorable. Hence, formation of a disordered absorbed-hexane layer on OTS monolayer is not possible.

- Hexane molecules lying flat: Flat-lying hexane molecules primarily expose CH_2 groups to the surface, thus eqn 5.8 becomes

$$\Delta\gamma_{CH3\rightarrow CH2} = \gamma_{CH2} + \gamma_{CH3\text{-}CH2} - \gamma_{CH3} \qquad (5.12)$$

Although these values depend on carbon number of n-alkane, it is found that γ_{CH3} is smaller than the γ_{CH2} irrespective of the carbon number.[24] Because, $\gamma_{CH3\text{-}CH2}$ is positive

$\Delta\gamma_{CH3\rightarrow CH2} > 0$, thus again making the formation of flat-lying molecules energetically unfavorble.

- Ordered hexane molecules: In the case of hexane molecules forming a well-ordered layer with the molecules aligned perpendicular to the substrate, i.e., hexane layer primarily exposing CH_3 groups to the surface, then

$$\Delta\gamma_{CH3\rightarrow CH3} = \gamma_{CH3} + \gamma_{CH3\text{-}CH3} - \gamma_{CH3} \qquad (5.13)$$

since $\gamma_{CH3\text{-}CH3} = 0$, $\Delta\gamma_{CH3\rightarrow CH3} = 0$, thus making the process energetically favorable. This agrees well with the experimental results observed.

5.4 Conclusions

In this chapter, we have investigated the absorption of vapors of acetone and hexane on different monolayers, varying in hydrocarbon chain length and in terminal functional group and successfully demonstrated the importance of the structure and terminal functional group on the absorption process. Acetone vapors showed preferred affinity towards the hydrophilic groups such as NH_2, C≡N and OH. The total amount of acetone absorbed is greater for hydrophilic terminated groups than for hydrophobic groups. The governing interactions that control the absorption process on these surfaces are discerned from the sensitivity of the vibrational frequencies of carbonyl and methylene groups of acetone and hexane vapors, respectively. The type of interaction, either specific hydrogen bonding or non-specific van der waals interactions depended on the surface on which the acetone vapors are absorbed onto. Acetone vapors physically adsorbed on to CH_3 terminated OTS monolayer through non-specific interactions. Because of the high packing density of OTS molecules, acetone vapors did not penetrate through the OTS monolayer. However, penetration is observed on inhomogeneous OTS surfaces. The absorption of acetone vapors agreed well with the langmuir-type model for

low partial pressures and deviated from the model for high partial pressures, at which physical sorption or condensation of the acetone vapors became prominent.

Interactions (absorption) of the hexane vapors depended on the properties of the underlying monolayers. Contrary to expectations, hexane also showed higher affinity towards the energetic, hydrophilic surfaces trying to reduce the surface tension of the absorbing surface. Moreover, alignment of the absorbed hexane vapors exhibited a strong correlation with the structure of the underlying monolayer. Structure of the absorbed hexane vapors varied from all-trans on OTS monolayer to liquid like structure on clean silicon wafer. Alignment of the hexane molecules on the OTS (methyl terminated) monolayer is modeled using interfacial energy arguments. From the model it is shown energetically it is favorable for the hexane molecules to align in an all-trans confuguration exposing the methyl groups to the surface. Both Langmuir and BET sorption models failed to describe the sorption properties of hexane vapors on the monolayers, as the sorption of hexane vapors.

5.5 References

1. Crooks, R. M.; Liu, Y.; Zhao, M.; Bergbreiter, D. E. **1997**.

2. Lahiri, J.; Isaacs, L.; Grzybowski, B.; D.Carbeck, J.; Whitesides, G. M. *Langmuir* **1999**, *15*, 7186-7198.

3. Laibinis, P. E.; Whitesides, G. M. *J. Am. Chem. Soc.* **1992**, *114*, 9022.

4. Lee, J.-Y.; Park, S.-M. *J. of Physical Chemistry* **1998**.

5. Ottova, A.; Tvarozek, V.; Racek, J.; Sabo, J.; Ziegler, W.; Hianik, T.; Tein, H. T. **1996**.

6. Rubinstein, I.; Steinberg, S.; Tor, Y.; Shanzer, A.; Sagiv, J. *Nature* **1988**, *332*, 426-429.

7. Schierbaum, K. D.; Weiss, T.; Velzen, E. U. T. v.; Engbersen, J. F. J.; Reinhoudt, D. N.; Gopel, W. *Science* **1994**, *265*, 1413-1415.

8. Steinberg, S.; Tor, Y.; Shanzer, A.; Rubinstein, I. *Thin Films* **1995**, *20*, 183-205.

9. Wulff, G. *Angew Chem. Int. Ed.* **1995**, *34*, 1812-1832.

10. Grate, J. W.; Patrash, S. J.; Abraham, M. H.; Du, C. M. *Analytical Chemistry* **1996**, *68*, 913-917.

11. Rose, G. D.; Quinn, J. A. *Journal of Colloid and Interface Science* **1968**, *27*, 193-207.

12. Rose, G. D.; Quinn, J. A. *Science* **1968**, *159*, 636-637.

13. Vanderlick, T. K.; Hanley, C. M.; Quinn, J. A. *AIChE Journal* **1996**, *42*, 1234-1243.

14. Marshbanks, T. L.; Ahn, D. J.; Franses, E. I. *Langmuir* **1994**, *10*, 276-285.

15. Long, F. A.; Thompson, L. J. *Journal of Polymer Science* **1955**, *15*, 413.

16. Perrin, L.; Nguyen, Q. T.; Sacco, D.; Lochon, P. *Polymer International* **1997**, *42*, 9-16.

17. Quickenden, T. I.; Barnes, G. T. *J. Colloid and Interface Science* **1978**, *67*, 415-422.

18. Sobotka, H. *Journal of Colloid Science* **1956**, *11*, 435-444.

19. Karpovich, D. S.; Blanchard, G. J. *Langmuir* **1997**, *13*, 4031-4037.

20. Archer, R. J.; La Mer, V. K. *J. Ohys. Chem* **1955**, *59*, 200.

21. Windreich, S.; Silberberg, A. *J. Colloid and Interface Science* **1980**, *77*, 427-434.

22. Langmuir, I. *J. Am. Chem. Soc* **1916**, *38*, 2221-95.

23. Kondoh, H.; Matsui, F.; Ehara, Y.; Yokoyama, T.; Ohta, T. *Langmuir* **2001**, *17*, 8178-8183.

24. Ocko, B. M.; Wu, X. Z.; Sirota, E. B.; Sinha, S. K.; Gang, O.; Deutsch, M. *Phys. Rev. E* **1997**, *55*, 3164.

25. Jasper, J. J. *J. Phys. Chem. Ref. Data* **1972**, *1*, 841.

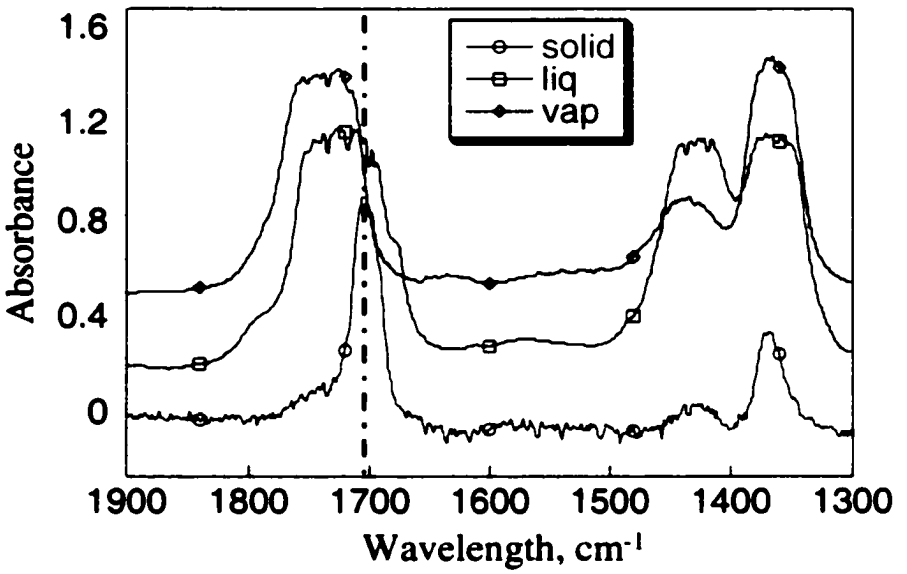

Figure 5.1: Spectra of acetone present in three different phases; clearly showing surface induced perturbation in C=O peak

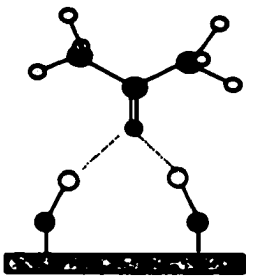

Cartoon depicting carbonyl group of acetone double hydrogen bonded to the substrate (1690 cm^{-1})

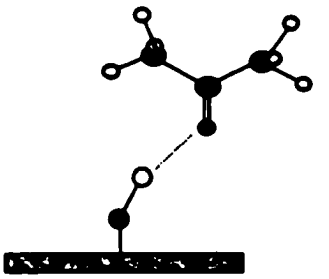

Cartoon depicting carbonyl group of acetone hydrogen bonded to the substrate (1705 cm^{-1})

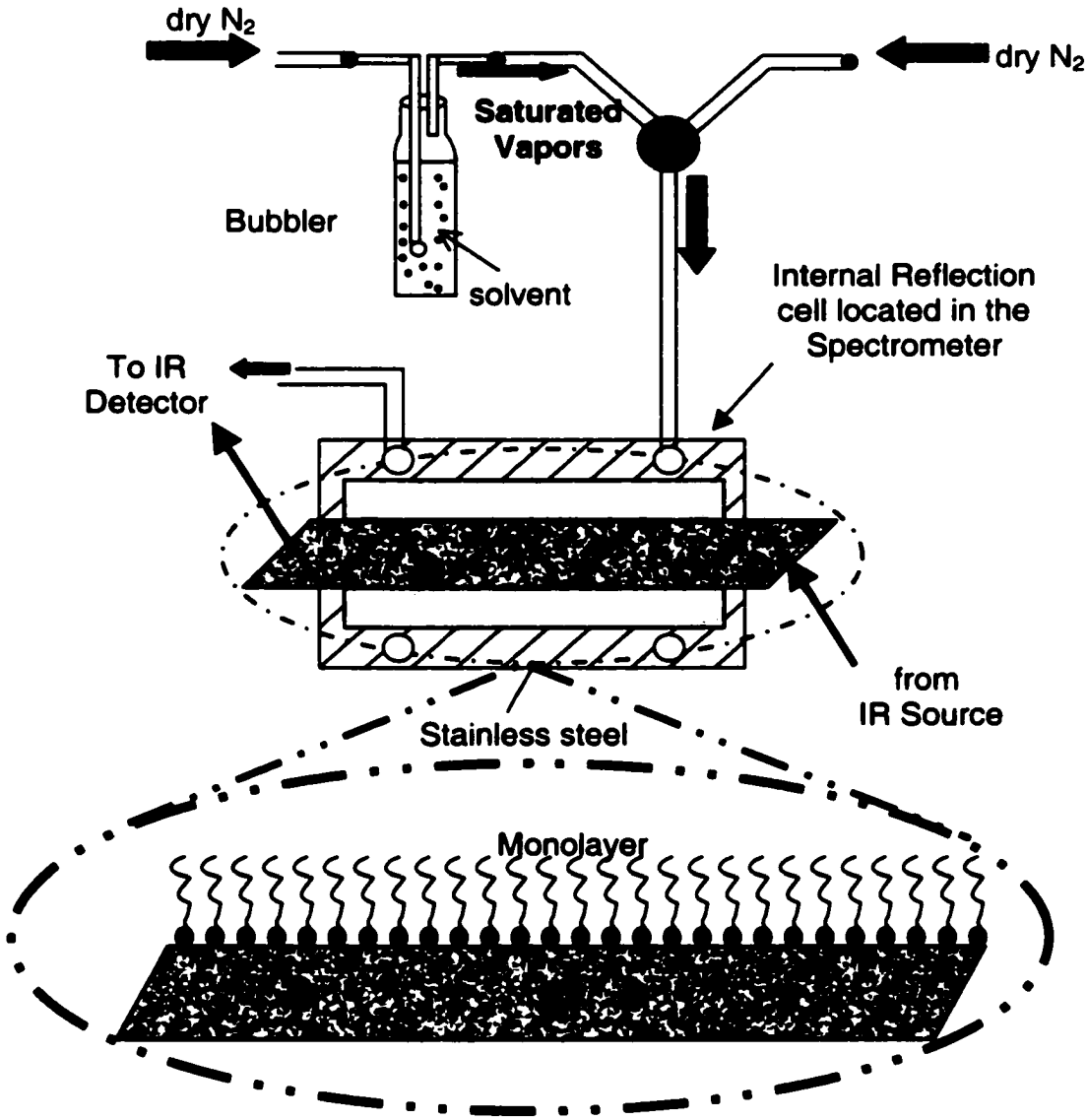

Figure 5.2: Experimental flow cell used to measure the sorption properties of volatile organic vapors

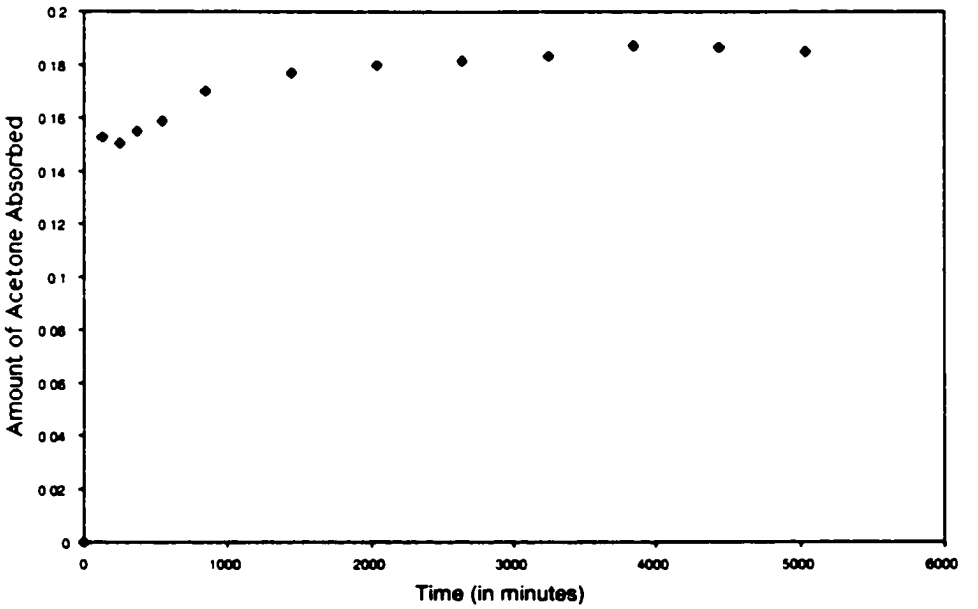

Figure 5.3: Kinetics of absorption of acetone vapor on clean Si surface

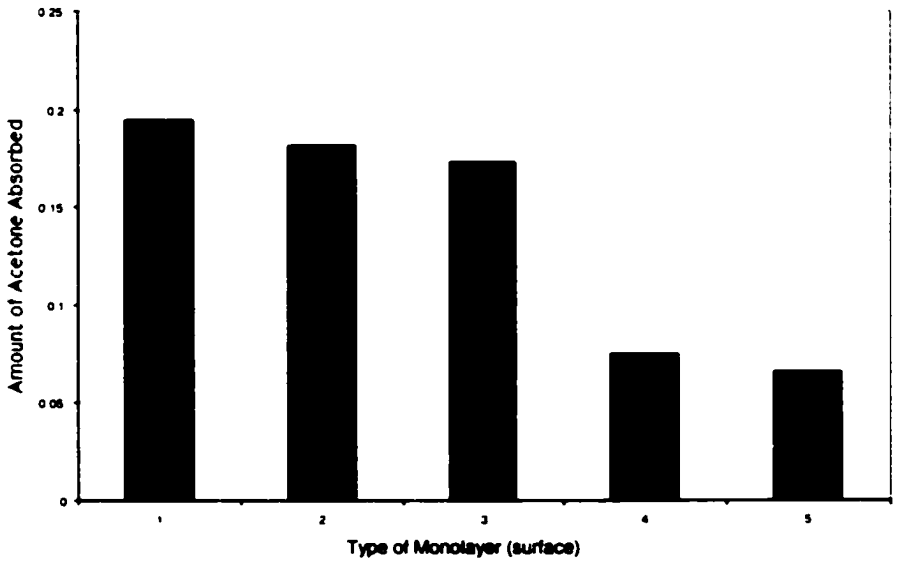

Figure 5.4: Amount of acetone absorbed on different surfaces

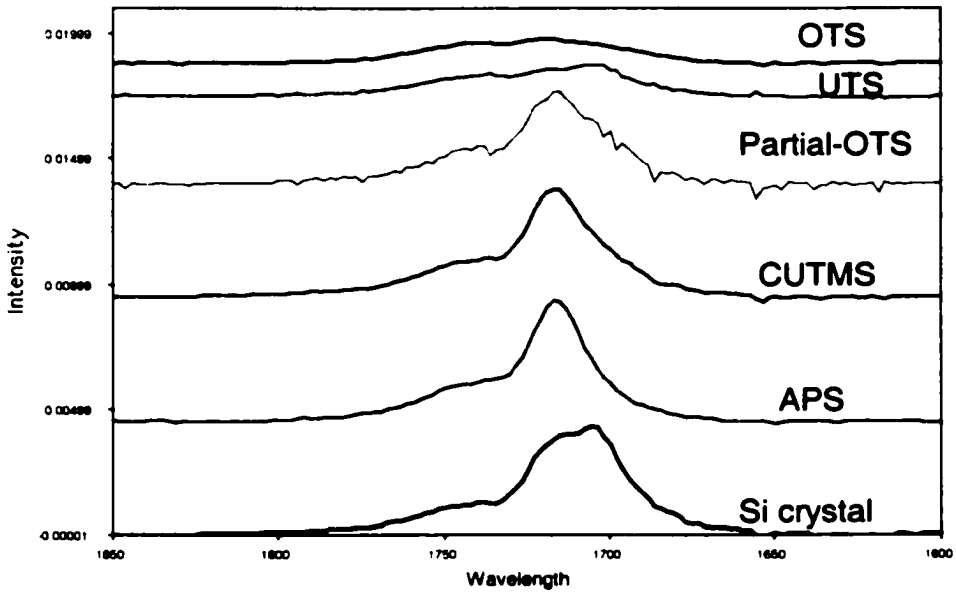

Figure 5.5: IR spectra of acetone absorbed on different monolayers

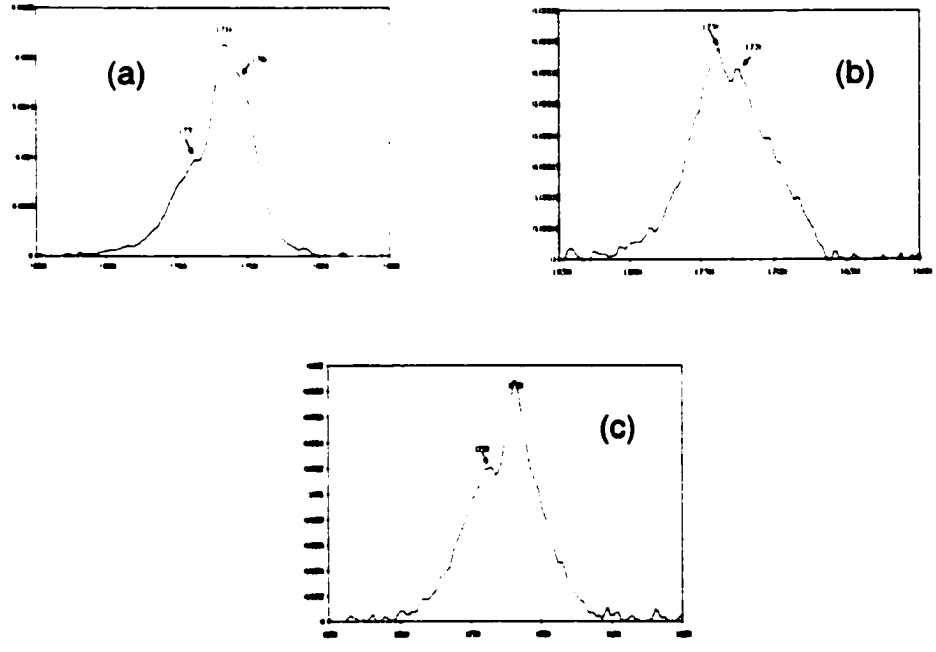

Figure 5.5: Zoomed IR spectra of acetone vapor absorbed on (a) CUTMS monolayer (b) OTS monolayer and (c) UTS monolayer

Monolayer	Hydrogen bonded C=O	Physically adsorbed or condensed C=O	Vapor Phase C=O
Clean Silicon	1703 cm^{-1}	1718 cm^{-1}	1737 cm^{-1}
APS		1716 cm^{-1}	1737 cm^{-1}
CUTMS	1704 cm^{-1}	1716 cm^{-1}	1737 cm^{-1}
UTS	1704 cm^{-1} (if molecules penetrate)	1719 cm^{-1}	1738 cm^{-1}
OTS	1704 cm^{-1} (if molecules penetrate)	1726 cm^{-1}	1739 cm^{-1}

Table 5.1: Showing the vibrational frequencies of C=O peak of acetone present in hydrogen bonded, physically adsorbed (or condensed) or vapor phase states in the presence of OTS, UTS, CUTMS and clean Silicon substrate.

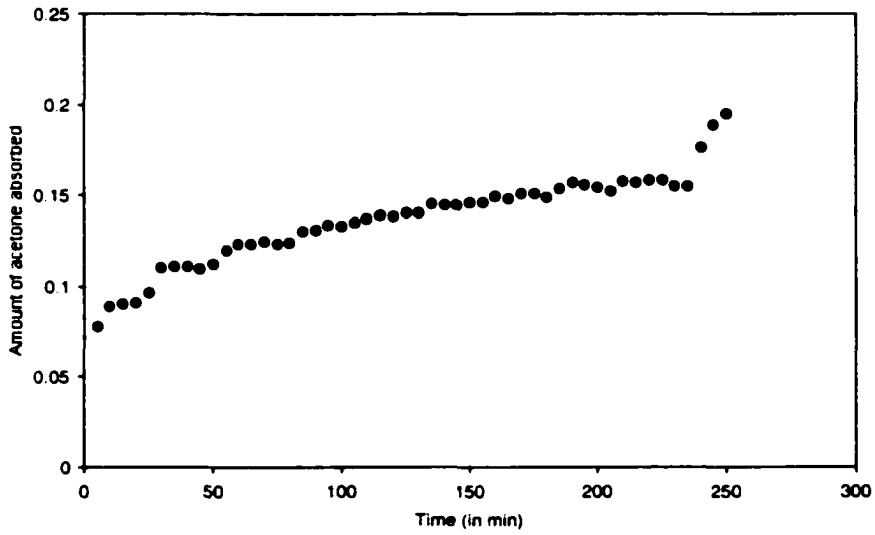

Figure 5.6: Effect of partial pressure on acetone absorption on Si surface with time

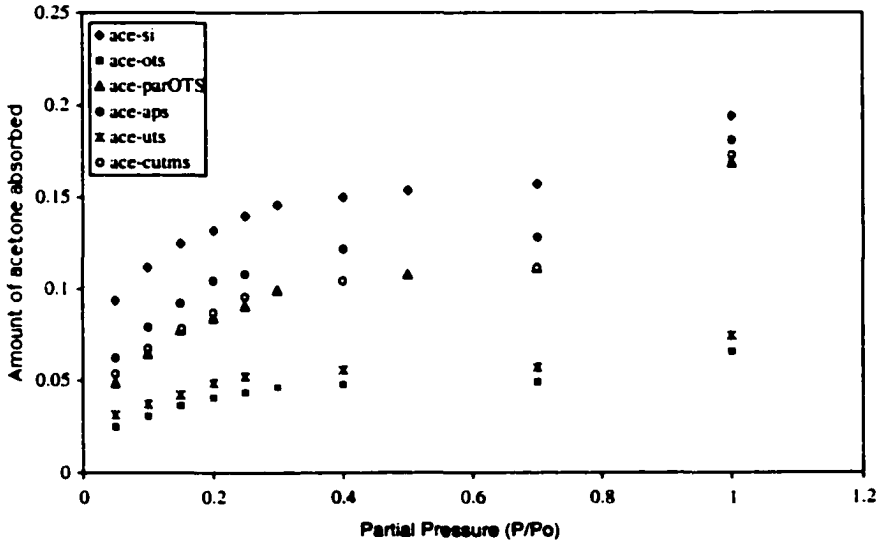

Figure 5.7: Effect of partial pressure on acetone absorption on different surfaces

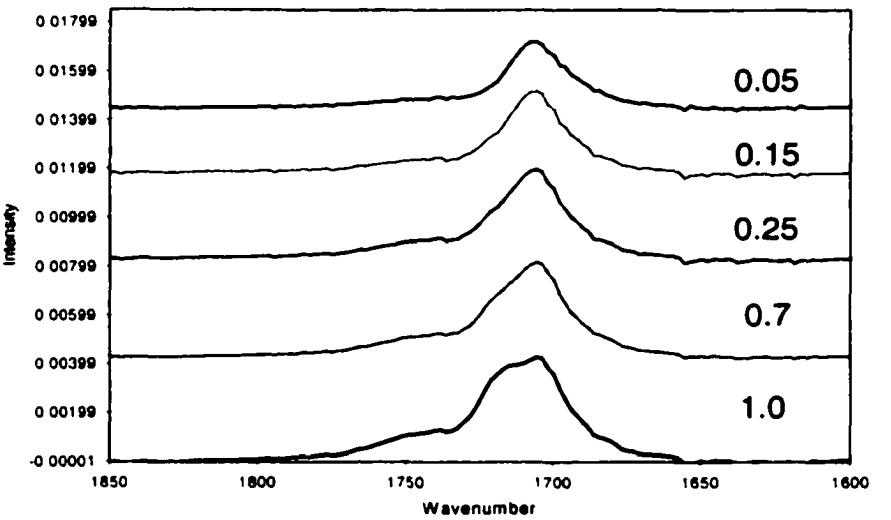

Figure 5.8: IR spectra of acetone vapors absorbed on Si crystal as a function of partial pressure

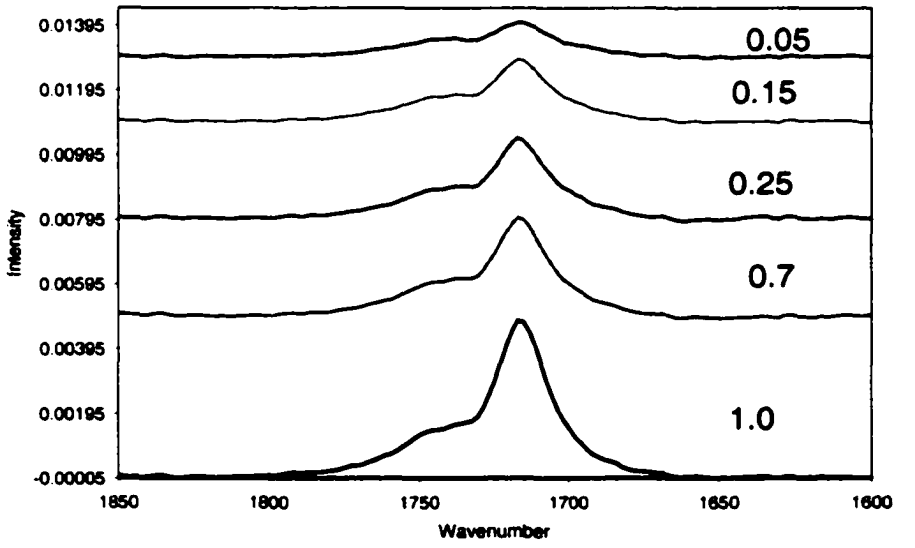

Figure 5.9: IR spectra of acetone vapors absorbed on APS monolayer as a function of partial pressure

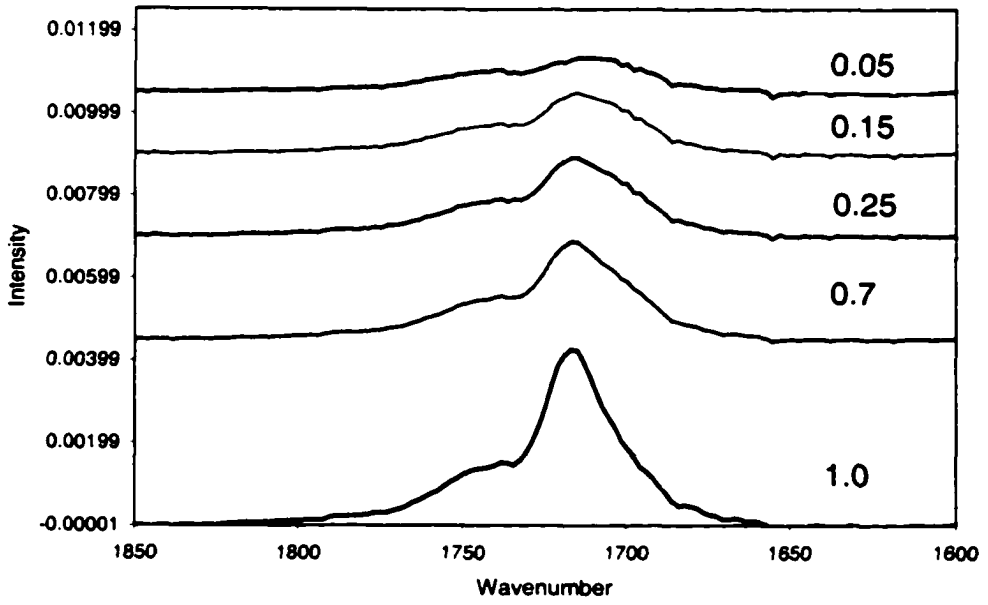

Figure 5.10: IR spectra of acetone vapors absorbed on CUTMS monolayer as a function of partial pressure

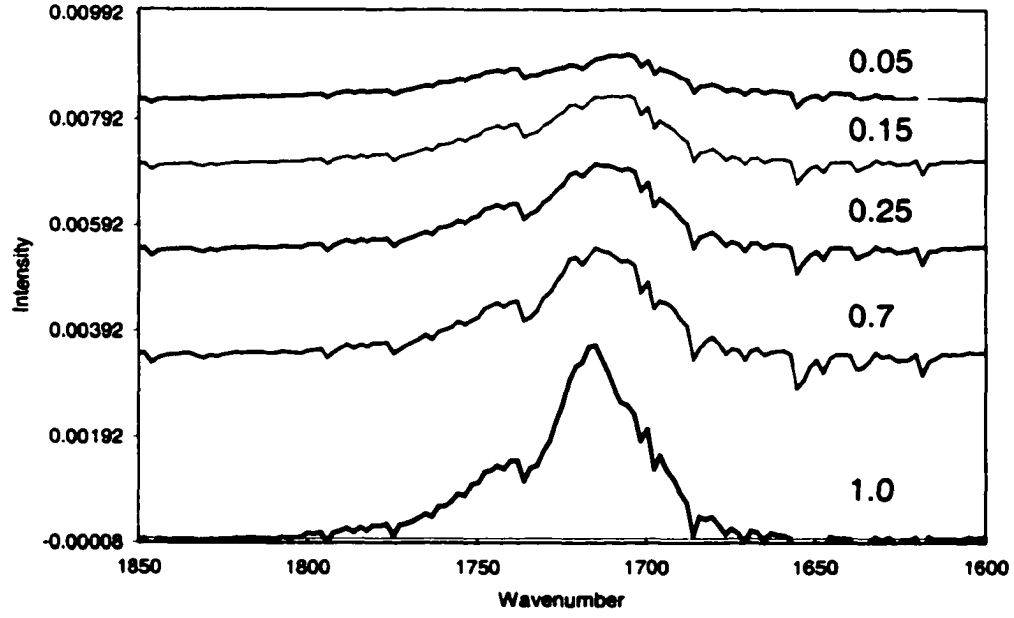

Figure 5.11: IR spectra of acetone vapors absorbed on partial-OTS monolayer as a function of partial pressure

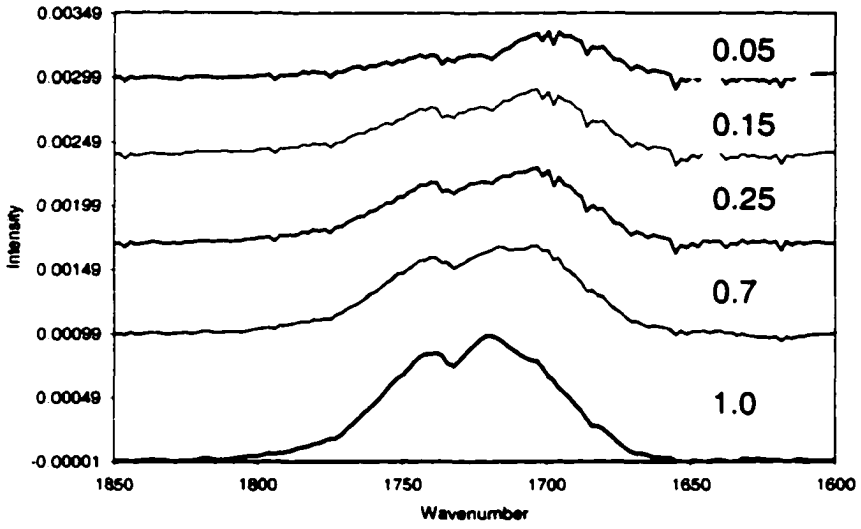

Figure 5.12: IR spectra of acetone vapors absorbed on OTS monolayer as a function of partial pressure

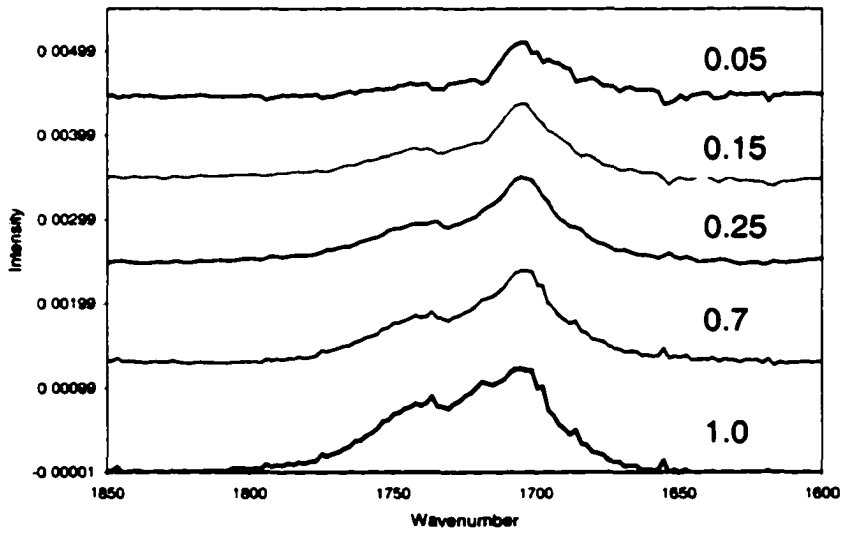

Figure 5.13: IR spectra of acetone vapors absorbed on UTS monolayer as a function of partial pressure

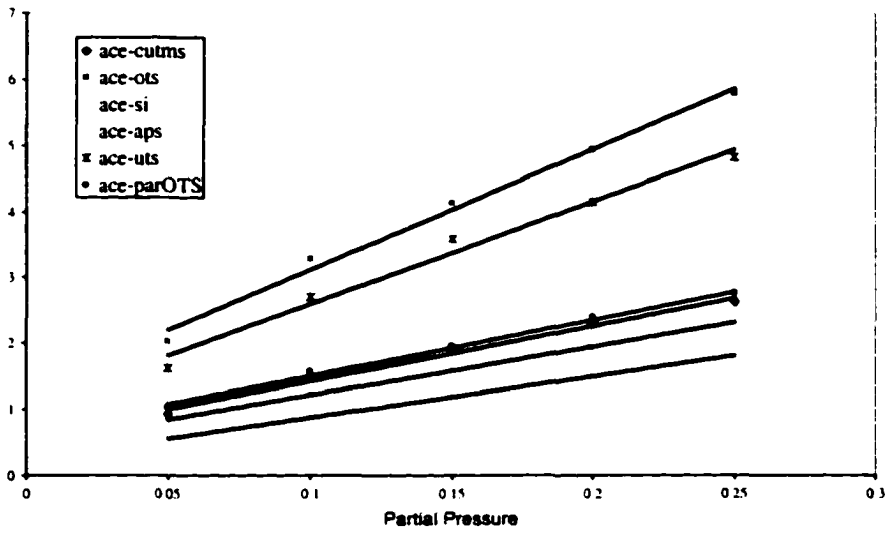

Figure 5.14 (a): Linear regime of Langmuir sorption model

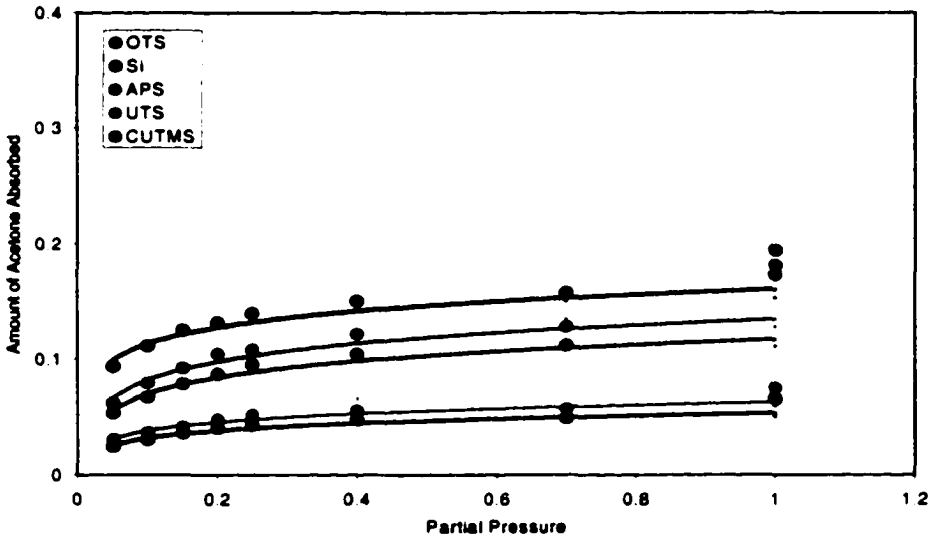

Monolayer	K=K1/K2	Vm (Monolayer Coverage)
Si	25.68	0.16
APS	15.14	0.136
CUTMS	14.2	0.119
UTS	15.35	0.064
Partial-OTS	13.19	0.117
OTS	14.44	0.054

Table 5.2: Langmuir parameters

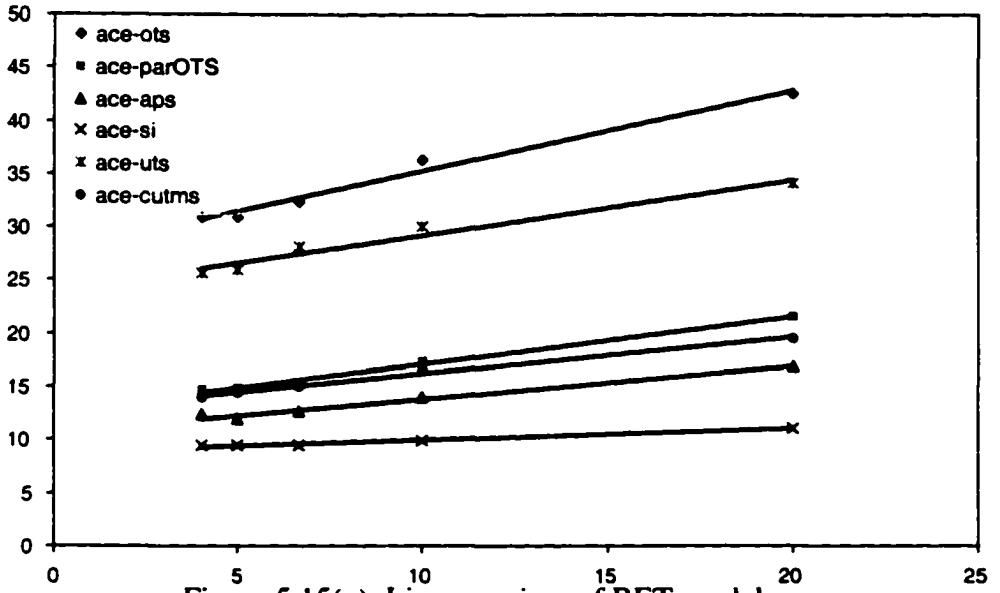

Figure 5.15(a): Linear regime of BET model

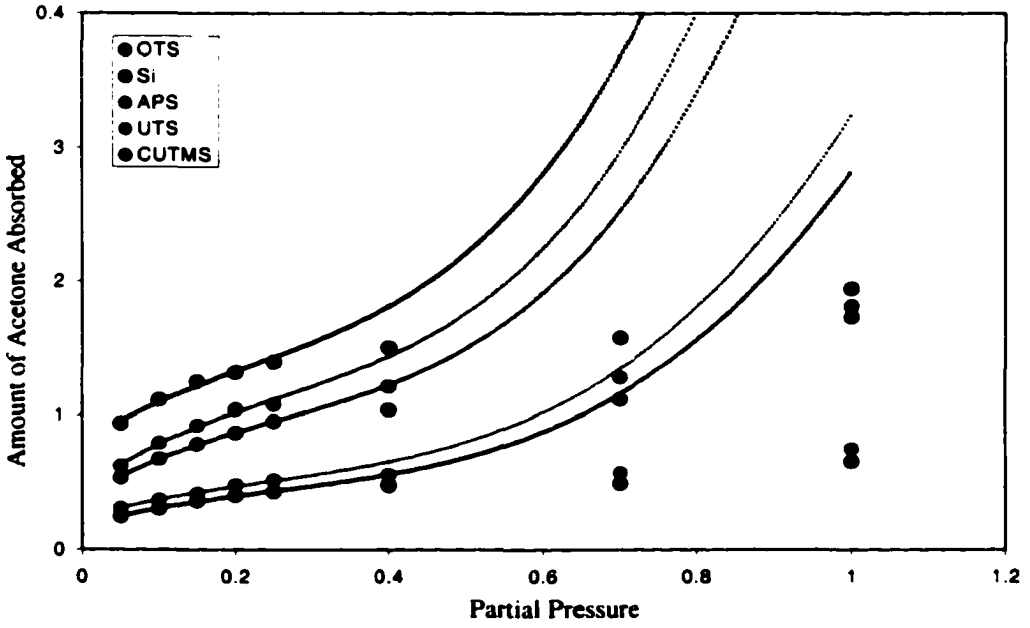

Figure 5.15(b): BET fit

Monolayer	C= K0/K1	Vm (monolayer coverage)
SI	82.55	0.111
APS	35.87	0.09
CUTMS	37.05	0.077
UTS	47.02	0.047
Partial-OTS	29.3	0.076
OTS	37.31	0.035

Table 5.3: BET model parameters

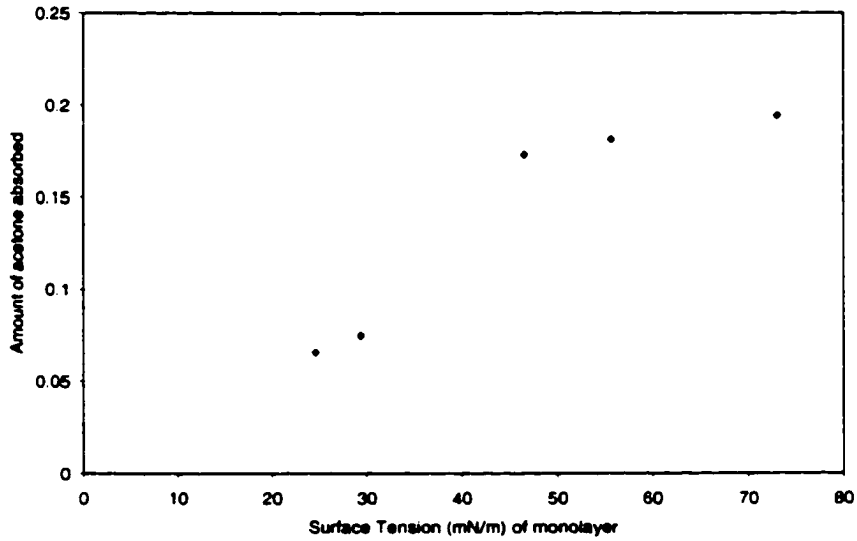

Figure 5.16(a): Effect of surface tension of the monolayers on the amount of acetone absorbed

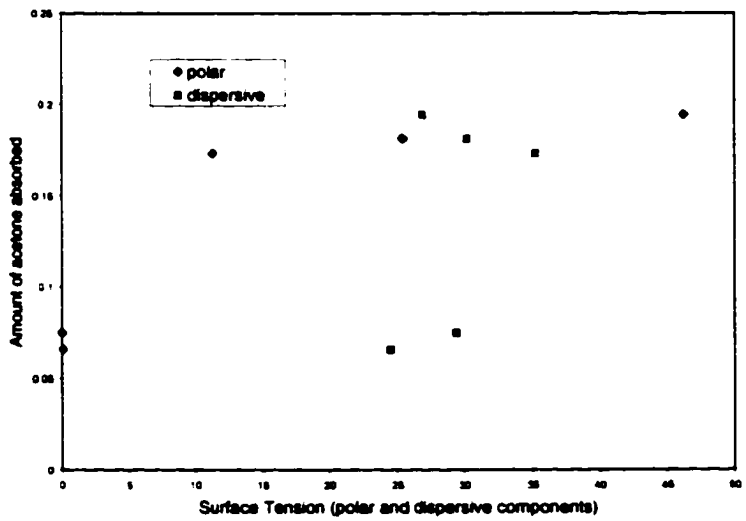

Figure 5.16(b): Effect of polar and dispersive components of surface tension of the monolayers on the amount of acetone absorbed

Monolayer	Gamma-p	gamma-d	gamma
Si	46.2	26.9	73.1
APS	25.4	30.2	55.6
CUTMS	11.3	35.2	46.5
UTS	0.004	29.4	29.404
OTS	0.08	24.5	24.58

Table 5.4: Polar and Dispersive components of surface tension of the monolayers

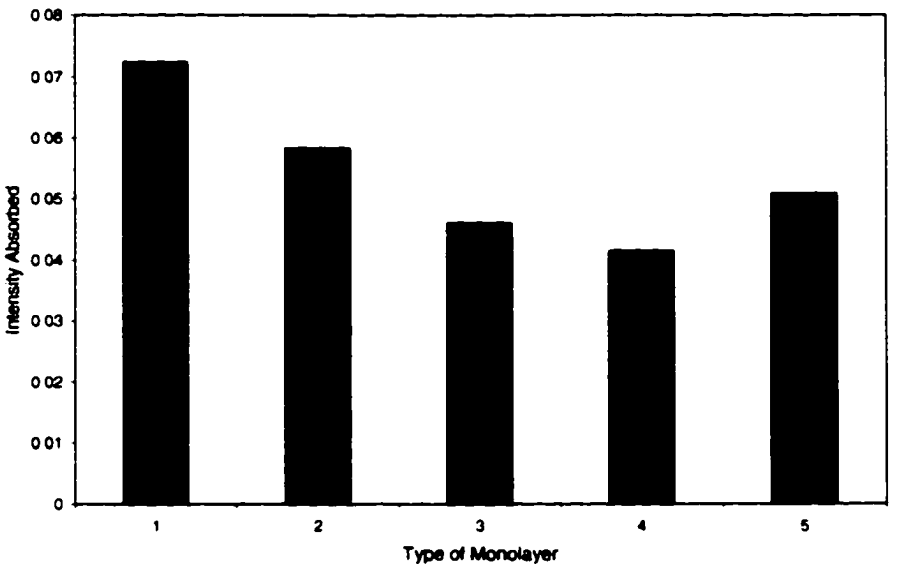

Figure 5.17: Amount of hexane absorbed on different monolayers

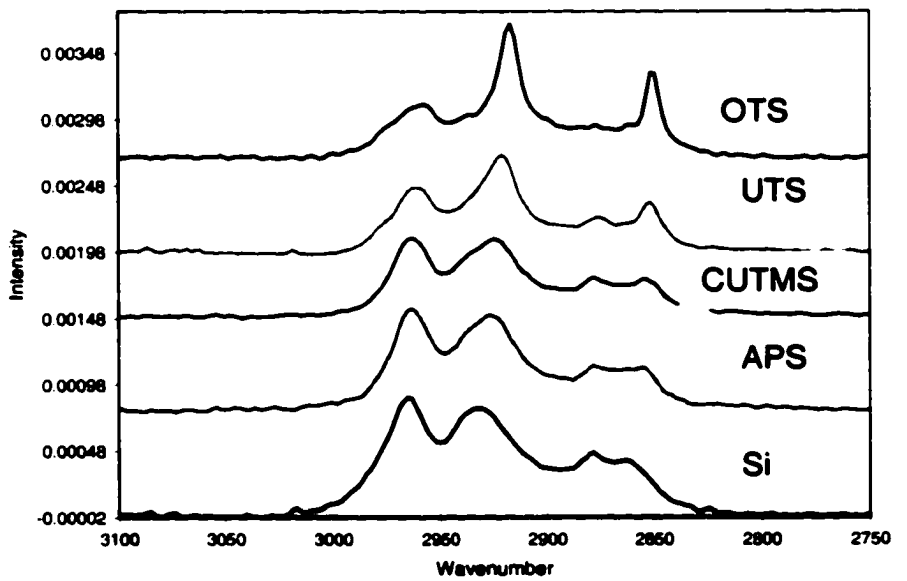

Figure 5.18: Spectra of absorbed hexane on different monolayer surfaces

Monolayer	CH_2 Asymm, cm^{-1}	CH_2 Symm, cm^{-1}	CH_3 Asymm, cm^{-1}
OTS	2917 (2919)	2850 (2851)	2957 (2960)
UTS	2920 (2924)	2851 (2854)	2961 (2960)
CUTMS	2924 (2927)	2854 (2856)	2963 (2960)
APS	2927 (2928)	2856 (2859)	2965 (2964)
Si	2932	2863	2965

Table 5.5: Showing the methylene asymmetric and symmetric stretches of absorbed hexane vapors. (values not in parenthesis). Values in the parenthesis represent that of the corresponding monolayers.

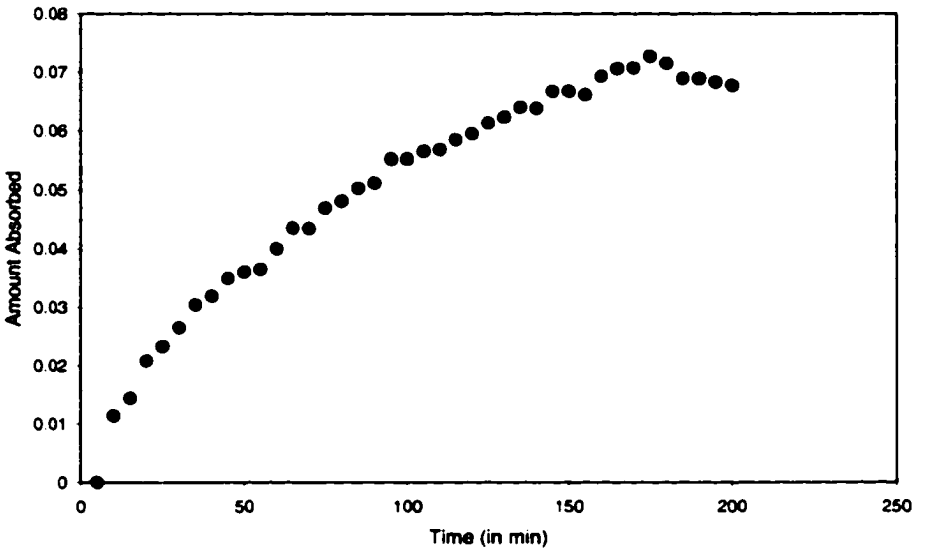

Figure 5.19: Amount of hexane absorbed as a function of partial pressure with time

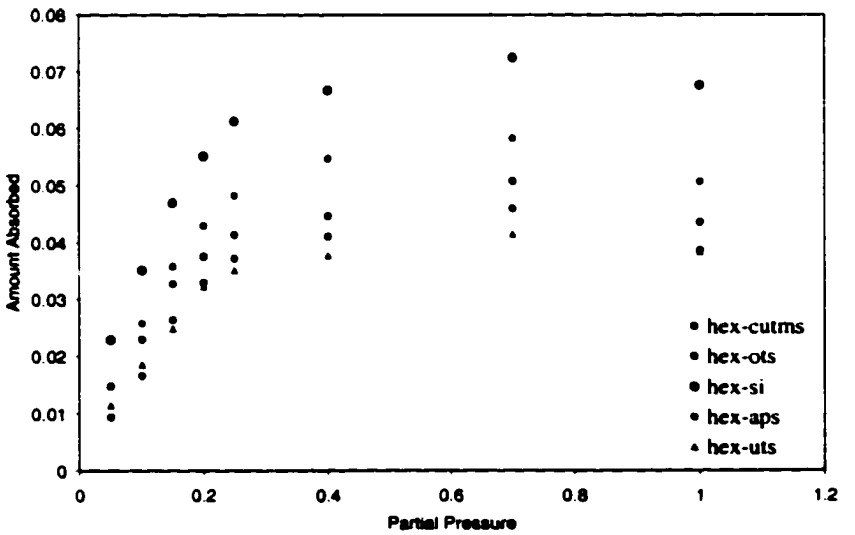

Figure 5.20: Amount of hexane absorbed as a function of partial pressure

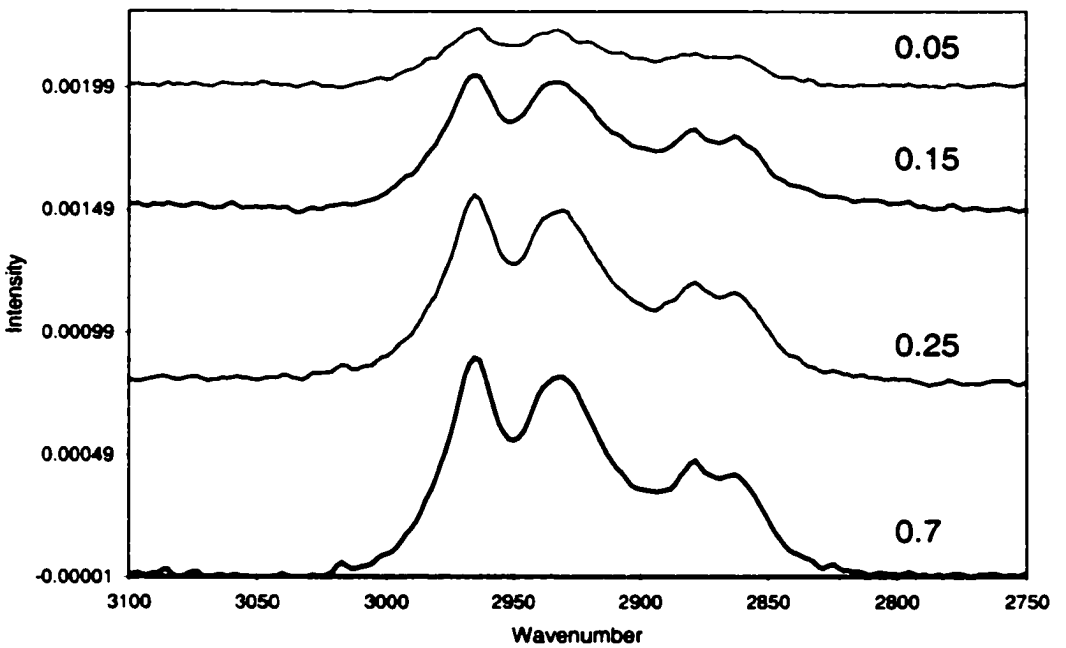

Figure 5.21: Spectra of absorbed hexane on Si crystal as a function of partial pressure

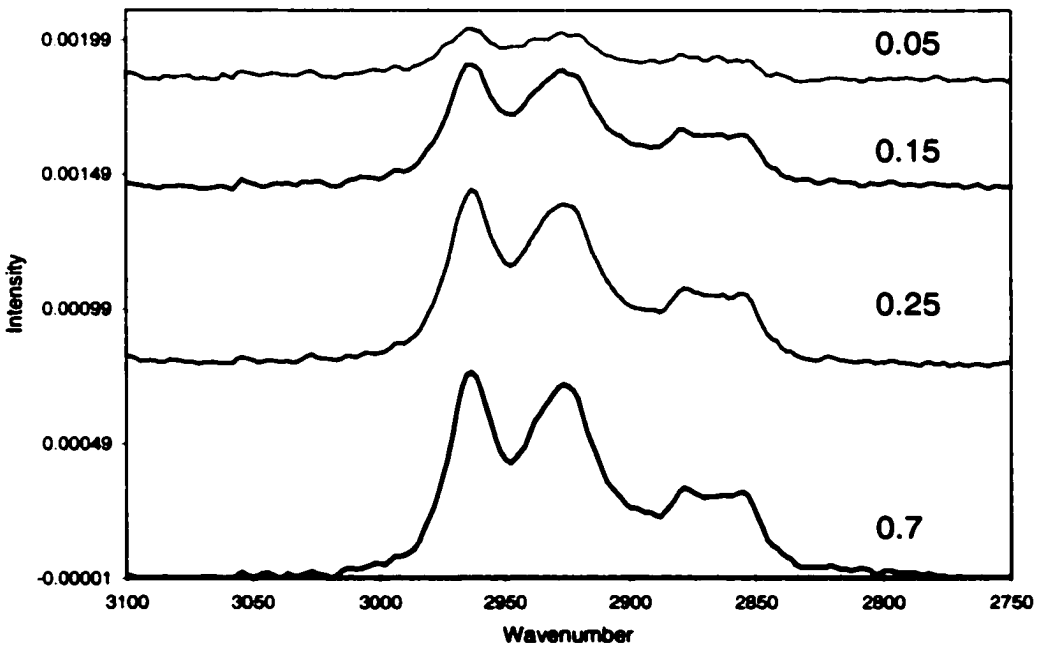

Figure 5.22: Spectra of absorbed hexane on APS monolayer as a function of partial pressure

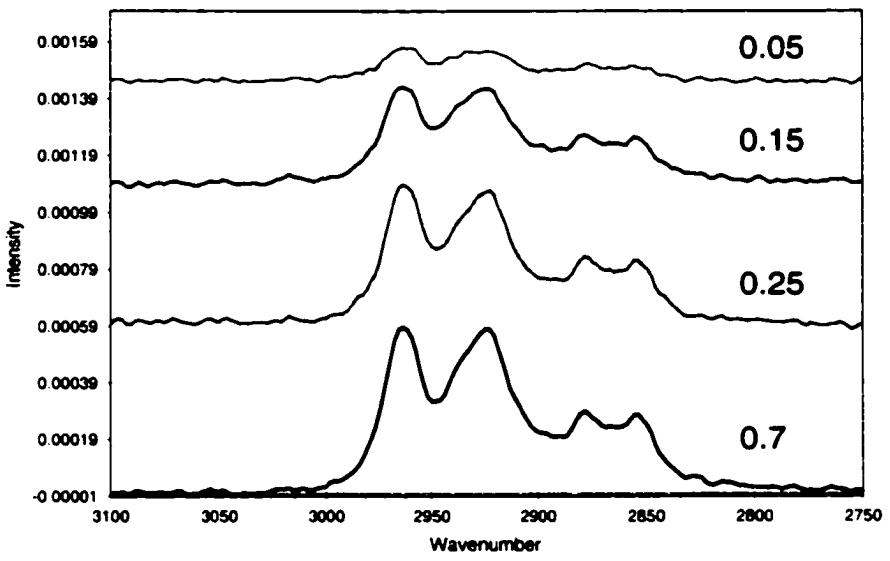

Figure 5.23: Spectra of absorbed hexane on CUTMS monolayer as a function of partial pressure

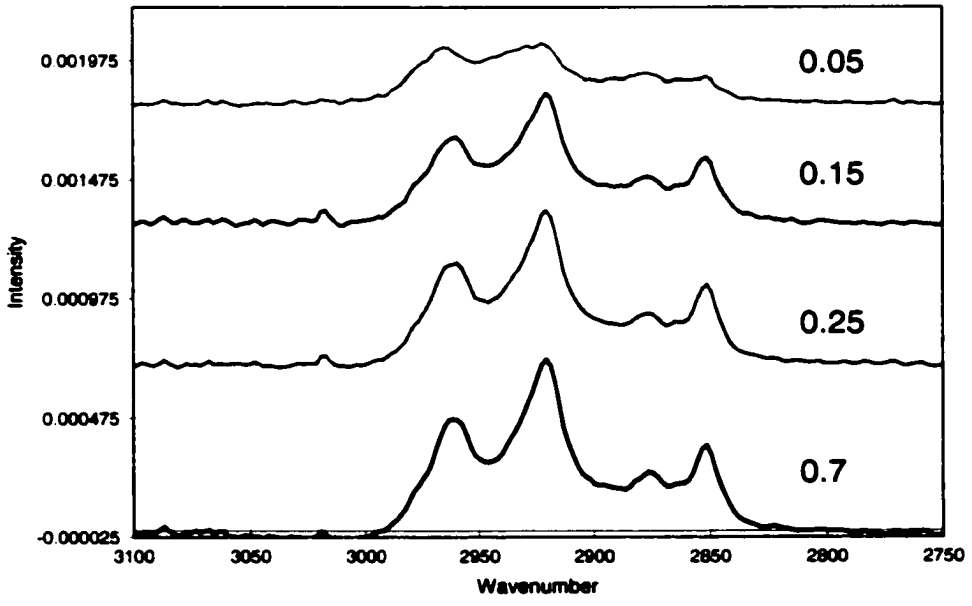

Figure 5.24: Spectra of absorbed hexane on UTS monolayer as a function of partial pressure

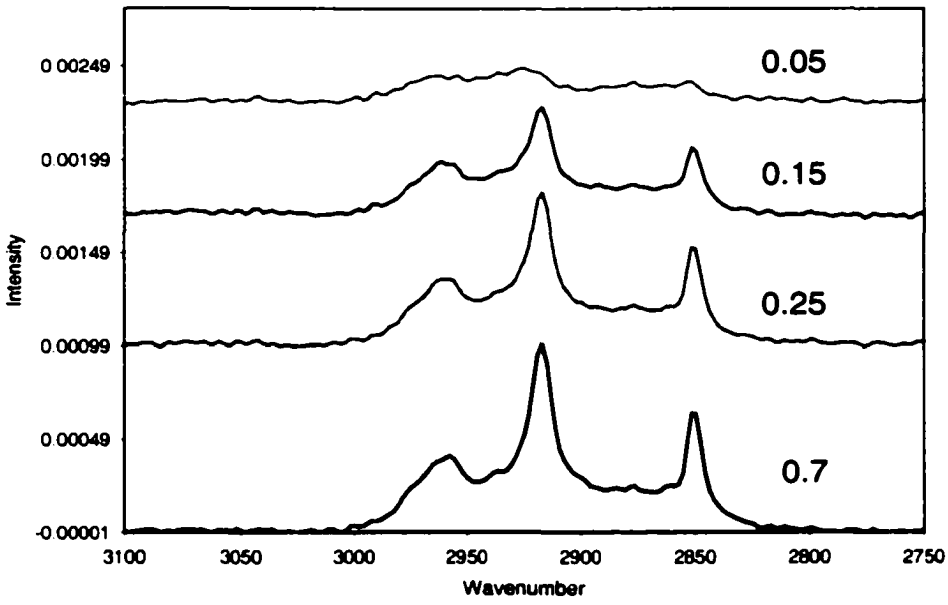

Figure 5.25: Spectra of absorbed hexane on OTS monolayer as a function of partial

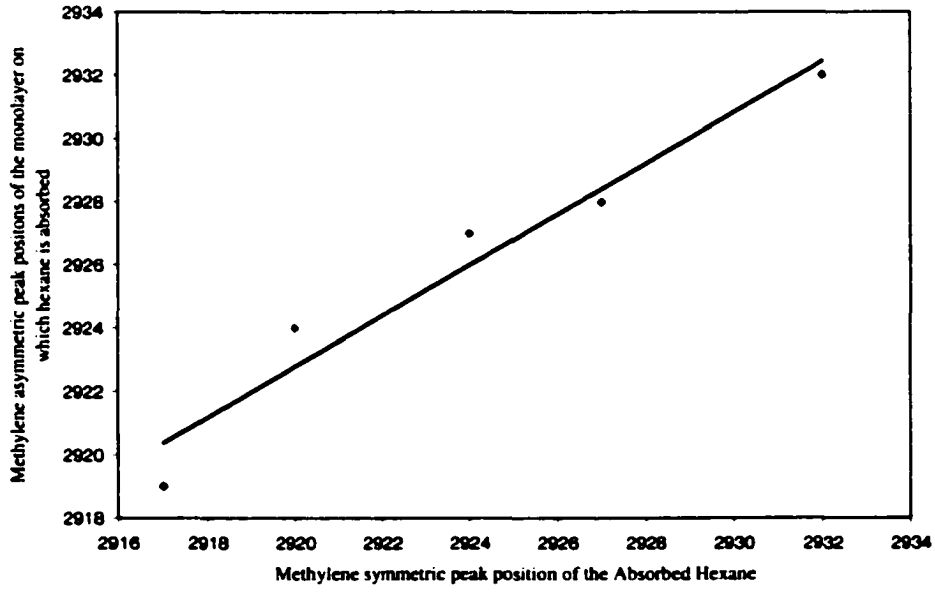

Figure 5.26: Showing the strong correlation between the structure of the absorbed hexane molecules on the monolayer and the structure of the corresponding underlying monolayer

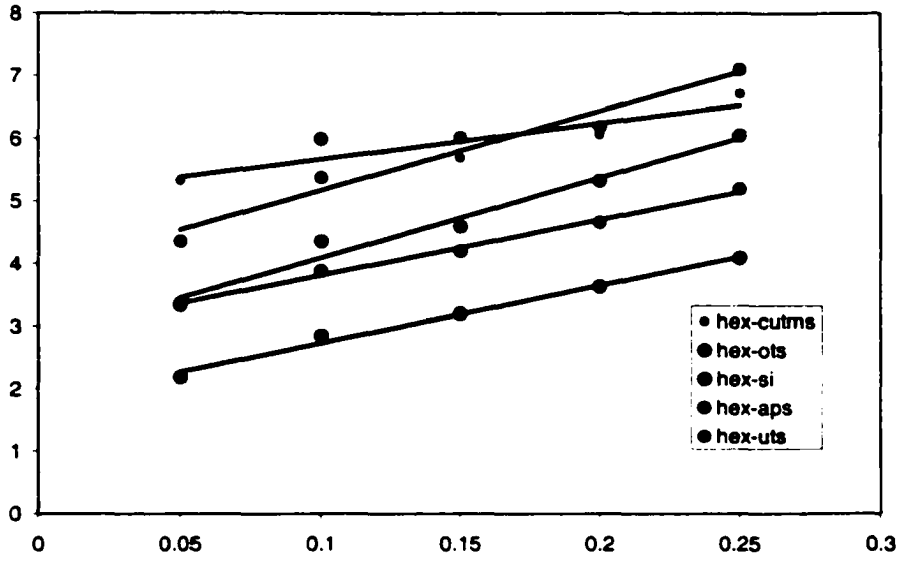

Figure 5.27(a): Linear regime of Langmuir plot

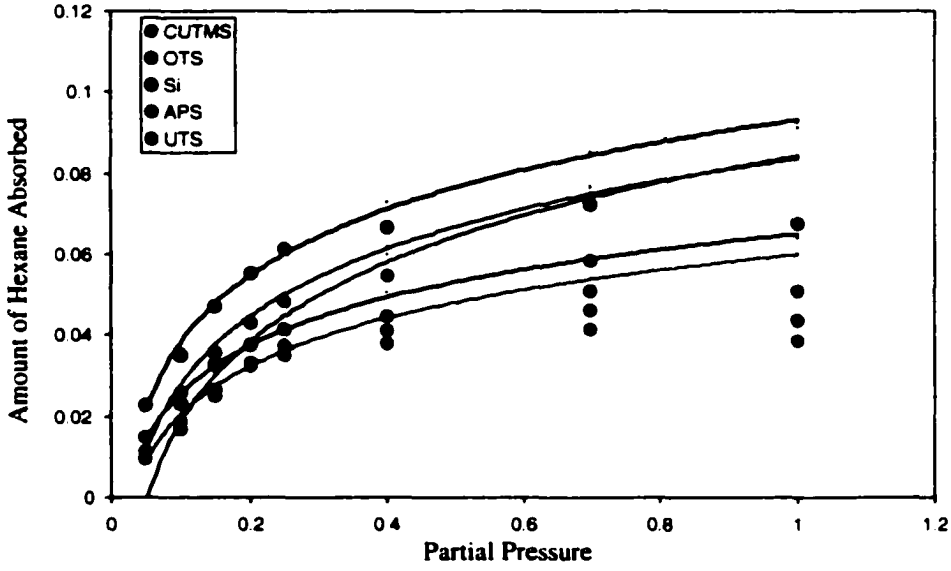

Figure 5.27(b): Langmuir fit

Table 5.6: Langmuir parameters

Monolayer	K= K1/K2	Vm (Monolayer Coverage)
Si	5.04	0.11
APS	3.04	0.112
CUTMS	1.12	0.174
UTS	3.23	0.079
OTS	4.56	0.078

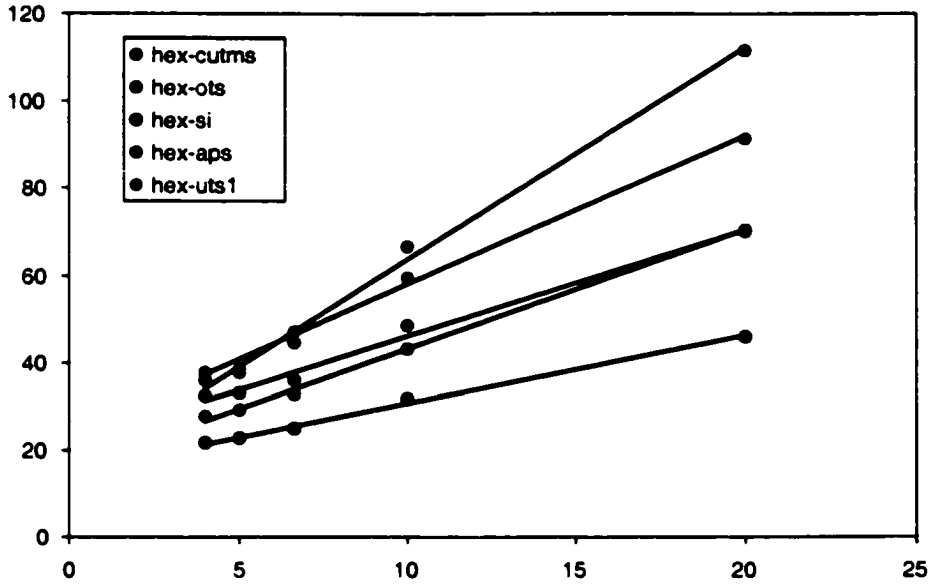

Figure 5.28(a): Linear regime of BET plot

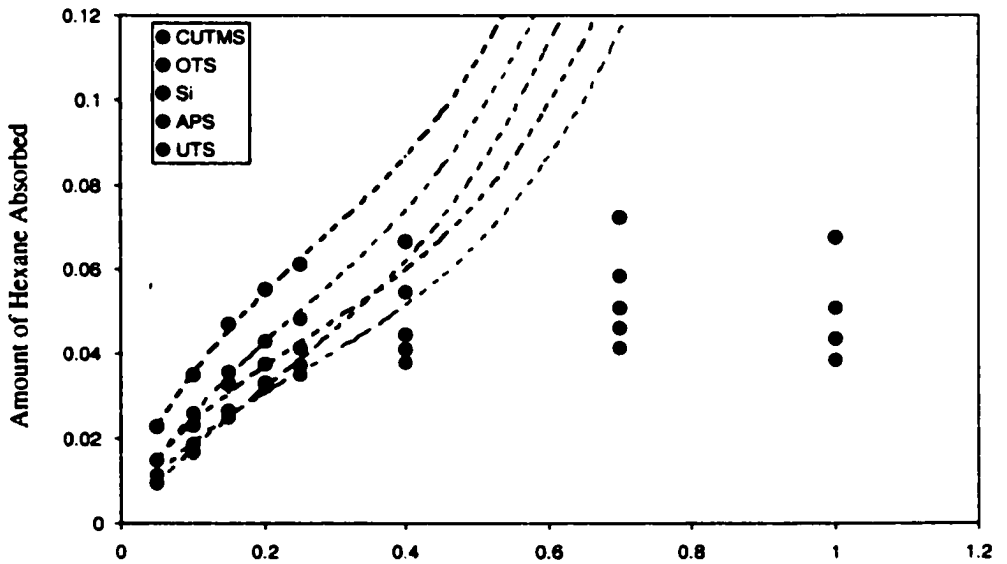

Figure 5.28(b): BET fit

Monolayer	C=K0/K1	Vm (Monolayer Coverage)
Si	10.93	0.059
APS	6.7	0.054
CUTMS	3.99	0.051
UTS	7.93	0.037
OTS	9.81	0.041

Table 5.7: BET parameters

Chapter 6

Future Work

In nature, self-assembly results in supermolecular hierarchical organizations of interlocking components that provides very complex systems. SAMs offer unique opportunities to increase fundamental understanding of self-organization, structure-property relationships, and interfacial phenomena.

6.1 Structure of the Monolayers

In chapter 3 we have shown that the intermolecular interactions, both weak van der Waals chain-chain interaction and the terminal group-substrate interactions, play an important role in determining the structure, mechanism of formation, and also packing density of the monolayers. General rule of thumb is, higher the chain length greater the order and packing density of the monolayers and higher the polarity of the terminal group, lower the order and packing density of the monolayers. We have also shown that the structure also depends on the temperature of deposition. Again the general tendency is that the molecules have higher phase transition temperature with increase in chain length and vice versa.

In future, it would be interesting to model the packing density of these monolayers using a simple lattice modeling. Apart from site-specific bonding, one has to take into account also the finite length of the molecule and how the orientation of the molecules effects the availability (activity) of the neighboring binding sites. Modeling successfully will give an estimate of the molecules structure and orientation, a priori to

running experiments. This also will give an insight into interactions that will play a prominent role and will help in designing or fabricating molecules for specific purpose with specific groups (properties) incorporated.

Other interesting aspect to look into is the phase transition regions for molecules of different lengths and terminal groups. Obtaining this will help in knowing a priori what state the monolayer is present - liquid expanded (LE), liquid condensed (LC) or mixed state. This also will provide information on the growth mechanism of the monolayer.

6.2 Surface Engineering of SAMs

In chapter 3, modification of cyano terminal group to carboxylic group is successfully demonstrated. It has also been shown the dependence of COOH/COO^- ratio on the pH. Our experiments with LB film of stearic acid have shown that there is a local structure (primarily a 2-D structure of COOH-COO^- surface arrangement) that can be controlled by controlling the pH.

Some of the questions to pose about this dependence of local structure on pH is:
(i) Whether there is a unique arrangement for a given number COOH and COO^- moieties present on the surface?
(ii) Is there any critical COOH/COO^- number ratio for which the electrostatic repulsive forces dominate?

We are trying to answer these questions in an indirect way by the formation of CdS (cadmium sulfide) nanoparticles. The idea is COO^- being negatively charged, acts as a nucleating site for the anchoring of Cd^{2+} ions, thus initiating the process of formation of

CdS nanoparticles. Therefore depending on the initial distribution of COOH and COO^- groups, the nanoparticles distribution will be related. Thus from this correlation one can determine the distribution of the COOH/COO^- groups, and its dependence on pH.

We did some preliminary experiments on the feasibility of the concept. On modified CN surface, CdS nanoparticles are formed, where as, no particles are formed on hydrophobic surface of OTS. Some of the results are shown in figure 6.1.

6.3 SAMs as Model Membranes

In chapter 5, we have investigated the absorption of vapors of acetone and hexane on SAMs, and have shown that these studies provide insight on fundamental understanding of the interactions that govern the absorption process. Extending these studies to various other VOCs (volatile organic vapors) like aromatic, cyclic, polar and non-polar analytes will help in better understanding of the interactions and will help in designing an efficient, energy effective, higher selective membrane for the separation processes.

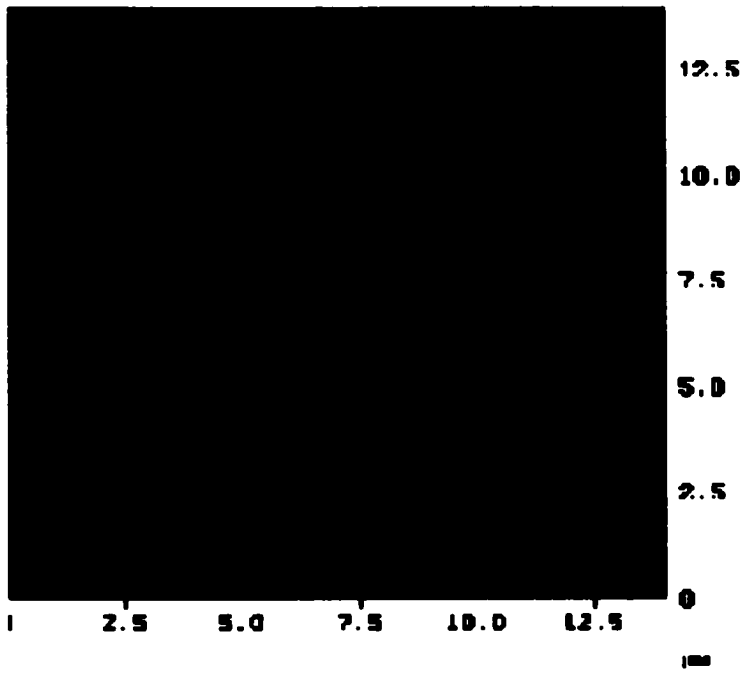

Figure 6.1 (a): CdS particles did not form on OTS surface even after long deposition times

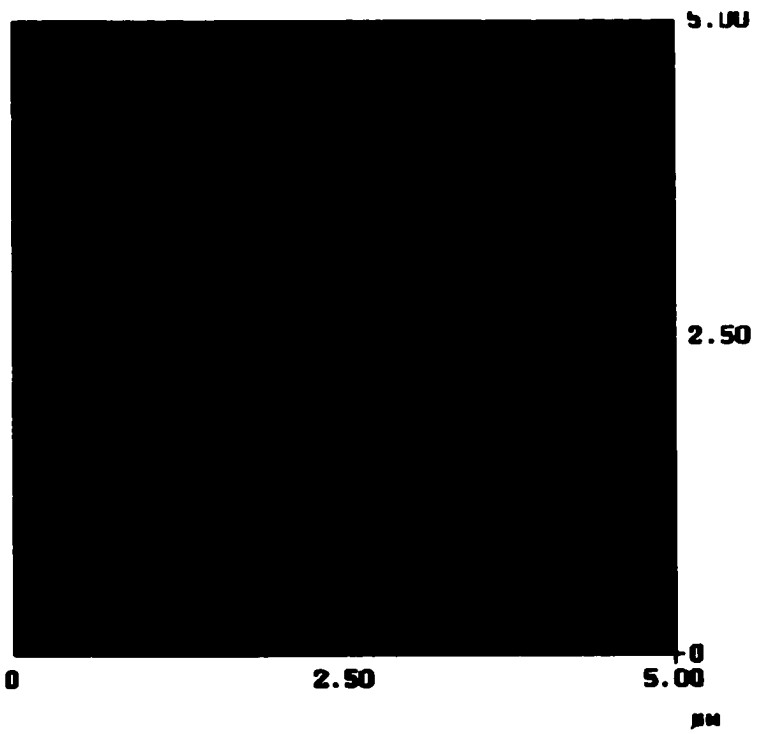

Figure 6.1 (b): CdS nanoparticles formed on modified CUTMS monolayer, (described in chapter4) containing COOH and COO^- groups on the surface

REFERENCES

References: Chapter 1

1. Barraud, A.; Rosilio, C.; Ruaudel-Teixier, A. *Thin Solid Films* **1980**, *68*, 99.

2. McCord, M. A.; Pease, R. F. W. *J. Vac. Sci. Technol., B* **1986**, *4*, 86.

3. Agarwal, D. K.; Srivastava, V. K. *Solid State Commun* **1972**, *11*, 1461.

4. Roberts, G. G.; Petty, M. C.; Baker, S.; Fowler, M. T.; Thomas, N. *J. Thin Solid Films* **1985**, *132*, 113.

5. Kajzar, F.; Messier, J.; Zyss, J.; Ledoux, I. *Opt. Commun.* **1983**, *45*, 13.

6. Chollet, P. A.; Kajzar, F.; Messier, J. *Thin Solid Films* **1985**, *132*, 1.

7. Sauteret, C.; Hermann, J. P.; Frey, R.; Pradere, F.; Ducuing, J.; Baughman, R. H.; Chance, R. R. *Phys. Rev. Lett.* **1976**, *36*, 956.

8. Bigelow, W. C.; Pickett, D. L.; Zisman, W. A. *J. Colloid Interface Science* **1946**, *1*, 513.

9. Nuzzo, R. G.; Allara, D. L. *J. Am. Chem. Soc.* **1983**, *105*, 4481.

10. Ulmann, A.; Kuhn, H. *Thin Films*; Academic Press: New York, 1995; Vol. 20.

11. Ball, P. *Designing the Molecular World*; Princeton University Press: Princeton, 1994.

12. Ulman, A.; Evans, S. D.; Shnidman, Y.; Sharma, R.; Eilers, J. E.; Chang, J. C. *J. Am. Chem. Soc.* **1991**, *113*, 1499.

13. Kumar, A.; Biebuyck, H. A.; Whitesides, G. M. *Langmuir* **1994**, *10*, 1498.

14. Allara, D. L. *Polymer Surfaces and Interfaces*; Wiley: Chichester, 1993; Vol. 2.

References: Chapter 2

1. Jennings, G. K.; Munro, J. C.; Yong, T.-H.; Laibinis, P. E. *Langmuir* **1998**, *14*, 6130-6139.

2. Gennes, P. G. d. *Rev. Mod. Phys.* **1985**, *57*, 827.

3. Lahiri, J.; Isaacs, L.; Grzybowski, B.; D.Carbeck, J.; Whitesides, G. M. *Langmuir* **1999**, *15*, 7186-7198.

4. Ottova, A.; Tvarozek, V.; Racek, J.; Sabo, J.; Ziegler, W.; Hianik, T.; Tein, H. T. **1996**.

5. Piletsky, S. A.; Wulff, G.; Piletskaya, E. V.; Panasyuk, T. L.; Elskaya, A. V.; Levi, R.; Karube, I. *Macromolecules* **1998**, *31*, 2137-2140.

6. Rubinstein, I.; Steinberg, S.; Tor, Y.; Shanzer, A.; Sagiv, J. *Nature* **1988**, *332*, 426-429.

7. Schierbaum, K. D.; Weiss, T.; Velzen, E. U. T. v.; Engbersen, J. F. J.; Reinhoudt, D. N.; Gopel, W. *Science* **1994**, *265*, 1413-1415.

8. Lockhead, M. J.; Letellier, S. R.; Vogel, V. *J. Phys. Chem. B* **1997**, *101*, 10821-10827.

9. Jiang, P.; Liu, Z.-F.; Cai, S.-M. *Surface Science* **2001**, *486*, L507-L512.

10. Li, L. S.; Lianhua Qu, R. L.; 1, X. P.; Zhao, Y.; Li, T. J. *Thin Solid Films* **1998**, *327–329*, 408–411.

11. Li, L. S.; Jin, J.; Tian, Y. Q.; Zhao, Y. Y.; Li, T. J.; Du, Z. L.; Ma, G. H.; Zheng, N. *Supramolecular Science* **1998**, *5*, 475-478.

12. Zhang, L.; Shen, G.; Pan, Z.; Lu, Z. *Materials Chemistry and Physics* **1998**, *55*, 160-163.

13. Sugimura, H.; Ushiyama, K.; Hozumi, A.; Takai, O. *Langmuir* **2000**, *16*, 885-888.

14. Whitesides, G. M.; Aizenberg, J.; Black, A. J. *nature* **1998**, *394*, 868-871.

15. Schon, J. H.; Bao, Z. *Applied Physics Letters* **2002**, *80*, 847-849.

16. Sagiv, J. *Journal of American chemical Society* **1980**, 92-98.

17. Kumar, N.; Malderelli, C.; Steiner, C.; Couzis, A. *Langmuir* **2001**, *17*, 7789-7797.

18. Sabatani, E.; Rubinstein, I.; Maoz, R.; Sagiv, J. *J. Electroanal. Chem.* **1987**, *219*, 365-371.

19. Angst, D. L.; Simmons, G. W. *Langmuir* **1991**, *7*, 2236-2242.

20. Bierbaum, K.; Grunze, M.; Basaki, A. A.; Chi, L. F.; Schrepp, W.; Fuchs, H. *Langmuir* **1995**, *11*, 2143-2150.

21. Parikh, A. N.; Allara, D. L.; Azouz, I. B.; Rondelez, F. *The Journal of Physical Chemistry* **1994**, *98*, 7577-7590.

22. Silberzan, P.; Leger, L.; Ausserre, D.; Benattar, J. J. *Langmuir* **1991**, *7*, 1647-1651.

23. Wasserman, S. R.; Tao, Y.-T.; Whitesides, G. M. *Langmuir* **1989**, *5*, 1074-1087.

24. Creager, S. E.; Clarke, J. *Langmuir* **1994**, *10*, 3675-3683.

25. Bain, C. D.; Whitesides, G. M. *Langmuir* **1989**, *5*, 1370-1378.

26. Cheng, S. S.; Scherson, D. A.; Sukenik, C. N. *Langmuir* **1995**, *11*, 1190-1195.

27. Wang, J.; Frostman, L. M.; Ward, M. D. *Journal of Physical Chemistry* **1992**, *96*, 5224-5228.

28. Sagiv, J.; Iscovici, R.; Gun, J. *J of colloid and interface science* **1984**, *101*, 201-213.

29. Maoz, R.; Sagiv, J. *J. of Colloid and interface science* **1984**, *100*, 465-496.

30. Iimura, K.-i.; Nakajima, Y.; Kato, T. *Thin Solid Films* **2000**, *379*, 230-239.

31. Brzoska, J. B.; Azouz, I. B.; Rondelez, F. *Langmuir* **1994**, *10*, 4367-4373.

32. Kallury, K. M. R.; Macdonald, P. M.; Thompson, M. *Langmuir* **1994**, *10*, 492-499.

33. Carraro, C.; Yauw, O. W.; Sung, M. M.; Maboudian, R. *The Journal of Physical Chemistry B* **1998**, *102*, 4441-4445.

34. Carraro, C.; Yauw, O. W.; Sung, M. M.; Maboudian, R.; Kim, Y. *Journal of Physical Chemistry B* **2000**, *104*, 1556-1559.

35. Bain, C. D.; Whitesides, G. M. *Langmuir* **1989**, *5*, 1370-1378.

36. Kumar, V.; Krishnan, S.; Steiner, C.; Maldarelli, C.; Couzis, A. *J. Phys. Chem B* **1998**, *102*, 5152-5159.

37. Brandow, S. L.; Chen, M. S.; Aggarwal, R.; Dulcey, C. S.; Calvert, J. M.; Dressick, W. J. *Langmuir* **1999**, *15*, 5429-5432.

38. Dulcey, W. J. D. C. S.; Chen, M.-S.; Calvert, J. M. *Thin Solid Films* **1996**, *284-285*, 568-572.

39. Heiney, P. A.; Gruneberg, K.; Fang, J.; Dulcey, C.; Sashidhar, R. *Langmuir* **2000**, *16*, 2651-2657.

40. Hooper, A. E.; Werho, D.; Hopson, T.; Palmer, O. *Surface and Interface Analysis* **2001**, *31*, 809-814.

41. Sieval, A. B.; Linke, R.; Heij, G.; Meijer, G.; Zuilhof, H.; Sudhoiter, E. J. R. *Langmuir* **2001**, *17*, 7554-7559.

42. Doudevski, I.; Hayes, W. A.; Woodward, J. T.; Schwartz, D. K. *Colloids and Surfaces: A Physicochemical and Engineering Aspects* **2000**, *174*, 233-243.

43. Bigelow, W. C.; Pickett, D. L.; Zisman, W. A. *J. Colloid Interface Science* **1946**, *1*, 513.

44. Sagiv, J.; Gun, J. *J of Colloid and interface science* **1986**, *112*, 457-472.

45. Sagiv, J.; Cohen, S. R.; Naaman, R. *J. of physical chemistry* **1986**, *90*, 3054-3056.

46. Ulman, A. *J. of Materials Education* , *11*, 207-279.

47. Kessel, C. R. *Langmuir* **1991**, *7*, 532-538.

48. McGovern, M. E.; Kallury, K. M. R.; Thompson, M. *Langmuir* **1994**, *10*, 3607-3614.

49. Angst, D. L.; Simmons, G. W. *Langmuir* **1991**, *7*, 2236-2242.

50. Grange, J. D. L.; Markham, J. L. *Langmuir* **1993**, *9*, 1749-1753.

51. Tripp, C. P.; Hair, M. L. *Langmuir* **1995**, *11*, 1215-1219.

52. Tripp, C. P.; Hair, M. L. *Langmuir* **1992**, *8*, 1120-1126.

References: Chapter 3

1. Iimura, K.-i.; Nakajima, Y.; Kato, T. *Thin Solid Films* **2000**, *379*, 230-239.

2. Jennings, G. K.; Munro, J. C.; Yong, T.-H.; Laibinis, P. E. *Langmuir* **1998**, *14*, 6130-6139.

3. Bierbaum, K.; Grunze, M.; Basaki, A. A.; Chi, L. F.; Schrepp, W.; Fuchs, H. *Langmuir* **1995**, *11*, 2143-2150.

4. Parikh, A. N.; Allara, D. L.; Azouz, I. B.; Rondelez, F. *The Journal of Physical Chemistry* **1994**, *98*, 7577-7590.

5. Parikh, A. N.; Liedberg, B.; Atre, S. V.; Ho, M.; L.Allara, D. *J. Physical Chemistry* **1995**, *99*, 9996-10008.

References: Chapter 4

1. Jennings, G. K.; Munro, J. C.; Yong, T.-H.; Laibinis, P. E. *Langmuir* **1998**, *14*, 6130-6139.

2. Gennes, P. G. d. *Rev. Mod. Phys.* **1985**, *57*, 827.

3. Lahiri, J.; Isaacs, L.; Grzybowski, B.; D.Carbeck, J.; Whitesides, G. M. *Langmuir* **1999**, *15*, 7186-7198.

4. Ottova, A.; Tvarozek, V.; Racek, J.; Sabo, J.; Ziegler, W.; Hianik, T.; Tein, H. T. **1996**.

5. Piletsky, S. A.; Wulff, G.; Piletskaya, E. V.; Panasyuk, T. L.; Elskaya, A. V.; Levi, R.; Karube, I. *Macromolecules* **1998**, *31*, 2137-2140.

6. Rubinstein, I.; Steinberg, S.; Tor, Y.; Shanzer, A.; Sagiv, J. *Nature* **1988**, *332*, 426-429.

7. Schierbaum, K. D.; Weiss, T.; Velzen, E. U. T. v.; Engbersen, J. F. J.; Reinhoudt, D. N.; Gopel, W. *Science* **1994**, *265*, 1413-1415.

8. Lockhead, M. J.; Letellier, S. R.; Vogel, V. *J. Phys. Chem. B* **1997**, *101*, 10821-10827.

9. Jiang, P.; Liu, Z.-F.; Cai, S.-M. *Surface Science* **2001**, *486*, L507-L512.

10. Li, L. S.; Lianhua Qu, R. L.; 1, X. P.; Zhao, Y.; Li, T. J. *Thin Solid Films* **1998**, *327–329*, 408–411.

11. Li, L. S.; Jin, J.; Tian, Y. Q.; Zhao, Y. Y.; Li, T. J.; Du, Z. L.; Ma, G. H.; Zheng, N. *Supramolecular Science* **1998**, *5*, 475-478.

12. Zhang, L.; Shen, G.; Pan, Z.; Lu, Z. *Materials Chemistry and Physics* **1998**, *55*, 160-163.

13. Sugimura, H.; Ushiyama, K.; Hozumi, A.; Takai, O. *Langmuir* **2000**, *16*, 885-888.

14. Whitesides, G. M.; Aizenberg, J.; Black, A. J. *nature* **1998**, *394*, 868-871.

15. Schon, J. H.; Bao, Z. *Applied Physics Letters* **2002**, *80*, 847-849.

16. Sabatani, E.; Rubinstein, I.; Maoz, R.; Sagiv, J. *J. Electroanal. Chem.* **1987**, *219*, 365-371.

17. Creager, S. E.; Clarke, J. *Langmuir* **1994**, *10*, 3675-3683.

18. Bain, C. D.; Whitesides, G. M. *Langmuir* **1989**, *5*, 1370-1378.

19. Cheng, S. S.; Scherson, D. A.; Sukenik, C. N. *Langmuir* **1995**, *11*, 1190-1195.

20. Wang, J.; Frostman, L. M.; Ward, M. D. *Journal of Physical Chemistry* **1992**, *96*, 5224-5228.

21. Lukkari, J.; Kleemola, K.; Meretoja, M.; Ollonqvist, T.; Kankare, J. *Langmuir* **1998**, *14*, 1705-1715.

22. Tillman, N.; Ulman, A. *Langmuir* **1989**, *5*, 101-111.

23. Delamarche, E.; Michel, B.; Kang, H.; Gerber, C. *Langmuir* **1994**, *10*, 4103.

24. Benesebaa, F.; Ellis, T. H.; Badia, A.; Lennox, R. B. *Langmuir* **1998**, *14*, 2361.

25. Tam-Chang, S.-W.; Biebuyck, H. A.; Whitesides, G. M.; Jeon, N.; Nuzzo, R. G. *Langmuir* **1995**, *11*, 4371.

26. Sung, M. M.; Kluth, G. J.; Yauw, O. W.; Maboudian, R. *Langmuir* **1997**, *13*, 6164-6168.

27. Sung, M. M.; Kluth, G. J.; Maboudian, R. *Langmuir* **1997**, *13*, 3775-3780.

28. Lee, Y. W.; Reed-Mundell, J.; Sukenik, C. N.; Zull, J. E. *Langmuir* **1993**, *9*, 3009-3014.

29. Balachander, N.; Sukenik, C. N. *Langmuir* **1990**, *6*, 1621-1627.

30. Barness, Y.; Gershevitz, O.; Sekar, M.; Sukenik, C. N. *Langmuir* **2000**, *16*, 247-251.

31. Collins, R. J.; Sukenik, C. N. *Langmuir* **1995**, *11*, 2322-2324.

32. Grisaru, H.; Cohen, Y.; Aurbach, D.; Sukenik, C. N. *Langmuir* **2001**, *17*, 1608-1619.

33. Fryxell, G. E.; Rieke, P. C.; Wood, L. L.; Engelhard, M. H.; Williford, R. E.; Graff, G. L.; Campbell, A. A.; Wiacek, R. J.; Lee, L.; Halverson, A. *Langmuir* **1996**, *12*, 5064-5075.

34. Koloski, T. S.; Dulcey, C. S.; Haralson, Q. J.; Calvert, J. M. *Langmuir* **1994**, *10*, 3122-3133.

35. Kakkar, A. K.; Yitzchaik, S.; Roscoe, S. B.; F., K.; Allan, D. S.; Marks, T. J. *Langmuir* **1993**, *9*, 388-390.

36. Yam, C. M.; Tong, S. S. Y.; Kakkar, A. K. *Langmuir* **1998**, *14*, 6941-6947.

37. Kim, T. K.; Yang, X. M.; Peters, R. D.; Sohn, B. H.; Nealey, P. F. *J. Phys. Chem. B* **2000**, *104*, 7403-7410.

38. Wade, N.; Gologan, B.; Vincze, A.; cooks, R. G.; Sullivan, D. M.; Bruening, M. L. *Langmuir* **2002**, *18*, 4799-4808.

39. Bain, C. D.; Whitesides, G. M. *Langmuir* **1989**, *5*, 1370-1378.

40. Parikh, A. N.; Allara, D. L.; Azouz, I. B.; Rondelez, F. *The Journal of Physical Chemistry* **1994**, *98*, 7577-7590.

41. Parikh, A. N.; Liedberg, B.; Atre, S. V.; Ho, M.; L.Allara, D. *J. Physical Chemistry* **1995**, *99*, 9996-10008.

42. Peters, R. D.; Nealey, P. F.; Crain, J. N.; Himpsel, F. J. *Langmuir* **2002**, *18*, 1250-1256.

43. Vallant, T.; Brunner, H.; Mayer, U.; Hoffmann, H.; Resch, R.; Grasserbauer, M.; Friedbacher, G. *J. Phys. Chem. B* **1998**, *102*, 7190-7197.

44. Kessel, C. R.; Granick, S. *Langmuir* **1991**, *7*, 532-538.

45. Oostendorp, D. J.; Bertrand, G. L.; O.Stoffer, J. *Silanes and Coupling Agents* **1992**, 159-179.

46. Osterholtz, F. D.; Pohl, E. R. *Silanes and other coupling agents* **1992**, 119-141.

47. Maoz, R.; Sagiv, J. *Langmuir* **1987**, *3*, 1034-1044.

48. Sagiv, J.; Gun, J. *thin solid films* **1985**, *132*, 135-151.

49. Wasserman, S. R.; Tao, Y.-T.; Whitesides, G. M. *Langmuir* **1989**, *5*, 1074-1087.

50. Crooks, R. M.; Sun, L.; Kepley, L. J. *Langmuir* **1992**, *8*, 2101-2103.

References: Chapter 5

1. Crooks, R. M.; Liu, Y.; Zhao, M.; Bergbreiter, D. E. **1997**.

2. Lahiri, J.; Isaacs, L.; Grzybowski, B.; D.Carbeck, J.; Whitesides, G. M. *Langmuir* **1999**, *15*, 7186-7198.

3. Laibinis, P. E.; Whitesides, G. M. *J. Am. Chem. Soc.* **1992**, *114*, 9022.

4. Lee, J.-Y.; Park, S.-M. *J. of Physical Chemistry* **1998**.

5. Ottova, A.; Tvarozek, V.; Racek, J.; Sabo, J.; Ziegler, W.; Hianik, T.; Tein, H. T. **1996**.

6. Rubinstein, I.; Steinberg, S.; Tor, Y.; Shanzer, A.; Sagiv, J. *Nature* **1988**, *332*, 426-429.

7. Schierbaum, K. D.; Weiss, T.; Velzen, E. U. T. v.; Engbersen, J. F. J.; Reinhoudt, D. N.; Gopel, W. *Science* **1994**, *265*, 1413-1415.

8. Steinberg, S.; Tor, Y.; Shanzer, A.; Rubinstein, I. *Thin Films* **1995**, *20*, 183-205.

9. Wulff, G. *Angew Chem. Int. Ed.* **1995**, *34*, 1812-1832.

10. Grate, J. W.; Patrash, S. J.; Abraham, M. H.; Du, C. M. *Analytical Chemistry* **1996**, *68*, 913-917.

11. Rose, G. D.; Quinn, J. A. *Journal of Colloid and Interface Science* **1968**, *27*, 193-207.

12. Rose, G. D.; Quinn, J. A. *Science* **1968**, *159*, 636-637.

13. Vanderlick, T. K.; Hanley, C. M.; Quinn, J. A. *AIChE Journal* **1996**, *42*, 1234-1243.

14. Marshbanks, T. L.; Ahn, D. J.; Franses, E. I. *Langmuir* **1994**, *10*, 276-285.

15. Long, F. A.; Thompson, L. J. *Journal of Polymer Science* **1955**, *15*, 413.

16. Perrin, L.; Nguyen, Q. T.; Sacco, D.; Lochon, P. *Polymer International* **1997**, *42*, 9-16.

17. Quickenden, T. I.; Barnes, G. T. *J. Colloid and Interface Science* **1978**, *67*, 415-422.

18. Sobotka, H. *Journal of Colloid Science* **1956**, *11*, 435-444.

19. Karpovich, D. S.; Blanchard, G. J. *Langmuir* **1997**, *13*, 4031-4037.

20. Archer, R. J.; La Mer, V. K. *J. Ohys. Chem* **1955**, *59*, 200.

21. Windreich, S.; Silberberg, A. *J. Colloid and Interface Science* **1980**, *77*, 427-434.

22. Langmuir, I. *J. Am. Chem. Soc* **1916**, *38*, 2221-95.

23. Kondoh, H.; Matsui, F.; Ehara, Y.; Yokoyama, T.; Ohta, T. *Langmuir* **2001**, *17*, 8178-8183.

24. Ocko, B. M.; Wu, X. Z.; Sirota, E. B.; Sinha, S. K.; Gang, O.; Deutsch, M. *Phys. Rev. E* **1997**, *55*, 3164.

25. Jasper, J. J. *J. Phys. Chem. Ref. Data* **1972**, *1*, 841.